Universidade do Minho
Escola de Engenharia

ANANTH RAJKUMAR

Improved methodologies for the design of extrusion forming tools

January 2017

ANANTH RAJKUMAR Improved methodologies for the design of extrusion forming tools

UMinho | 2017

Universidade do Minho
Escola de Engenharia

ANANTH RAJKUMAR

Improved methodologies for the design of extrusion forming tools

Doctoral Dissertation for PhD degree in
Engineering Design and Advanced Manufacturing –
The Leaders for Technical Industries
(MIT – Portugal Program)

Thesis Supervisors
Professor João Miguel de Amorim Novais da Costa Nóbrega
Professora Olga Machado de Sousa Carneiro
Professor Zeljko Tukovic

January 2017

STATEMENT OF INTEGRITY

I hereby declare having conducted my thesis with integrity. I confirm that I have not used plagiarism or any form of falsification of results in the process of the thesis elaboration.

I further declare that I have fully acknowledged the Code of Ethical Conduct of the University of Minho.

University of Minho, _____

Full name: ANANTH RAJKUMAR

Signature: 

I would like to dedicate this thesis to my family,

Specially to my brothers

&

My kids (Balian, Rihanna &, Jade)

Abstract

Thermoplastic profiles cover a wide range of applications (window frames, structural components, vehicle door seals, medical catheters, etc.). The inherent design freedom promoted by the employment of thermoplastic profiles is one of the major reasons for their attractiveness. In the current market situation, extrusion industries aim for competitive advantages by delivering quality products within a short time. In order to produce any specific thermoplastic profile, a considerable amount of time is spent on the design of the required extrusion forming tools (namely, the extrusion die and the calibration/cooling system) since this task is usually carried out based on experimental trial-and-error procedures. This approach is highly dependent on the experience of the persons involved and usually requires high consumption of resources. Often, these limitations either inhibit the achievement of an optimal solution or increase significantly the development costs and, consequently, the final price of the produced profiles. As a major consequence, even with obvious advantages in terms of performance, the employment of thermoplastic profiles is still restricted. Obviously, these difficulties are more evident when the new profile to be produced comprises a complex geometry and there is lack of previous experience with similar products.

Numerical tools, on the other hand, can provide an alternative route to design/optimize the extrusion forming tools. Even though, most of the profile extrusion forming tool designers prefer to follow the time consuming experimental trial-and-error approach, because of the cost involved in acquiring commercial modeling tools and the lack of knowledge/experience in numerical modeling.

The main objective of this PhD project is to establish new and improved design procedures for the extrusion forming tools. These procedures are implemented with the aid of free/open source softwares that can attract the interest of profile extrusion industries.

A new die design methodology was proposed along with the development of a solver to model the polymer melt flow inside the extrusion die. The numerical code is developed within the OpenFOAM framework, and verified for proper implementation. The proposed design methodology was used to solve two industrial case studies, proposed by a profile extrusion company.

An innovative die design methodology was developed to provide simplified guidelines for the design of complex profile extrusion dies, which can be decomposed in *L* and *T* elementary geometries. The methodology is based on surrogate models, its application does not rely on any numerical tools, and it was developed mainly for designers with no access to computational modelling tools. The efficiency of the methodology was proved by assessing it with some illustrative case studies.

The range of application of the simplified die design methodology was further enlarged by taking into account the processing and rheological features of the flowing polymeric material. Here, the Power-Law index ‘n’, which has the most influence on the flow distribution, was included in the model. Again, the improved methodology was assessed with complex geometries made of *L* and *T* shaped profiles, and proved to be valid for typical thermoplastic polymers.

Regarding the calibration system, a numerical code, developed in the OpenFOAM framework to model the heat transfer occurring during the extrusion profile cooling process, was validated with experimental data. A study based on numerical trial-and-error approach was used to illustrate the usefulness of applying numerical tools to aid the design of the calibration systems, and a better alternative for an industrial calibration system was proposed.

The work was undertaken in close cooperation with Soprefa, a Portuguese company that has been working for more than two decades in the design and production of extruded thermoplastic profiles. The developed/proposed design methodologies for extrusion forming tools were evaluated in their premises, with case studies proposed by them.

Keywords: Extrusion forming tools, thermoplastic profile, complex geometry, Extrusion die design, Calibration system design, numerical modelling, OpenFOAM.

Resumo

Os perfis termo-plásticos estão presentes numa ampla gama de aplicações, tais como caixilharia de janelas, componentes estruturais, vedações de porta de veículos, cateteres médicos, etc. A sua vasta utilização deve-se fundamentalmente à liberdade de formas geométricas que os mesmos permitem criar. Na actual situação de mercado, a competividade das empresas está fortemente dependente da rapidez com que conseguem colocar produtos de qualidade no mercado. No entanto, na produção de perfis termo-plásticos é habitualmente gasto um tempo considerável na concepção das ferramentas de processamento (nomeadamente, a cabeça de extrusão e o sistema de calibração/arrefecimento), uma vez que essa tarefa é, na maioria das vezes, realizada com base em procedimentos de tentativa e erro de base experimental. Deste ponto de vista, o processo torna-se muito dependente da experiência prévia das pessoas envolvidas, e requer a utilização de uma grande quantidade de recursos. Consequentemente, estas limitações inibem a obtenção de uma solução óptima ou aumentam significativamente os custos de desenvolvimento e, dessa forma, o preço final dos perfis produzidos. Assim, mesmo com vantagens óbvias em termos de desempenho, o uso de perfis termo-plásticos é ainda restrito. Estas dificuldades são ainda mais evidentes quando o novo perfil a ser produzido tem uma geometria complexa e existe falta de experiência com produtos similares.

Por outro lado, a utilização de livrarias numéricas podem ajudar a projetar e otimizar as ferramentas de processamento por extrusão. Mesmo assim, a maioria dos projetistas de perfis produzidos por extrusão preferem seguir a morosa abordagem de tentativa e erro, isto porque o custo associada a ferramentas numéricas comerciais é bastante elevado e devido à falta de conhecimento/experiência em modelação numérica.

O principal objectivo deste projecto de doutoramento é estabelecer procedimentos novos e melhorados para a conceção de ferramentas de processamento por extrusão. Estes procedimentos são suportados pelo recurso a ferramentas numéricas com código livre/aberto, o que pode atrair significativamente o interesse das indústrias de processamento de perfis por extrusão.

Neste trabalho é proposta uma nova metodologia de concepção de perfis por extrusão juntamente com o desenvolvimento de um algoritmo numérico capaz de modelar o fluxo de polímero fundido dentro da cabeça de extrusão. O código numérico é desenvolvido recorrendo à biblioteca de código aberto OpenFOAM e a sua implementação é verificada em diversos estudos analíticos. Adicionalmente, a metodologia de concepção de perfis proposta foi usada para resolver dois problemas associados a aplicações industriais.
Uma metodologia inovadora para a concepção de cabeças de extrusão foi também desenvolvida neste trabalho, aplicável a geometrias que podem ser decompostas em secções elementares em forma de “L” e “T”, na qual apenas é necessário seguir

indicações simples. Esta metodologia, baseada em modelos de substituição, foi desenvolvida visando utilizadores sem acesso a ferramentas numéricas, possibilitando um uso mais alargado no contexto da concepção de cabeças de extrusão. A eficácia da metodologia proposta foi testada em geometrias complexas.

A metodologia desenvolvida para a concepção de cabeças de extrusão foi ainda melhorada de forma a ter em conta as características reológicas e de processamento do material polimérico usado. Desta forma, o parâmetro de comportamento do fluído no modelo de viscosidade da Lei de Potência, *n*, que tem maior influência na distribuição do fluxo, foi incluído nos modelos de substituição. Novamente, a metodologia melhorada foi testada com geometrias complexas, compostas por secções elementares em forma de "L" e "T" e mostrou ser válida para a generalidade de materiais termoplásticos.

No que diz respeito ao sistema de calibração efectuou-se a validação experimental de um código numérico desenvolvido na biblioteca OpenFOAM, que permite modelar a transferência de calor ocorrida durante o estágio de arrefecimento do perfil extrudido. Neste caso, realizou-se um estudo numérico, baseado em tentativa e erro, para ilustrar as vantagens da aplicação de ferramentas numéricas no apoio à conceção do sistema de calibração, tendo-se identificado uma alternativa melhor para um sistema de calibração existente numa empresa.

Este projeto foi realizado em estreita colaboração com a Soprefa, empresa portuguesa que trabalha há mais de duas décadas na concepção e produção de perfis termoplásticos extrudidos. As metodologias desenvolvidas para a concepção de cabeças de extrusão foram testadas nas instalações da referida empresa e com casos de estudo propostos pela mesma.

Keywords: ferramentas de processamento por extrusão, termoplásticos extrudidos, geometria complexa, cabeças de extrusão, sistema de calibração, ferramentas numéricas, OpenFOAM.

Acknowledgement

I sincerely acknowledge the support of MIT-Portugal program and the Portuguese Foundation for Science and Technology (FCT) for the financial support through PhD student grant SFRH/ BD/51943/2012.

I am grateful to my supervisors, Professor Miguel Nóbrega and Professor Olga Carneiro for their guidance, understanding and support. I highly appreciate and always be thankful for their patience and presence throughout this work. I would also like to express my gratitude to my other supervisor Professor Zeljko Tukovic.

I also show my gratitude to the computing facilities provided by the Project "Search-ON2: Revitalization of HPC infrastructure of UMinho" (NORTE-07-0162-FEDER-000086), co-funded by the North Portugal Regional Operational Programme (ON.2–O Novo Norte), under the National Strategic Reference Framework (NSRF), through the European Regional Development Fund (ERDF).
I am highly indebted to Soprefa for the technical support, tools and guidance. Personally, I express my gratitude to Mr. Alberto Sacramento for his support, I also take this opportunity to thank Mr. Helder and Mr. Luis.

I am utterly thankful to Luis Ferrás, Célio Fernandes and Sacha Mould. Luis Ferrás for providing support for solving mathematical issues and for the motivation from his side. Célio Fernandes and Sacha Mould for supporting me, technically and personally.
I thank all my colleagues in Polymer Engineering Department of University of Minho, Paulo Teixeira, Rui Gomes and João Vidal and all other persons I had the privilege to work with.
I am also grateful to Florian Habla and Martin Becker, for the timely response to my doubts.

Most importantly, I thank my wife Ignasious Premi, for understanding my situation, and also for her patience, support and motivation.

Table of Contents

List of Figures

List of Tables

Chapter 1

Introduction

Extrusion is one of the most common techniques used to manufacture polymeric parts. In this processing technology, the polymer, usually in the form of pellets or powder, is fed to the extruder where it is melted, homogenized and pushed through a die, which shapes it. Then the polymer is cooled, and either cut into sections or rolled up. Some examples of extruded products include tubings, pipes, films, sheets, and profiles. The latter play a significant role that encompass the production of complex shaped profiles for various applications. Some of the products obtained through profile extrusion are home siding, window frames, medical tubing, etc. (Gentran).

Profile extrusion is a steady-state process for converting a polymer raw material to a finished or near-by finished product (Rauwendaal, 2014). A typical profile extrusion line comprises an extruder, an extrusion die, a calibration/cooling system, a haul-off unit and a saw, as shown in Figure 1.1. Each unit has its particular function, as described below:

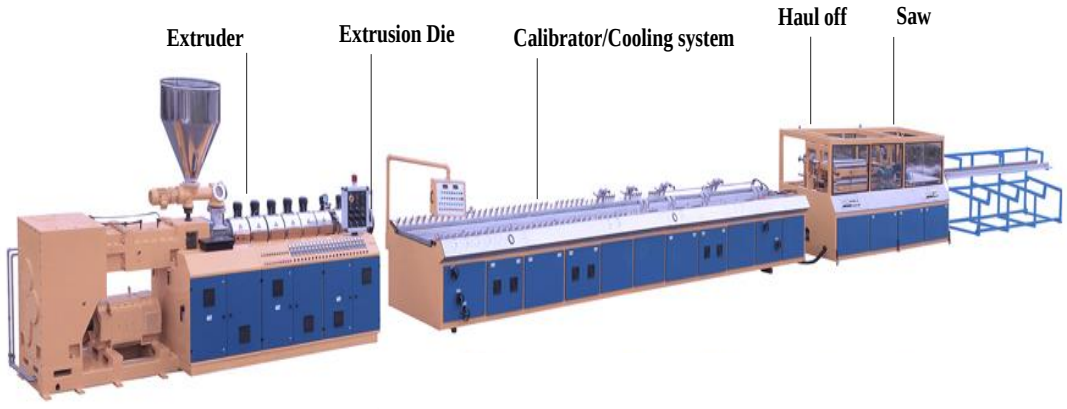

Figure 1.1: Profile extrusion line (SAInternational).

Extruder – is a plasticating unit responsible to melt, homogenize and push the molten polymer towards the extrusion die;

Extrusion die – is a metallic tool responsible to shape the molten polymer into the desired cross section;

Calibration/Cooling system – a system responsible to cool and assure that the profile meets the specified dimensions;

Haul-off – is a unit that pulls the profile at a specified linear velocity;

Saw – cuts the continuous profile into segments with the desired length.

Among the above mentioned extrusion line components, the extrusion die and the calibration system are the most relevant extrusion line components that play an important role in establishing the product dimensions, morphology and properties, and are also those that establish the maximum allowable production rate (Michaeli, 1992; Kent, 1998).

1.1 Extrusion forming tools

1.1.1 Extrusion dies

As mentioned above, the extrusion die is the tool responsible to shape the molten polymer on to the desired profile geometry. In the particular case of profile extrusion, three different design construction of the die are distinguished: plate dies, stepped dies and streamlined dies. Plate dies comprise the simplest design approach, mainly consisting on a single metallic block containing the flow channel. This type of construction allows easy operation/handling and cheap manufacturing, but in the downside, it potentiates the occurrence of hot spots which turns its use prohibitive for thermally sensitive materials (Nóbrega, 2004). Stepped dies, in turn, provides better

performance than plate dies and still benefit of low manufacturing costs. The construction consists on a sequence of metallic plates which progressively shape the molten polymer into the final product. These type of dies are usually employed on the production of simple profiles without hollow sections. An example of a plate die and a stepped die is shown in Figure 1.2.

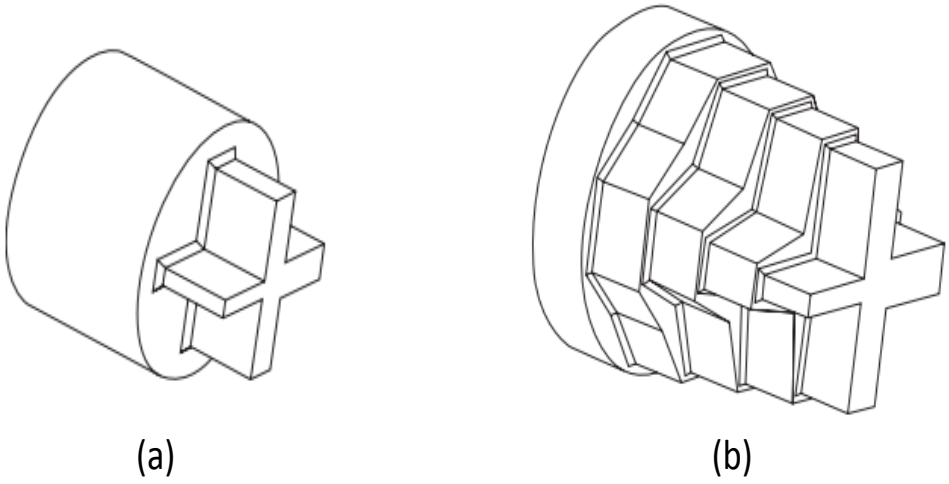

Figure 1.2: Flow channel used for the production of cross-shaped profile: (a) plate die, (b) stepped die (Carneiro and Nóbrega, 2012).

The streamlined dies are developed based on the concept of constant area reduction along the length of the die (Narayanasamy et al., 2003), allowing smooth transition of material flow. The die can produce profiles with high dimensional accuracy at high rates, but are expensive from the machining point of view (Nóbrega, 2004). The streamlined dies are built of four unique components namely: (i) Adapter; (ii) Transition Zone; (iii) Pre-Parallel Zone; and (iv) Parallel Zone. Figure 1.3 shows a typical streamlined die evidencing its corresponding sections.

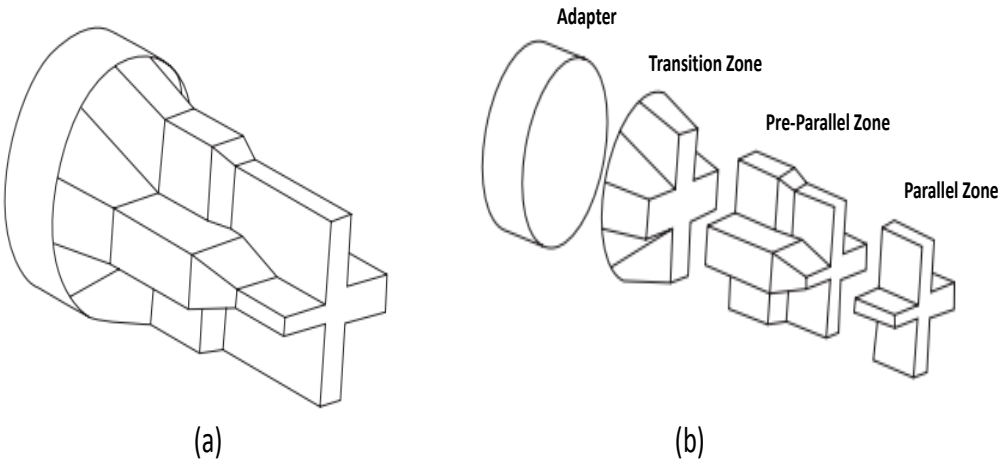

Figure 1.3: Flow channel used for the production of cross-shaped profile: (a) streamlined die, (b) different zones of the die (Carneiro and Nóbrega, 2012)

As the material enters the Adapter zone, it gets accommodated and take the circular shape of the zone. After the Adapter, the material exits to the Transition Zone which has an approximate shape of the profile. The Transition Zone transforms the material cross section smoothly from the Adapter exit to the Pre-Parallel Zone inlet. The Pre-Parallel Zone is the functional zone that allows to control the material flow distribution by adjusting the location of the convergences to the Parallel Zone. Finally, the Parallel Zone provides a constant dimensional passage over a length imposing the shape to the extrudate leaving the die (Kostic and Reifschneider, 2006; Carneiro and Nóbrega, 2012).

Extrusion die design procedure involves several functional requirements and challenges, in order to obtain a quality die that expedite the production of the required profile with acceptable quality. Regarding the operation point of view, a good die should ensure easy maintenance, easy assembly and disassembly (Giles et al., 2004). The challenges encountered during the design process from the polymer point of view are the avoidance of rheological defects (the melt flow instabilities that may occur during the flow through the extrusion die, eg. sharkskin, melt fracture) (Nóbrega, 2004; Carneiro and Nóbrega, 2012) the prevention of thermal degradation of polymer

melt (Carneiro et al., 2001) and the anticipation of the effect of the post-extrusion phenomena (eg. extrudate-swell, draw-down and shrinkage) (Pauli et al., 2013).

Concerning to the process, the main design challenge encountered is the flow balance at the die exit, i.e., achieving uniform average melt velocities in all the regions of the die exit cross-section, which allow the production of the desired profile. This particular extrusion die design problem is concentrated throughout the course of this PhD project.

Naturally, more material flows through the thicker sections compared to that of the thinner ones, creating an uneven flow and unable to produce the defined profile. Moreover, the polymer melt rheological properties along with the complex shape of the profile having different wall thickness makes the flow balancing process more difficult. A proper design of die flow channel, which allows to control the flow based on the restrictions, aids the achievement of flow balanced conditions (Murray, 1978).

In the search for a flow channel, resulting in a balanced flow distribution, the recommended approaches by some of the researchers are to change the parallel zone cross-section or the flow channel length (Busby, 1996; Svabik et al., 1997). Some claim that in order to achieve flow balance, the adjustment has to be done only on the flow channel length and not on the parallel zone cross section (Kuhnle, 1986; Hurez et al., 1991; Lee and Stevenson, 1992; Hurez et al., 1993; Hurez et al., 1996).

The optimization techniques based on modification of the flow channel length, can be inadequate to achieve flow balancing for a geometry profile with high differences in flow restriction (Sun and PENG, 1991); in such situation the use of flow separators can provide a better solution (Kuhnle, 1986; Hurez et al., 1996). However, the use of flow separators, may produce weld lines in the profiles, affecting its mechanical properties. Regarding the other optimization approach based on the adjustment of Parallel Zone cross section, it can lead to a more robust die, which is less sensitive to the change in process conditions or material rheology (Svabik et al., 1997; Nóbrega et al., 2003b).

1.1.2 Cooling/Calibration system

The cooling system in the extrusion line may be performed by wet, dry or combined cooling methods. In the wet cooling method the heat is removed directly by the cooling fluid since it is in direct contact with the profile. It is commonly used on the cooling of hollow profiles (Carneiro and Nóbrega, 2012), but unpleasant profile distortions (e.g., twisting and wrapping) may appear if the temperature difference between the profile and the cooling water is high (CONAIR). In dry cooling, there is no direct contact between the hot profile and the cooling medium. Instead, the profile is cooled by a metallic calibrator which contains its own cooling system. This method is suitable in high speed profile extrusion, being the most reliable alternative among all. Lastly, the combined wet/dry method is also used for high speed profile extrusion, where the system consist of a dry vacuum calibrator followed by a water bath (Michaeli, 1992; Carneiro and Nóbrega, 2012).

The calibration/cooling system should ensure easy assembly and disassembly, and should also be easy to operate. The design challenges regarding to the process are setting the system geometry (number of calibration units, unit length, distance between the calibrators), cooling conditions (temperature of inlet water, flow rate, flow direction), vacuum conditions (vacuum pressure, number and location of holes) and extrusion conditions (mass flow rate and die exit cross-temperature profile field) (Nóbrega, 2004; Goncalves, 2013). The calibration/cooling system design process should ensure proper cooling of the incoming melted polymer profile to keep the desired cross section geometry (Michaeli, 1992). The cooling should be ensured at a fast rate and in a uniform manner, in order to have adequate morphology and a reduced level of thermal residual stresses (Carneiro et al., 2004a).

The calibrator should also provide efficient cooling to obtain enough profile strength, to avoid deformation due to various external forces applied along the production line

(Michaeli, 1992; Carneiro et al., 2004a). These objectives are conflicting since fast cooling rates increase the temperature non-homogeneity (and level of thermal residual stresses). A proper heat transfer between the polymer and the calibrator is a looked-for issue for achieving uniform cooling in calibrator design process, and this challenge is discussed in this work.

1.2 Design of extrusion forming tools

Extrusion forming tools design is more an art than a science (Kostic and Reifschneider, 2006; Carneiro and Nóbrega, 2012), due to the complex rheology of polymer melts and the difficulties in understanding their behavior. The usual methodologies employed to design extrusion forming tools are based on experimental trial–and–error approaches which consume lot of time and resources (Michaeli et al., 2001). In order to reduce the resources involved during the design process and, thus, improve the design performance, a deep knowledge about the extrusion process is required. With the development of powerful computing hardware and proficient numerical techniques, fast and reliable numerical models can be developed in order to simulate the flow through the extrusion forming tools (Karadogan, 2005; Kostic and Reifschneider, 2006). The numerical solution approach provides predictions for the details of the extrusion process, such as velocity, shear stress, pressure, and temperature fields and other phenomena which are impossible to obtain experimentally (Kostic and Reifschneider, 2006). The use of numerical simulation can reduce significantly the extrusion forming tools design cost and development time.

1.2.1 Die design methods

The studies related to the design of profile extrusion die flow channels are being carried out for a long time (Corbett, 1954). As a result, the literature is rich in experimental and numerical studies. At the early stages, series of experimental studies were made to improve the design process. As a result, practical rules and guidelines facilitating die tool design, were provided by various researchers (Corbett, 1954; Murray, 1978; Levy, 1981; Rauwendaal, 1991), which are based on knowledge gathered from practical experience.

In some other studies (Reynolds, 1886; Tadmor and Gogos, 2006), analytical calculations were used along with those recommendations suggested from the accumulated experience. Based on this approach, Michaeli (1984) proposed a study that uses the combination of analytical computation and an experimental trial-and-error technique, aiming to obtain uniform flow distribution at each section of the extrusion die by adjusting the flow channel length and the die entry angle. These partly empirical procedures delivered a better awareness to the die designer regarding the phenomena involved in the design process (Michaeli, 1984). Also, an analytical approach aiming to simplify the die design process for rigid PVC was proposed by Summers and Brown (1981). As a result, the study delivered simplified equations and practical rules in a tabular format, in order to facilitate the average design engineer in building dies.

Huneault et al. (1996), delivered a flow network model named FAN (flow analysis network). This method uses analytical relationships focused to optimize the flow distribution at the die exit. The results predicted from this model proved to be in good agreement with the experimental data. In a research study by Hurez et al. (1996), a design procedure for complex profile extrusion dies, based on the resolution of the

flow inverse problem, was developed. The procedure is a combination of the network approach (that explains the complex layout of flow channel in the die land) and the cross-section method (to determine the individual channels pressure drop), in which the Power-Law model is used to study the flow of the material. The method facilitates the determination of the channel topology that indorses a balanced flow at the die exit cross-section, and it has been proven to perform very well for the flow balancing of multiple channel dies. Formerly, many researchers used a neural network algorithm to optimize the die design process, but this method consumes a lot of time in order to train a network and to exactly predict the flow. In an attempt to reduce the time needed to obtain an optimized die using the network approach, Mehta et al. (1999), introduced a new methodology combining the neural network and the results from a design of experiments. The recommendation from the experimental results indicates the important variables to be used in the optimization process, thereby reducing the data set needed for training a neutral network to achieve an optimized die.

In an another work, Reid et al. (2003) used a simple method based on a 1-D design equation to analyze the influence of the fluid rheology on the flow distribution in coat hanger die design. As a result of their investigation, the authors declares that the effect of Power-Law index ‘n’ on the flow uniformity is very small; however, the study neglected the influence of lateral flows.

All these analytical approaches support the flow balancing of simple flows and are limited towards complex geometries, since a huge amount of these works contemplate 1 and 2-dimensional flow analysis (Wu et al., 2006). Thereby, these methods are not able to consider the full influence of the lateral flow, and their use to design complex profile extrusion dies may mislead.

The enhancement in computer technology, along with the significant development of computational fluid dynamics, fast and accurate development in numerical tools, motivated many researchers to use numerical simulation to study the extrusion die design process (Sebastian and Rakos, 1985; Menges, 1986). Due to this, a huge amount of numerical based studies for extrusion die design, are available in the literature. A while back, McKelvey and Ito (1971), performed a research study to analyze the flow distribution in flat sheet dies by considering a Power-Law model, in order to describe the flow under isothermal flow condition. They established a method to predict the die dimensions promoting an even flow distribution at a specific pressure drop and flow rate. The study also concludes that the flow distribution is highly influenced by the Power Law index "n". Procter (1972), studied and analyzed the effect of inelastic Power Law fluids under isothermal condition for different extrusion dies. The result provided by the study states that the axial flow distribution in the extrusion dies depends mainly on the Power Law index and also on a number of flow channel design parameters. Wortberg et al. (1982), proposed a study that investigate the main stages of the extrusion process namely the extruder, die forming and cooling. The study uses a Finite Element Method (FEM) based numerical code to calculate the three dimensional (3D) flow patterns in Y and T shaped profile extrusion dies.

Later, Legat and Marchal (1993), developed a numerical scheme to solve the inverse extrusion problem by means of an implicit Newton-Raphson iterative technique. The method was used to predict the die cross section geometry that produces an extrudate with the prescribed shape, thereby minimizing the trial-and-error iterative procedure. They also studied the flow of Newtonian and non-Newtonian (shear thinning) fluids under isothermal conditions and presented the benchmark results for geometries with square and rectangular shapes, and also for geometries with multiple corners. Na and Lee (1997), proposed a shape optimization study of polymer extrusion dies, and in this work the numerical simulations are performed with a FEM based numerical code and the optimization is done using a solution strategy of inverse problem. The search

for an optimum solution of the extrusion die was drafted as a quadratic optimization problem, where the optimized geometry can be predicted by the quadratic optimization problem in several iterations.

A different approach, called Taguchi method, was used by Chen et al. (1997) to analyze the effect of various parameters namely, the materials, die geometry and processing conditions in the optimization of a manifold profile (coat-hanger die). The method provides the influence of parameters on the manifold design, and a significant influence was obtained for the die geometry parameters and the Power Law index. Yu and Liu (1998), used the lubrication approximation to devise a simple numerical approach to optimize a linearly tapered coat-hanger die. The method deals with any generalized Newtonian fluid model. The results predicted with this methodology are compared with those obtained from the 3-D FEM simulations of the complete geometry, and it proves to be reasonably accurate. Ulysse (1999), presented the design study of a plane strain two-hole extrusion die using the combination of FEM and mathematical optimization techniques. The method determines an optimal bearing length to promote a uniform flow at the exit of the extrusion die. The study assumes a power-law model under isothermal conditions. The accuracy of this numerical method is assessed with experimental results, showing a good agreement. Later, the same author (Ulysse, 2002), extended the design model to improve the flow control at the die exit, by including temperature distribution in the material flow calculation and also by considering the thermal effects in the analytical sensitivity formulation.

A FEM based numerical design method was developed by Wu and Hsu (2002) to optimize the shape design of extrusion dies. The optimization process was done using an improved genetic algorithm, providing an optimal shape with minimum force and strain. Lehnhäuser and Schäfer (2005), presented and analyzed a numerical based method for the shape optimization of the fluid flow domains, by modeling a steady state incompressible Newtonian fluid. The procedure encompasses: a numerical

solver to simulate the flow, a mathematical optimization tool and an efficient shape altering technique. The study illustrates the applicability of the method over certain engineering interest involved in the production process. Sienz et al. (2006), used FEM based simulation to study the performance of a slit die towards optimum flow distribution. In this study, the results obtained from three methods used namely, a generic algorithm, a multipoint approximation optimization method, and a gradient-based optimization method, were compared to reach an optimum solution for melt flow distribution. Lebaal et al. (2009), proposed a computational approach that incorporates a software for performing FEM simulations and an optimization algorithm built using global response surfaces with the Kriging Interpolation and SQP algorithm that optimize the velocity distribution at the die exit with a constraint over the pressure drop in the die. Soury et al. (2009), provided a study that holds both the simulation work (done using a numerical code) and the experimental verification for an extrusion die used to produce a wood-plastic composite profile, thereby providing a numerical based trial-and-error approach, similar to the one proposed in this PhD project. An I-shaped profile extrusion die was used to perform the optimization study and, as a result, the prediction given by the simulation led to the production of the profile with acceptable quality.

Recently, Sienz et al. (2010), used a direct differentiation method that can be coded in FEM, for performing sensitive analysis in the profile extrusion die design process. The study indicates that the essential derivatives needed to evaluate the design sensitivity can be attained from a post-processing step and by using the same code that solves the discrete governing equations. Mu et al. (2010), used the combination of FEM simulation, the back-propagation neural network, and the non-dominated sorting genetic algorithm II (NSGA-II), to propose an optimization strategy for the polymer extrusion die design process. The numerical procedure to model the polymer melts flow is based on the penalty method, the simulated results are analyzed by the NSGA-II to predict the optimal design variables, and the neural network was used to evaluate the objective functions. The optimization methodology proves to be

successful for designing a die for tubular products of low-density polyethylene. Elgeti et al. (2012), proposed a new design concept based on numerical shape optimization. The design concept consists of two steps: systematic design of initial geometry, and numerical shape optimization of the flow channel. The framework was applied to two profile extrusion dies, namely a simple slit profile and a complex floor skirting. The results obtained with a Newtonian fluid and a non-Newtonian one (Carreau model) were also compared in the study. The study concludes that the Carreau model displays a significant influence on the quality of the solution. Yilmaz et al. (2014), studied the optimization of profile extrusion dies' geometry parameters using a range of objective function definitions based on Simulated Annealing-Kriging Meta-Algorithm, and the numerical simulation is performed using a FEM based code. The algorithm used in the study searches for an optimum solution from the map developed based on the results of the objective functions.

Furthermore, a wide range of commercial softwares are available to aid the design of profile extrusion dies. These are, among others, ANSYS Polyflow, Die Flow, Compuplast and Polydynamics. The availability of those tools indicates that they are a suitable alternative to the experimental trail-and-error die design procedure, the most common practice employed in the extrusion industry. However, the decisions regarding the consecutive adjustment of the die design until an acceptable optimum result is attained, are still committed to the designers (Rezaei et al., 2010). Consequently, the designer intervention and knowledge are still required. Moreover, higher computational time and resources are required to model the polymer flow in 3D geometries (Vincent et al., 2002).

Aiming to automatize the extrusion die design process, Michaeli and Kaul (2004) proposed a calculation method based on the network theory and a genetic algorithm. As a result, the study delivers an algorithm for the automatic optimization of flow channels in profile extrusion dies. Regarding to the automatic approach, some

research works were done by Ettinger et al. (2004), in which the main parameters and optimization strategies needed to automatize the design of profile extrusion dies were identified. In that study, 3D die geometries are represented using two dimensional (2D) geometry called 'die-slices', which are subjected to numerical optimization. The same team developed a computational optimization approach for dealing with the complex type die required for the production of uPVC profiles (Ettinger et al., 2013). However, the approach is 2D, which causes limited applicability. The research team from the University of Minho, Carneiro et al. (2001), proposed a moderately comprehensive methodology for the optimization of the profile extrusion die design process. A 3D computational code based on Finite Volume method (FVM) was developed for performing numerical simulations, and the Pre-Parallel Zone length distribution was optimized in order to achieve flow balance. In their work, they identified the main steps needed for the automatic design process (Nóbrega et al., 2003a). The group performed a series of simulations with the numerical code developed and advanced on the automatic optimization design concept (Nóbrega et al., 2003b; Nóbrega, 2004; Nóbrega et al., 2004a; Carneiro et al., 2004b). The optimization design strategies used are based on changes performed in the Pre-Parallel Zone and Parallel Zone (or die land) cross section. However, the numerical code used for this purpose is limited to simple geometry problems, due to the use of structured meshes. Later, a numerical code was developed to simulate complex geometries, based on unstructured meshes, and a generalized Newtonian fluid was used to model the flow under isothermal conditions (Goncalves, 2013). The difficulties faced in using those in-house developed codes are that they require the knowledge of the designer who devised them.

As a conclusion, the use of numerical simulation in extrusion industries is very limited and improved design methods are still required to attract their interest.

1.2.2 Calibration/Cooling system design methods

The preliminary attempts to model the cooling of plastic profiles were made with 1D models (Menges et al., 1982; Kurz, 1988). Later, a study with a 2D approach was provided by Menges et al. (1987), that is said to handle any complex shape profile. Based on this method, Sheehy et al. (1994) developed a method named 'Corrected slice method', to deal with 3D geometries. Fradette et al. (1996), also used Menges et al. (1987) method, along with the correlation developed to describe heat transfer, to study a specific experimental case. Both, Sheehy et al. (1994) and Fradette et al. (1996), validated their numerical model with real calibrators, and provided a fairly good agreement. Szarvasy (2000), included a more realistic boundary condition for the heat exchange within the internal cavities of hollow profiles. Pittman and Farah (1996), presented an inclusive mathematical model along with FEM simulation to study the cooling process in plastic pipes, and the method was used to predict the sag flow in thick wall pipes. However all these works use 2D approaches.

Ren et al. (2010), presented an optimization method for designing heterogeneous cooling systems (i.e. calibrators built with different materials e.g. copper and steel). FEM and Finite Difference Method (FDM) are used to model the cooling process of the plastic profile within the calibrator. The study indicates that the uniform cooling of the plastic profile by the heterogeneous calibrator improves by changing the cooling channels location, size, and number, and by adjusting the material distribution in the calibrator. The University of Minho research team (Nóbrega et al., 2004b; Nóbrega et al., 2004c; Nóbrega and Carneiro, 2006; Nóbrega et al., 2008), established and verified an algorithm comprising a non-isothermal 3D code, used to model the thermal interchanges that take place during the cooling stage of profile extrusion, and geometry and mesh generators. They also provided an optimization routine aiming to determine the optimal cooling conditions. The developed numerical code is not able

to deal with very complex geometries, due to the use on structured meshes. Taking into account this limitation, and considering the effectiveness of open source codes, more recently, Habla et al. (2016), developed a model to study the heat transfer between the polymer and calibrator phases for complex profiles. However, a valid experimental assessment to recognize its accountability in industrial context was not performed.

1.3 The OpenFOAM® computational library

OpenFOAM® is a free and open source computational library that is gaining recognition among the academic researchers and industrial users, predominantly in CFD (Jasak et al., 2007). The software is distributed absolutely under the General Public License (GPL), which gives the liberty for the users to change and restructure the software and also assures the free use (Hammouda et al., 2012). OpenFOAM® is an object-oriented library, written in C++ programming language used primarily to develop applications (solvers and utilities). The solvers are coded to solve a precise problem in continuum mechanics, and the utilities are created for data manipulation. The framework holds numerous applications covering a wide range of problems (Moukalled et al., 2015).

The main mesh generation utilities available in OpenFOAM® framework are blockMesh and SnappyHexMesh (Moukalled et al., 2015). The blockMesh utility is used to create simple meshes with hexahedral cells (Moukalled et al., 2015), and is not apt for complex geometries. SnappyHexMesh utility have the capability to handle complex geometries, generating hexahedral and split-hexahedral cells in an automatic manner from triangulated surface of the geometries (Moukalled et al., 2015). Both

mesh generation utilities are considered in this work, keeping in mind their applicability.

1.4 Motivation

The design process of extrusion forming tools to produce quality profiles is influenced by various parameters such as the flow channel geometry, the rheological properties of the material used and the operating conditions (Carneiro et al., 2001). The usual procedure for obtaining those parameters are based on experimental trial–and–error approaches, highly dependent on the designer's experience, leading to high consumption of resources. The difficulty of this process is more evident when a complex new profile needs to be produced and there is no previous experience with similar geometries. In order to contribute solving this problem, many numerical modeling tools are currently available (Compuplast; Polydynamics; Die Flow; ANSYS Polyflow). These commercial softwares usually comprise high licensing costs and experienced users to perform the numerical simulations, and, in some cases, also require heavy computational resources to solve complex 3D problems. The in-house codes developed by the University of Minho research team (Nóbrega et al., 2003b; Nóbrega, 2004; Nóbrega et al., 2004a; Carneiro et al., 2004b; Nóbrega et al., 2004b; Nóbrega et al., 2004c; Nóbrega and Carneiro, 2006; Nóbrega et al., 2008; Goncalves, 2013), can be used to aid the design of profile extrusion forming tools, but have limitations concerning the complexity of the geometries that can be handled and are difficult to adapt and/or improve.

Extrusion industries are mainly concerned about the lead time of the product, delivering quality product to their customer within a short time. The profile production is mainly delayed by the forming tools design process, due to the usual experimental trial-and-error approach. The use of numerical tools for the design

process would definitely be a suitable alternative for the usual method, because it can minimize the lead time and the resources involved. However, the costs for acquiring the commercial modelling codes and the insufficient knowledge and practice in numerical modeling, are believed to be the motivation for most of the extrusion industries to rely on accumulated knowledge and on exclusive experimental procedures.

The currently available free open-source numerical modelling codes, would be an interesting option for the extrusion companies because they do not involve licensing costs, which may encourage the companies to acquire knowledge in numerical modelling. The investment in this expertise is expected to be low, especially in long term perspectives, and savings in physical resources and time should also be considered, when compared to the usual experimental trial-and-error method.

In order to evaluate in detail the advantages of using the new and innovative design methodologies developed in this project, the work was made in close cooperation with Soprefa Plastics. Soprefa Corporation is one of the biggest Portuguese companies of welts and shoe products, established 30 years ago. It is an industrial company, headquartered in Santa Maria da Feira - Portugal. Having initiated its activity in the components for footwear, it is figured as the world's larger welts manufacturer with plants in Portugal, India and Brazil (Soprefa). Soprefa Plastics, being the youngest sector of the group is, however, the area in which the company invested more time and resources in the past few years. Having started as a department for an economic welts alternative it has evolved into the production of other extruded products for industries such as the freezing and office furniture ones. Two major directives of the company are the "Just in Time" concept, a full dynamic management, perfectly adapted to their goals and, on the other hand, the notion of "Customer Satisfaction", which means the plain fulfilment of the customer's needs (Soprefa).

1.5 Objective

The main objective of this work is to establish improved design procedures for the forming tools employed in thermoplastic profile extrusion, namely the extrusion die and the calibration/cooling system, that should allow to minimize the resources and time spend on the design process, and to encourage the extrusion companies, such as Soprefa Plastics, to use numerical modeling for this purpose.

In order to accomplish the main objective, the following partial objectives must be achieved:

- To develop an improved solver in OpenFOAM® framework that can model the steady non-isothermal flow of incompressible generalized Newtonian fluids in the extrusion dies.

- To propose a new methodology for the design of complex profile extrusion dies in a framework of open-source softwares (numerical trial-and-error method), that can be easily ported to industry.

- To study numerically the effects of the main extrusion die design parameters, namely, i) the geometrical parameters of the flow channel, ii) the material rheology, and, iii) the processing conditions, on the flow balancing process, in order to better understand the behavior of the system and to provide simplified guidelines to aid the design of medium complexity profile extrusion dies. This should allow to undertake the design task without using numerical modelling codes, being, therefore, adequate for the designers with no access to numerical modeling tools.

- To assess the applicability of a previously developed numerical code, in OpenFOAM® framework, to model the heat transfer between the polymer and the calibrator, for industrial situations.

1.6 Thesis Structure

The first (this) chapter starts with a basic insight about the profile extrusion process, and the extrusion forming tools, followed by a detailed information about the available research studies devoted to the design of extrusion forming tools. Then, the motivation and objective of this thesis are presented.

The subsequent four chapters of this thesis correspond to manuscripts that are accepted, or submitted, for publication in peer-reviewed scientific journals related to this field.

Chapter 2 describes the open-source software implemented/specified to design complex geometry profile extrusion dies, which comprises a new numerical code developed to model the non-isothermal flow of generalized Newtonian fluids. The verification and experimental assessment of the code, taking into account two industrial case studies, are also provided.

Chapter 3 presents the development of a new methodology used to balance the flow distribution of complex profile extrusion dies (made of '*L*' and '*T*' shaped geometries). For this purpose a surrogate model is devised by performing a detailed numerical study with '*L*' and '*T*' shaped geometries, and two design methods (Average Method and Minimum Method) are also proposed. The developed die design methodology is assessed with some case studies.

Chapter 4, fulfills the limitation of the methodology presented in the previous chapter (Chapter 3). For this purpose, an improved surrogate model is developed in this

chapter which can be applied for a range of materials. A detailed numerical study is performed to determine the influence of the rheological properties of the materials and the processing conditions on the flow balancing of complex profile extrusion dies containing *L* and *T* shaped geometries. The influential parameter is added to the surrogate model, and some case studies are used to assess the improved die design methodology.

Chapter 5, presents a valid experimental assessment of a previously developed numerical code used to model the heat transfer that occur at the calibration stage and taking into account complex extrusion profiles. The chapter also provides some numerical studies based on a numerical trial-and-error approach to demonstrate the design improvement of the calibration system under study.

The thesis ends with the main conclusions and proposals for future work.

1.7 References

ANSYS Polyflow (2016).
URL: http://www.ansys.com/Products/Fluids/ANSYS-Polyflow.

Busby, J.W. (1996). PVC Profile Die Design by Simulation. PVC '96, *Conference proceeding*, Brighton.

Carneiro, O.S. and Nóbrega, J.M. (2012). *Design of Extrusion forming Tools*, Smithers Rapra Technology Ltd.

Carneiro, O.S., Nóbrega, J.M., Oliveira, P.J. and Pinho, F.T. (2004a). A study on the thermal performance of calibrators. *Antec-conference proceedings.*

Carneiro, O.S., Nóbrega, J.M., Oliveira, P.J. and Pinho, F.T. (2001). Computer aided rheological design of extrusion dies for profiles, *Journal of materials processing technology* **114**(1): 75-86.

Carneiro, O.S., Nóbrega, J.M., Oliveira, P.J. and Pinho, F.T. (2004b). Automatic balancing of profile extrusion dies: Experimental assessment. *Antec-conference proceedings.*

Chen, C., Jen, P. and Lai, F. (1997). Optimization of the coat hanger manifold via computer simulation and an orthogonal array method, *Polymer Engineering & Science* **37**(1): 188-196.

Compuplast (2016).
URL: http://www.compuplast.com/product.

CONAIR (2016).
URL: http://www.conairgroup.com/.

Corbett, H. (1954). Extrusion die design. *SPE Journal*: 15-18.

Die Flow (2016).
URL: http://www.dieflow.com/.

Elgeti, S., Probst, M., Windeck, C., Behr, M., Michaeli W.and Hopmann C. (2012). Numerical shape optimization as an approach to extrusion die design, *Finite Elements in Analysis and Design* **61**: 35-43.

Ettinger, H., Pittman J. and Sienz J. (2013). Optimization-driven design of dies for profile extrusion: Parameterization, strategy, and performance, *Polymer Engineering & Science* **53**(1): 189-203.

Ettinger, H., Sienz, J., Pittman J. and Polynkin A. (2004), Parameterization and optimization strategies for the automated design of uPVC profile extrusion dies, *Structural and Multidisciplinary Optimization* **28**(2-3): 180-194.

Fradette, L., Tanguy, P., Hurez P. and Blouin D. (1996). On the determination of heat transfer coefficient between PVC and steel in vacuum extrusion calibrators, *International Journal of Numerical Methods for Heat & Fluid Flow* **6**(1): 3-12.

Gentran (2016).
URL: http://www.gentran-corp.com/extrusion.html.

Giles, H., Mount, E. M. and Wagner J. R. (2004). *Extrusion: the definitive processing guide and handbook*, William Andrew.

Goncalves, N.D. (2013). *Computer aided design of extrusion forming tools for complex geometry profiles*, Ph.D Thesis, University of Minho.

Habla, F., Fernandes, C., Maier, M., Densky, L., Ferrás, L., Rajkumar, A., Carneiro, O., Hinrichsen, O. and Nóbrega, J. (2016). Development and validation of a model for the temperature distribution in the extrusion calibration stage, *Applied Thermal Engineering* **100**: 538-552.

Hammouda, I., Lundell, B., Mikkonen, T. and Scacchi, W. (2012), Open Source Systems: Long-Term Sustainability: *8th IFIP WG 2.13 International Conference*, Hammamet, Tunisia.

Huneault, M., P. Lafleur and P. Carreau (1996). "Evaluation of the FAN technique for profile die design." *International Polymer Processing* **11**(1): 50-57.

Hurez, P., Tanguy, P. and Blouin, D. (1993). Numerical simulation of profile extrusion dies without flow separation, *Polymer Engineering & Science* **33**(15): 971-979.

Hurez, P., Tanguy, P. and Blouin, D. (1996). A new design procedure for profile extrusion dies, *Polymer Engineering & Science* **36**(5): 626-635.

Hurez, P., Tanguy, P. and Blouin, D. (1991). Finite element based design of profile extrusion dies, *Annual Technical Conference Proceedings*, Soc of Plastics Engineers.

Jasak, H., Jemcov, A. and Tukovic, Z. (2007). OpenFOAM: A C++ library for complex physics simulations, *International workshop on coupled methods in numerical dynamics*, IUC Dubrovnik, Croatia.

Karadogan, C. (2005). *Advanced methods in numerical modeling of extrusion processes*, Zürich.

Kent, R. J. (1998). *Plastics Profile Extrusion*, Smithers Rapra Publishing.

Kostic, M. and Reifschneider, L. (2006). Design of extrusion dies, *Encyclopedia of Chemical Processing DOI* **10**.

Kuhnle, H. (1986). Rheological Design of Profile Extrusion Dies, *Kunststoffe-German Plastics* **76**(3): 276-281.

Kurz, H. (1988). Fixing the dimensions of extruded high-mw polyolefin pipes during cooling, *Kunststoffe-German Plastics* **78**(11): 1052-1058.

Lebaal, N., Schmidt, F. and Puissant, S. (2009). Design and optimization of three-dimensional extrusion dies, using constraint optimization algorithm, *Finite Elements in Analysis and Design* **45**(5): 333-340.

Lee, C.C. and Stevenson, J. F. (1992). The face-relief strategy for design of profile dies, *International Polymer Processing* **7**(2): 186-189.

Legat, V. and Marchal, J. M. (1993). Die design: an implicit formulation for the inverse problem, *International journal for numerical methods in fluids* **16**(1): 29-42.

Lehnhäuser, T. and M. Schäfer (2005). A numerical approach for shape optimization of fluid flow domains, *Computer methods in applied mechanics and engineering* **194**(50): 5221-5241.

Levy, S. (1981). The technology of plastics profile tooling, *Advances in Polymer Technology* **1**(1): 8-53.

McKelvey, J. M. and Ito, K. (1971). Uniformity of flow from sheeting dies, *Polymer Engineering & Science* **11**(3): 258-263.

Mehta, B. V., Ghulman, H. and Gerth, R. (1999). Extrusion die design: a new methodology of using design of experiments as a precursor to neural networks, *Journal of Materials* **51**(9).

Menges, G., Haberstroh, E. and Janke, W. (1982). Systematic lay-out of cooling lines for film, sheet and pipe extrusion plant, *Kunststoffe-german plastics* **72**(6): 332-336.

Menges, G., Kalwa, M. and Schmidt, J. (1987). Finite element simulation of heat transfer in plastics processing, *Kunststoffe-german plastics* **77**(8): 797-802.

Michaeli, W. (1984). *Extrusion Dies Design and Engineering Computations*, Hanser Publishers, Munich.

Michaeli, W. (1992). *Extrusion Dies for Plastics and Rubber: Design and Engineering Computations*, Hanser Publishers, Munich.

Michaeli, W. and Kaul, S. (2004). Approach of an automatic extrusion die optimization, *Journal of polymer engineering* **24**(1-3): 123-136.

Michaeli, W., Kaul, S. and Wolff, T. (2001). Computer-aided optimization of extrusion dies, *Journal of polymer engineering* **21**(2-3): 225-238.

Moukalled, F., Mangani, L. and Darwish, M. (2015). *The Finite Volume Method in Computational Fluid Dynamics: An Advanced Introduction with OpenFOAM® and Matlab*, Springer.

Mu, Y., Zhao, G., Wu, X.and Zhang, C. (2010). An optimization strategy for die design in the low-density polyethylene annular extrusion process based on FES/BPNN/NSGA-II, *The International Journal of Advanced Manufacturing Technology* **50**(5-8): 517-532.

Murray, T. A. (1978). Here's Your Guide to Die Design, *Plastics Technology: 99 - 105*.

Na, S. Y. and Lee, T.Y. (1997). Shape optimization of polymer extrusion die by three-dimensional flow simulation, *High Performance Computing on the Information Superhighway*, IEEE.

Narayanasamy, R., Srinivasan, P. and Venkatesan, R. (2003). Computer aided design and manufacture of streamlined extrusion dies, *Journal of materials processing technology* **138**(1): 262-264.

Nóbrega, J.M. and Carneiro, O.S. (2006). Optimising cooling performance of calibrators for extruded profiles, *Plastics, rubber and composites* **35**(9): 387-392.

Nóbrega, J.M., Carneiro O.S., Covas, J., Pinho F.T. and Oliveira P.J. (2004b). Design of calibrators for extruded profiles. Part I: Modeling the thermal interchanges, *Polymer Engineering & Science* **44**(12): 2216-2228.

Nóbrega, J.M., Carneiro O.S., Gaspar A. C. and Gonçalves N.D. (2008). Design of calibrators for profile extrusion–optimizing multi-step systems, *International Polymer Processing* **23**(3): 331-338.

Nóbrega, J.M., Carneiro, O.S., Oliveira, P.J. and Pinho, F.T. (2003a). Flow Balancing in Extrusion Dies for Thermoplastic Profiles Part I : Automatic Design, *International Polymer Processing* **XVIII**.

Nóbrega, J.M., Carneiro, O.S., Oliveira, P.J. and Pinho, F.T. (2003b). Flow Balancing in Extrusion Dies for Thermoplastic Profiles: Part II: Influence of the Design Strategy, *International Polymer Processing* **18**(3): 307-312.

Nóbrega, J.M., Carneiro, O.S., Oliveira, P.J. and Pinho, F.T. (2004a). Flow Balancing in Extrusion Dies for Thermoplastic Profiles: Part III: Experimental Assessment, *International Polymer Processing* **19**(3): 225-235.

Nóbrega, J.M., Carneiro, O.S., Oliveira, P.J. and Pinho, F.T. (2004c). Accounting for temperature-dependent properties in viscoelastic duct flows, *International journal of heat and mass transfer* **47**(6): 1141-1158.

Nóbrega, J. M. (2004). *Computer aided design of forming tools for the production of Extruded profiles*, Ph.D Thesis, University of Minho.

Pauli, L., Behr, M. and Elgeti, S. (2013). Towards shape optimization of profile extrusion dies with respect to homogeneous die swell, *Journal of Non-Newtonian Fluid Mechanics* **200**: 79-87.

Pittman, J. and Farah, I. (1996). Comprehensive simulation of cooling process in plastic pipe manufacture, *Plastics rubber and composites processing and applications* **25**(6): 305-312.

Polydynamics (2016).
URL: http://www.polydynamics.com/index.html.

Procter, B. (1972). Flow analysis in extrusion dies, *SPE Journal* **28**(2): 34-&.

Rauwendaal, C. (1991). How proper die design can improve profile quality, *Plastics world* **49**(12): 73-75.

Rauwendaal, C. (2014). *Polymer extrusion*, Carl Hanser Verlag GmbH Co KG.

Reid, J., Campanella, O., Corvalan, C. and Okos, M. (2003). The influence of power-law rheology on flow distribution in coathanger manifolds, *Polymer Engineering & Science* **43**(3): 693-703.

Ren, L., Yang, R. and Zhang, W. (2010). Optimization design in cooling system of heterogeneous calibrator for plastic profile extrusion, *Artificial Intelligence and Computational Intelligence (AICI)*, IEEE.

Reynolds, O. (1886). On the Theory of Lubrication and Its Application to Mr. Beauchamp Tower's Experiments, Including an Experimental Determination of the Viscosity of Olive Oil, *Proceedings of the Royal Society of London* **40**(242-245): 191-203.

Rezaei , S., Behravesh, A., Bakhshi M. and Soury, E. (2010). Design, optimization, and manufacturing of a multiple-thickness profile extrusion die with a cross flow, *Polymer Engineering & Science* **50**(12): 2417-2424.

SAInternational (2016).
URL:http://www.kdseair.com/html/Products_Services/Plastics_Machinery/Profile_Extrusion_Line/2015/0518/85.html.

Sebastian, D. H. and Rakos, R. (1985). Interactive software package for the design and analysis of extrusion profile dies, *Advances in Polymer Technology* **5**(4): 333-339.

Sheehy, P., Tanguy, P. and Blouin, D. (1994). A finite element model for complex profile calibration, *Polymer Engineering & Science* **34**(8): 650-656.

Sienz, J., Bates, S. J. and Pittman, J. F. (2006). Flow restrictor design for extrusion slit dies for a range of materials: Simulation and comparison of optimization techniques, *Finite elements in analysis and design* **42**(5): 430-453.

Sienz, J., Goublomme, A. and Luege, M. (2010). Sensitivity analysis for the design of profile extrusion dies, *Computers & structures* **88**(9): 610-624.

Soprefa (2016).
URL: http://www.soprefa.com/.

Soury, E., Behravesh, A. H., Nasrabadi, H. and Zolfaghari, A. (2009). Design and manufacture of an extrusion die for wood—plastic composite, *Journal of Reinforced Plastics and Composites* **28**(12): 1433-1439.

Summers, J. and Brown, R. (1981). Practical principles of die design—a simplified procedure, in table form, for rigid PVC, *Journal of Vinyl Technology* **3**(4): 215-218.

Sun, D.W. and Peng, Y.C. (1991). A practical method to design hollow profile dies, *Plastics rubber and composites processing and applications* **16**(2): 109-114.

Svabik, J., Mikulenka, T., Manas, M. and Busby, J. (1997). Evaluation of profile die design strategies. *Conference of polymer processing*, Europe/Africa Region Meeting.

Szarvasy, I. (2000). Simulation of Complex PVC Window Profile Cooling During Calibration with Particular Focus on Internal Heat Exchange. *3rd ESAFORM Conference on Material Forming*.

Tadmor, Z. and Gogos, C. G. (2006). *Principles of polymer processing*, John Wiley & Sons.

Ulysse, P. (1999). Optimal extrusion die design to achieve flow balance, *International journal of machine tools and manufacture* **39**(7): 1047-1064.

Ulysse, P. (2002). Extrusion die design for flow balance using FE and optimization methods, *International Journal of Mechanical Sciences* **44**(2): 319-341.

Vincent, M., Vergnes, B., Demay, Y., Coupez, T., Billon, N. and Agassant, J. (2002). Present Challenges in the Numerical Modeling of Polymer-forming Processes, *The Canadian Journal of Chemical Engineering* **80**(6): 1143-1152.

Wortberg, J., Haberstroh, E., Lutterbeck, J., Masberg, U., Schmidt, J. and Targiel, G. (1982). Designing of extrusion lines, *Advances in Polymer Technology* **2**(2): 75-106.

Wu, C.Y. and Hsu, Y.C (2002). Optimal shape design of an extrusion die using polynomial networks and genetic algorithms, *The International Journal of Advanced Manufacturing Technology* **19**(2): 79-87.

Wu, T., Jiang, B., Xu, S. and Bi, C. (2006). Nonisothermal comprehensive 3D analysis of polymer melt flow in a coat-hanger die, *Polymer Engineering & Science* **46**(4): 406-415.

Yilmaz, O., Gunes, H. and Kirkkopru, K. (2014). Optimization of a profile extrusion die for flow balance, *Fibers and Polymers* **15**(4): 753-761.

Yu, Y.W. and Liu, T.J. (1998). A simple numerical approach for the optimal design of an extrusion die, *Journal of Polymer Research* **5**(1): 1-7.

Chapter 2

An Open-source framework for the Computer Aided Design of Complex Profile Extrusion Dies

Abstract

In this work we present a detailed description of how to use open source based computer codes to aid the design of complex profile extrusion dies, aiming to improve its flow distribution. The work is presented in a simple way, so that both academics and industrials feel motivated to consider numerical methodologies in their future developments. The text starts by describing the overall computer aided design methodology, comprising: (i) material rheological characterization (ii) geometry and mesh generation, (iii) the computational framework and (iv) assessment case studies. In order to consider more realistic thermoplastic polymer flow conditions, where heat exchange has an important role, a new solver was implemented in OpenFOAM®, capable of simulating the steady non-isothermal flow of an incompressible generalized Newtonian fluid. The proper implementation of the solver was verified using the Method of Manufactured Solutions (MMS). The technique used to design the profile extrusion die, i.e., to balance the flow distribution, is based on a numerical trial-and-error procedure. The capability of the proposed design methodology was assessed with two industrial case studies. The results obtained clearly demonstrate that the computational design aid is an excellent alternative to the exclusively experimental trial-and-error procedure commonly used in industry.

This chapter was adapted from: Rajkumar, A., Ferrás, L.L., Fernandes, C., Sacramento, A., Carneiro,O.S., Nóbrega J.M.(2016). "An Open-source framework for the Computer Aided Design of Complex Profile Extrusion Dies", submitted to Polymer Engineering and Science.

2.1 Introduction

Extruded thermoplastic profiles are applied in many fields, such as automotive, household, civil construction, electrical, health, among many others. Designing an extrusion die capable to generate an uniform velocity distribution of the polymer melt at its outlet is difficult due to the complex geometry of the profile cross section and the existence of walls with different thicknesses (Michaeli, 2003; Carneiro and Nóbrega, 2012). Moreover, the growth in competition, combined with an increasingly demanding market (requiring higher production rates and improved product quality (Hristov and Vlachopoulos, 2007; Gonçalves et al., 2013)), imposes short time to market and improvements in the production technique.

The usual approach for designing extrusion dies, employed by most of the profile extrusion die manufacturers, is the experimental trial-and-error procedure (Carneiro and Nóbrega, 2012) performed by die designers with a deep knowledge on the design process, who rely on several years of accumulated experience. Usually, the design procedure involves a number of iterations before achieving the desired solution, i.e., the one that leads to the required profile geometry. Also, the number of iterations increases significantly with the profile/die geometry complexity (Michaeli, 2003). As a consequence, the design process consumes a lot of time and a huge amount of raw-material, considerably increasing the cost of the design process (Michaeli, 2003; Tadmor and Gogos, 2006) and the time to market of a new product.

It is well known that the aid of computational codes helps improving the manufacture efficiency (Karadogan, 2005; Kostic and Reifschneider, 2006). When die design is considered, this aid gives rise to more efficient processes, by transforming the experimental trial-and-error design procedure into a numerical based operation.

Some of the currently available commercial softwares developed to aid the design of extrusion dies are DIEFLOW, ANSYSPOLYFLOW, FLOW2000 and PROFILECAD

and some of them have the ability to predict the flow channel cross section needed to produce the desired profile (i.e., they solve the inverse problem) (Legat and Marchal, 1993; Marchal and Goublomme, 2000). As an example of the use of PolyFlow (Ettinger et al., 2004), where they studied the main parameters and optimization strategies needed to automatize the design of profile extrusion dies, and later the development of an optimization approach dealing with complex shaped dies required for the production of uPVC profiles (Ettinger et al., 2013).

These particular studies, and also most of the commercial codes, use 2.5D approaches. In fact, the codes that allow to solve 3D problems are usually avoided because of the huge computational time and resources they require (J.F.Agassant, 2000). Moreover, commercial software licenses are expensive. A possible solution is the use of in-house developed codes. As an example, we can refer the 3D computational code, based on the Finite Volume Method, presented by Nóbrega et al. (Nóbrega et al., 2003a; Nóbrega et al., 2003b; Nóbrega et al., 2004), capable to numerically model the fluid flow through profile extrusion dies, where the optimization design strategies used encompass modifications performed in the pre-parallel and parallel zones of the flow channel. However, this code employed had limitations concerned to the extrusion die geometry, being only able to deal with structured meshes. In order to overcome this limitation, a numerical code able to cope with unstructured meshes was also put forward by the same group (Gonçalves et al., 2013), considering generalized Newtonian fluids under isothermal conditions. The major drawbacks of in-house codes are that they rely on the expertise of their developers and they are not user friendly.

Considering the cost of the commercial numerical modelling software and the lack of know-how and experience in numerical modeling, most of the extrusion companies still adopt the experimental trial-and-error method.

Nowadays there are many free open-source numerical modelling codes. The use of this type of codes, is free of charge and, thus, may motivate extrusion companies to invest in acquiring the knowledge to use them, aiming to improve their design processes.

However, in what concerns to extrusion die design applications, there is still some work to be done, namely the identification of adequate software to use on the several steps of the design process and the development (or identification) of numerical solvers that can adequately model the forming process.

Having in mind the current industrial reality, the main objective of this work is to propose a new methodology to design complex profile extrusion dies in a framework of open-source software, in which the numerical modelling code is developed using the OpenFOAM® computational library.This is a free open-source and expandable set of numerical tools, which includes routines for creating the geometry and generating the computational mesh, and also allows parallel computing. For this purpose, a new solver was developed in the OpenFOAM®, to model the steady non-isothermal flow of incompressible generalized Newtonian fluids. Prior to its use, the developed solver was verified using the Method of Manufactured Solutions (MMS)(Roache, 2002). The capability of the proposed design methodology was assessed through two experimental industrial case studies.

The remainder of this chapter is organized as follows. In Section 2.2 the developed design methodology is presented and discussed, explaining in detail the main stages involved. In Section 2.3 we present and verify the new solver developed in the OpenFOAM® framework. In Section 2.4 two assessment industrial case studies are presented: the first exemplifying the design of a new extrusion die, and the second illustrating its usefulness to improve the performance of an existing die. The chapter ends with the main conclusions.

2.2 Die-Design Method

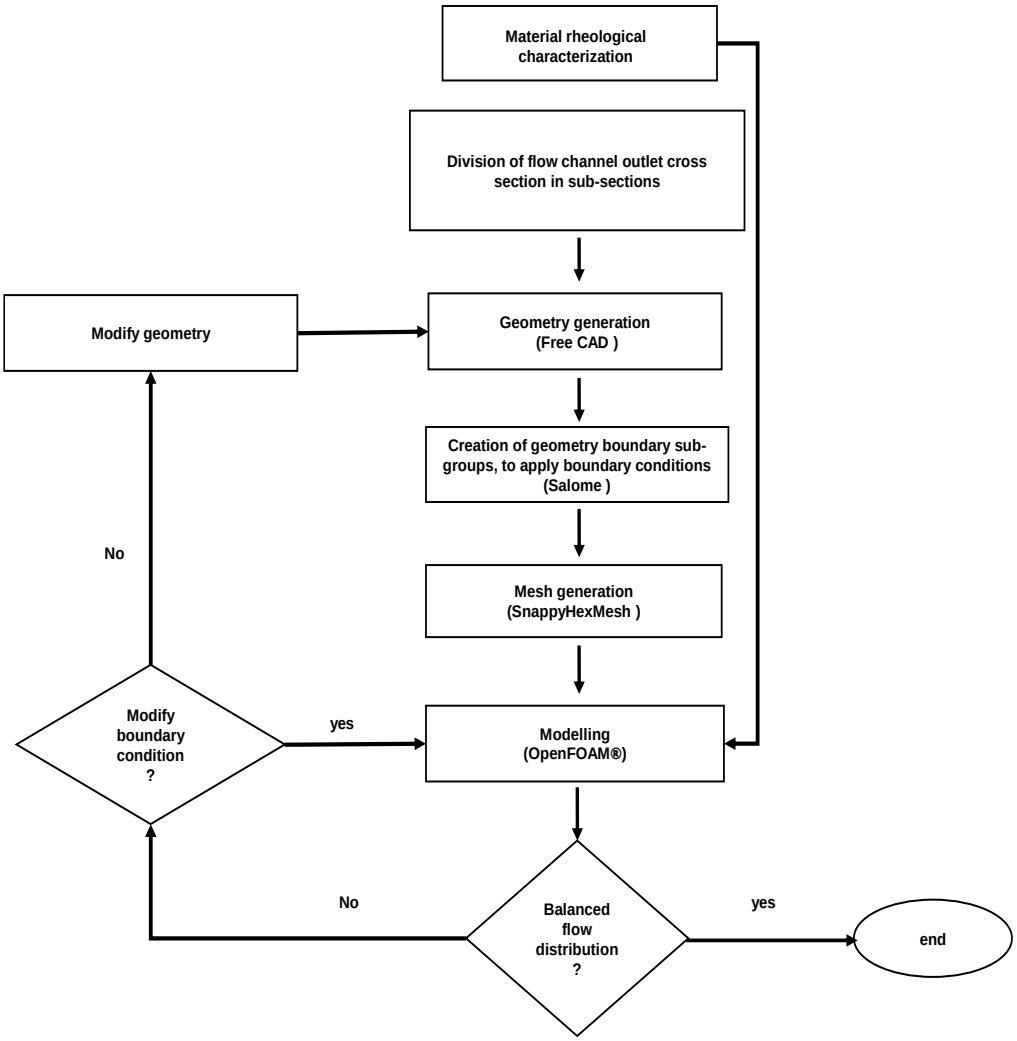

Figure 2.1:Proposed die-design methodology

The design procedure encompasses a series of stages involving the use of different software packages, as illustrated in Figure 2.1

The procedure starts with the material rheological characterization, to determine the relevant rheological parameters for modelling purposes. Then, and before generating the flow channel geometry of the die, the die exit (outlet), which is similar to that of the profile, is divided into Elemental Sections (ESs) and Intersection Sections (ISs).

These subsections will be used to monitor the flow distribution (or flow rate) at the flow channel outlet. An example of this step is provided in Figure 2.2.

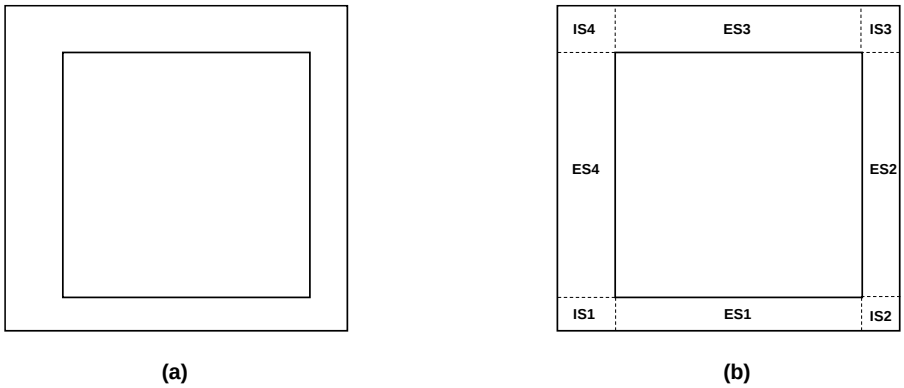

Figure 2.2: A square shaped profile: (a) die exit; (b) division of die exit into ESs and ISs.

The generation of the flow channel geometry is done using a CAD software, as FreeCAD. The generated geometry is imported to Salome and the geometry boundary is divided in different groups to allow applying different boundary conditions. The defined regions are exported as STL ASCII files from Salome and used as input to the mesh generation code.

The computational mesh is generated using SnappyHexMesh, a mesh generation utility included in OpenFOAM® framework, which creates unstructured meshes in a semi-automatic manner, based on STL files. Finally, the numerical simulation is performed in the OpenFOAM® framework using the developed solver, followed by the post-processing, in which the predicted results are used to access the flow distribution quality. A standard post processing utility from OpenFOAM®, patchIntegrate, was used to compute the flow rate in each subsection of the flow channel outlet (see Figure 2.2). The numerically obtained flow rate is then used to calculate the flow distribution objective function ($F_{obj,i}$) at each ESs and ISs, using the following equation,

$$F_{obj,i} = \frac{\frac{U_i}{U_{av}} - 1}{\max\left(\frac{U_i}{U_{av}}, 1\right)} \quad (2.1)$$

where, U_i and U_{av} are the ESi (or ISi) and the global average velocities, respectively. These velocities are obtained by dividing the computed flow rate by the respective subsection area. The objective function ($F_{obj,i}$) was defined in a way to provide similar importance to the ratio $\frac{U_i}{U_{av}}$ when, for example, it is half or the double of the value required for flow balancing. Under these conditions, the absolute $F_{obj,i}$ value for the $\frac{U_i}{U_{av}}$ = 0.5 case will be the same of that corresponding to a ratio value of 2. In the case of perfect flow balancing, i.e., when the average velocity is the same at all the subsections and, thus, equal to the global average velocity, the $F_{obj,i}$ value will be zero. The performance of each iteration is quantified using the sum of the absolute values of all the local objective function ($F_{obj,i}$), as indicated in Eq. 2.2.

$$F_{obj} = \sum_{i=ES+IS} \left\| F_{obj,i} \right\| \quad (2.2)$$

Note that the lower the value of F_{obj} the higher the die performance is.

The assessment of the flow distribution quality is done, at this stage, based on the results of the global and local objective function (F_{obj}, $F_{obj,i}$). If the balanced flow condition is not reached, a decision must be taken: either to modify the boundary conditions (and model the flow with the same flow channel geometry), or to modify the die geometry, using again the geometry generation software (see Figure 2.1). The iterative process is repeated by adjusting the geometry and/or boundary conditions until a balanced flow distribution is achieved.

2.3 The Numerical Modelling Code implementation and verification

As referred in Section 2.1, , the numerical code to be developed should be able to model the flow with an incompressible inelastic fluid under non-isothermal conditions. This required the implementation of a new solver in OpenFOAM® computational library able to solve the relevant governing equations presented in subsection 2.3.1. This new solver if briefly described in Subsection 2.3.2, being its verification presented in Subsection 2.3.3.

2.3.1 Governing equations

The equations used to model the flow are, the mass conservation,

$$\nabla \cdot \mathbf{u} = 0 , \tag{2.3}$$

and the linear momentum conservation,

$$\nabla \cdot \left(\rho \mathbf{u}\mathbf{u} \right) = -\nabla p + \nabla \cdot \boldsymbol{\tau} . \tag{2.4}$$

The energy conservation equation must be also considered to predict the temperature distribution,

$$\nabla \cdot \left(\rho c_p \mathbf{u} T \right) - \nabla \cdot (k \nabla T) = \boldsymbol{\tau} : \nabla \mathbf{u} . \tag{2.5}$$

In the above equations, ρ is the density, $\mathbf{u}$ the velocity vector, p the pressure, $\boldsymbol{\tau}$ the deviatoric stress tensor, T the temperature, c_p the specific heat, and k the thermal conductivity. The last term on the RHS of Eq. 2.5, $\boldsymbol{\tau} : \nabla \mathbf{u}$, accounts for the viscous dissipation contribution.

For generalized Newtonian fluids the deviatoric stress tensor is,

$$\boldsymbol{\tau} = 2\eta(\dot{\gamma},T)\,\mathbf{D} \tag{2.6}$$

where, $\mathbf{D}$ is the rate of strain tensor, given by,

$$\mathbf{D} = \frac{1}{2}\left(\left[\nabla\mathbf{u}\right]+\left[\nabla\mathbf{u}\right]^{\mathrm{T}}\right), \tag{2.7}$$

where $\nabla\mathbf{u}$ is the velocity gradient tensor, and $\eta(\dot{\gamma},T)$ is the shear viscosity that depends both on temperature (T) and shear rate ($\dot{\gamma}$), being a function of the second invariant of the rate of deformation tensor,

$$\dot{\gamma} = \sqrt{2\mathrm{tr}\mathbf{D}^2}\,. \tag{2.8}$$

To consider the effect of both temperature and shear rate on the shear viscosity, the Bird-Carreau model was coupled to an Arrhenius law, leading to:

$$\eta\left(\dot{\gamma},T\right) = a_T\eta_\infty + \frac{a_T\left(\eta_0-\eta_\infty\right)}{\left(1+\left(a_T\lambda\dot{\gamma}\right)^2\right)^{\frac{1-n}{2}}} \tag{2.9}$$

where η_0 and η_∞ are the zero and infinite shear rate viscosities, respectively, λ is the relaxation time and n is the power-law exponent. In Eq. 2.9 the temperature shift factor, a_T, is given by,

$$a_T = \exp\left(\frac{E}{R}\left(\frac{1}{T}-\frac{1}{T_0}\right)\right), \tag{2.10}$$

with R the universal gas constant, E the activation energy and T and T_0 the temperature and its reference value (both in Kelvin), respectively.

2.3.2 Solver Implementation

Since the available SimpleFOAM solver, is only capable to solve the system of Navier-Stokes equations for steady state incompressible flows of generalized Newtonian fluids, but under isothermal conditions, it was modified by implementing the energy conservation equation (Eq. 2.5) and a more realistic rheological equation for the shear viscosity (Eq. 2.9). The main part of the code developed to add the energy conservation equation (Eq. 2.5) into the OpenFOAM® framework is given in Figure 2.3, in which is clear the mimic language used to expand the calculation features of the OpenFOAM® computational library.

```
tau = nu * (grad U + grad U.T());
Solve
 (
      fvm : : div (phi , T)
    - fvm : : laplacian (DT , T)
  == (1 / cp) * (tau  &&  grad U)
)
```

Figure 2.3: Energy equation programmed in OpenFOAM.

The energy conservation equation (Eq. 2.5) can be rewritten dividing all the terms by ρc_p (both constants), giving:

$$\nabla \cdot (\mathbf{u}T) - \nabla \cdot \left(\frac{k}{\rho c_p} \nabla T \right) = \frac{1}{\rho c_p} \boldsymbol{\tau} : \nabla \mathbf{u} \cdot \qquad (2.11)$$

To discretize Eq. 2.11, we first integrate in space all the terms, and then use the Gauss theorem to convert the volume integrals into surface integrals. The variables are then evaluated at the cell faces.

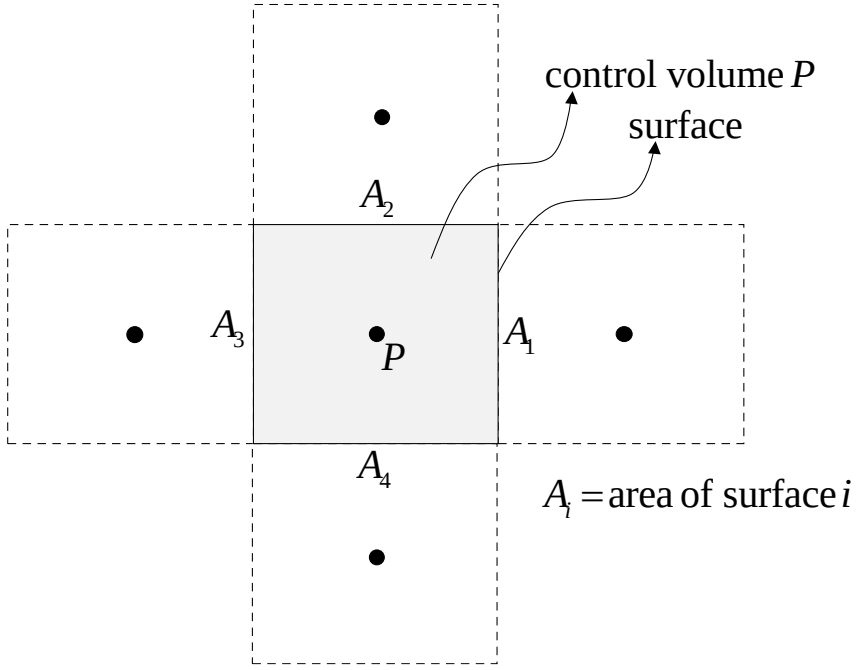

Figure 2.4: Schematic of a control volume.

$$\begin{aligned} &\int_V \nabla\cdot(\mathbf{u}T)\,dV - \int_V \nabla\cdot\left(\frac{k}{\rho c_p}\nabla T\right)dV = \int_V \nabla\cdot\left(\frac{1}{\rho c_p}\boldsymbol{\tau}:\nabla\mathbf{u}\right)dV \\ \underset{Gauss\,theor.}{\Leftrightarrow} &\int_s (\mathbf{u}T)\cdot\mathbf{n}ds - \int_s \left(\frac{k}{\rho c_p}\nabla T\right)\cdot\mathbf{n}ds = \frac{1}{c_p}\int_V \tilde{\boldsymbol{\tau}}:\nabla\mathbf{u}dV \end{aligned} \tag{2.12}$$

where $\tilde{\boldsymbol{\tau}} = \boldsymbol{\tau}/\rho$.

If we consider a control volume cell, as the one given in Figure 2.4, we have a well-defined boundary surface, formed by 4 rectilinear surfaces. Therefore, the previous expression can be approximated by:

$$\sum_{i=1}^{4}(\mathbf{u}T)_i A_i - \frac{k}{\rho c_p}\sum_{i=1}^{4}(\nabla T)_i A_i = \frac{1}{c_p}(\tilde{\boldsymbol{\tau}}:\nabla\mathbf{u})_p V_p \tag{2.13}$$

The following correspondence between the different terms of the energy equation and the code language was used:

$$\tilde{\boldsymbol{\tau}} = \frac{\eta(\dot{\gamma},T)}{\rho}\left([\nabla \mathbf{u}] + [\nabla \mathbf{u}]^{\mathrm{T}}\right) \rightarrow tau = nu * (grad\,U + grad\,U.T()), \tag{2.14}$$

with $nu = \frac{\eta}{\rho}$ being the kinematic viscosity.

$$\nabla \cdot (\mathbf{u}T) \rightarrow div(phi, T), \tag{2.15}$$

where $phi \equiv \mathbf{u}A$ is the flux (obtained after discretization), as shown in Eq. (2.13).

$$\nabla \cdot \left(\frac{k}{\rho c_p}\nabla T\right) = \Delta\left(\frac{k}{\rho c_p}T\right) \rightarrow laplacian(DT, T), \tag{2.16}$$

with $\frac{k}{\rho c_p} \equiv DT$ being the thermal diffusivity.

Finally, we have,

$$\frac{1}{c_p}\tilde{\boldsymbol{\tau}} : \nabla \mathbf{u} \rightarrow \left(\frac{1}{c_p}\right) * (tau \,\&\&\, grad\,U). \tag{2.17}$$

In this language, the tensor double dot operation is represented by "&&", the variable "nu" is a vector that stores all the discretized values of viscosity, "phi" is also a vector that stores all the cell face fluxes, and DT is a constant.

The FVM class (Moukalled et al., 2015) is used to discretize each term, meaning that the terms with "fvm::" are evaluated implicitly, while the remaining term, the one that accounts for viscous dissipation (see Equation 2.11), is evaluated explicitly, using the previous iteration values.

Second order approximations are used to approximate the derivatives at the volume face, and also to interpolate variables to the cell faces. This discretization approach is expected to give rise to an overall convergence order of 2.

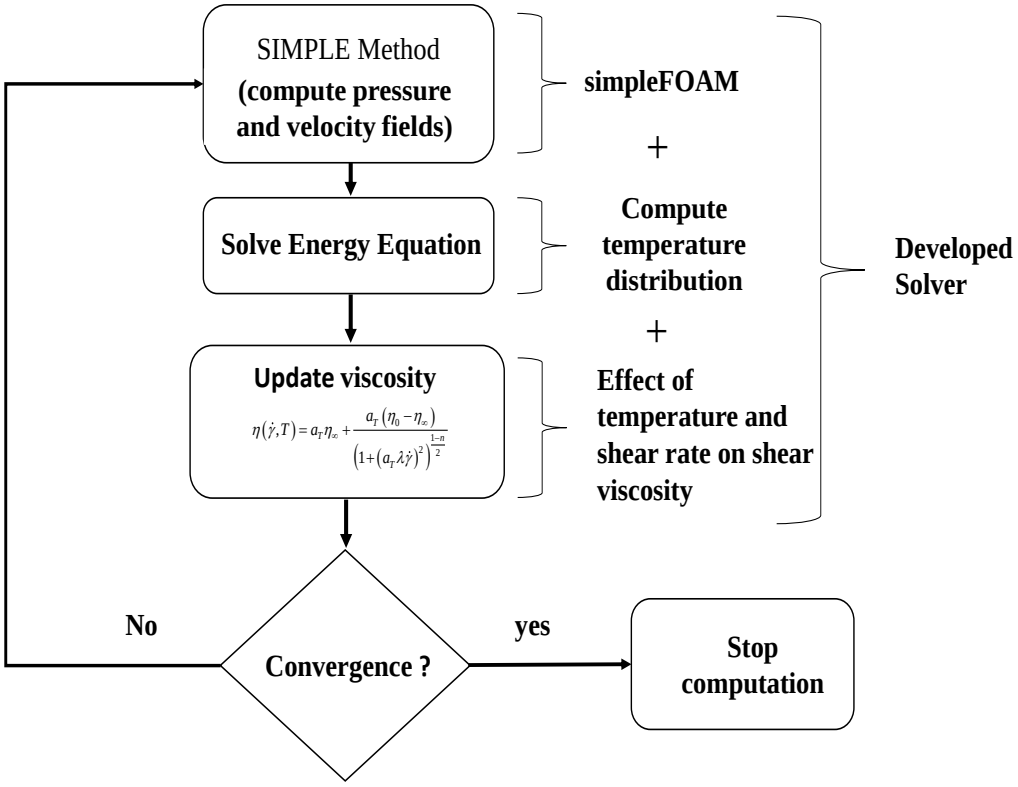

Figure 2.5: Iterative procedure for the solution of the governing equations used in the developed solver.

The pressure and the velocity fields were coupled using the SIMPLE method (Patankar and Spalding, 1972). As illustrated in the flowchart given in Figure 2.5, at each iteration the energy equation is solved after updating the velocity and pressure fields. Then, the shear viscosity is computed as a function of the newly predicted temperature and velocity fields. The flow sequence of the computation process stops after reaching convergence.

The convergence of the simulation is controlled by monitoring the residuals obtained from the system of equations that are solved for velocity, pressure and temperature. In our case, the convergence is reached when the residuals falls below a certain defined value that assures a sufficiently accurate numerical solution. Since we use an iterative procedure, we start by providing an initial guess.

2.3.3 Solver verification

The best way to verify numerical modelling codes is to apply them to solve problems for which analytical solutions exist. However, analytical solutions can only be obtained for very simple geometries and material models. The Method of the Manufactured Solutions (MMS) (Roache, 2002) is a straightforward way to obtain analytical solutions for problems similar to those being solved and, thus, a simple way to verify the new solver.

The MMS starts by the establishment of a guessed solution for the problem. In general, that solution will not verify the original differential governing equation and, thus, when inserted in the governing equation, a residual source term will remain. If the symmetric of that source term is inserted into the original governing equation, the solution of this new equation will be the guess solution used at the beginning of the process.

Since the energy conservation equation (Eq.2.4) was the new contribution to the calculation procedure, the MMS was only used to verify the numerical implementation of this governing equation.

In the following verification, the flow between two parallel plates, a 2D case illustrated in Figure 2.6, is modeled for a Newtonian fluid.

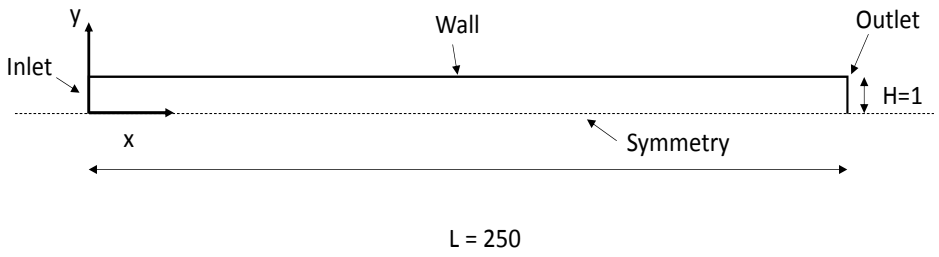

Figure 2.6: Geometry used for the solver verification case studies (for symmetry reasons, only half of the geometry is illustrated; all the dimensions are in mm).

The numerical simulation was performed by imposing a fully developed velocity profile at the inlet, given by Eq. 2.18,

$$u = \frac{3}{2} U \left[1 - \left[\frac{2\,y}{H}\right]^2\right] \quad , \tag{2.18}$$

Where, U is the mean velocity with a value of 0.2 m/s and H is the flow channel width.

For the velocity field, a zero gradient boundary condition was imposed at the outlet and a no slip boundary condition is used at the walls. Concerning the boundary condition for pressure, we assumed zero pressure at the outlet and a zero gradient variation at the inlet and walls. For the temperature, a constant value was considered at the walls and inlet, equal to 230 ºC, and a zero gradient boundary condition was considered at the outlet.

Two different manufactured solutions were used for the temperature distribution: a constant temperature, 230˚ C, and a complex temperature profile function (Eq. 2.19),

similar to the temperature development along a channel with isothermal walls (Carley, 1989) in which viscous dissipation plays an important role.

$$T\,(x,y) = T_w + T_{add}\left[-\left[\left[1-\frac{x}{L}\right]\left[\frac{2y}{H}\right]^2 + \frac{x}{L}\right]\left[\left[\frac{2y}{H}\right]^2 - 1\right]\frac{x}{L}\right] \qquad (2.19)$$

Where T_w is the wall temperature (230 ºC), and T_{add} (10 ºC) the symmetry plane increase in temperature at the channel outlet. The evolution of the temperature profile given for this last trial solution is shown in Figure 2.7.

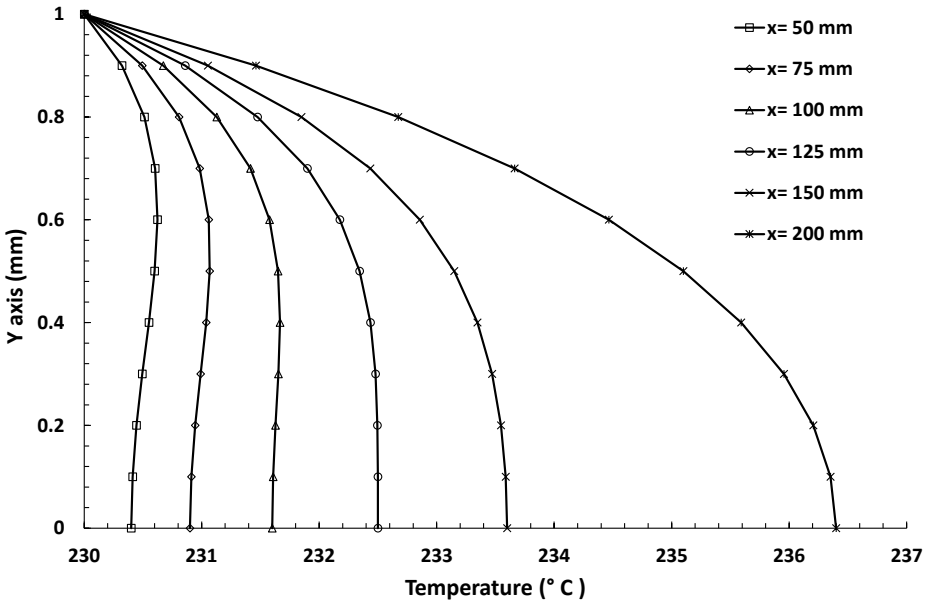

Figure 2.7: Development of the temperature profile along the flow channel length, given by the complex function used as manufactured solution (for symmetry reason, only half of the profiles are shown).

Eqs. 2.20 to 2.22 show the source terms obtained from the different terms composing the energy equation, for the manufactured solution of constant temperature.

$$\nabla.(u\,T) \;=\; 0 \tag{2.20}$$

$$DT\,\nabla.(\nabla\,T) \;=\; 0 \tag{2.21}$$

$$\frac{1}{c_p}[\tau:\nabla u] \;=\; \frac{\eta}{\rho\,c_p}\left[\frac{12\,U\,y}{H^2}\right]^2 \tag{2.22}$$

In this case the single extra source term to add to the manufactured solution results from the viscous dissipation term (Eq. 2.22), as the advective and diffusive terms do not provide any source.

Eqs. 2.23 to 2.24 show the source terms obtained for the manufactured solution of a complex temperature profile.

$$\nabla.(u\,T) = \frac{3}{2}U\left[1-\left[\frac{2y}{H}\right]^2\right]\left(\frac{T_{add}\,x\,(-1+\frac{4y^2}{H^2})(-\frac{1}{L}+\frac{4y^2}{H^2L})}{L}+\frac{T_{add}(-1+\frac{4y^2}{H^2})(-\frac{x}{L}-\frac{4(1-\frac{x}{L})y^2}{H^2})}{L}\right) \tag{2.23}$$

$$DT\,\nabla.(\nabla\,T) = DT\,\frac{T_{add}\,x\,(-\frac{128(1-\frac{x}{L})y^2}{H^4}-\frac{8(1-\frac{x}{L})(-1+\frac{4y^2}{H^2})}{H^2}+\frac{8(-\frac{x}{L}-\frac{4(1-\frac{x}{L})y^2}{H^2})}{H^2})}{L}+\frac{2T_{add}(-1+\frac{4y^2}{H^2})(-\frac{1}{L}+\frac{4y^2}{H^2L})}{L} \tag{2.24}$$

The viscous dissipation contribution is the same of the previous example, Eq. 2.22, since the velocity and stress fields are not affected by this manufactured solution.

For verification purposes, the new solver was modified, by adding to the original equation source term the symmetric of the terms calculated for each MMS solution (Eq. 2.22 for the constant temperature MMS and Eq. 2.22, 2.23 and 2.24 for the complex temperature profile), and used to compute the temperature distribution. Both

case studies were tested with different mesh refinements, namely with 100 x 10, 200 x 20, 400 x 40 and 800 x 80 computational cells along the x and y directions. This allowed to determine the order of convergence of the new solver, by comparing the calculation errors obtained between consecutive mesh refinements.

Three error norms, namely L_1, L_2 and L_∞, indicated by $E(L_1)$, $E(L_2)$ and $E(L_\infty)$ respectively, were used to estimate the calculation error (i.e. the difference between the numerically predicted temperature and the imposed manufactured solution). $E(L_1)$ and $E(L_2)$ norms were computed with Eqs. 2.25 and 2.26,

$$E(L_1) = \frac{\sum_{i=1}^{N} |error| \, V_i}{\sum_{i=1}^{N} V_i} \tag{2.25}$$

$$E(L_2) = \sqrt{\frac{\sum_{i=1}^{N} |error|^2 \, V_i}{\sum_{i=1}^{N} V_i}} \tag{2.26}$$

where, V_i is the cell volume and N is the number of cells.

$E(L_\infty)$ is the maximum value of the absolute temperature error. The order of convergence (p) of the method was calculated (Roy, 2003) using the Eq. 2.27 for all the three error norms considered,

$$order\ of\ Convergence(p) = \frac{\ln\left[\frac{E_m}{E_{m+1}}\right]}{\ln\left[\frac{N_{m+1}}{N_m}\right]} \tag{2.27}$$

where, E is the error value obtained for each employed error norms, N is the number of computational cells used for each mesh refinement, and m is the mesh refinement case. The results of the error norms and the order of convergence obtained with both manufactured solutions are given in Table 2.1 and Table 2.2.

Table 2.1: Error norms (E) values and order of convergence (p) for the constant temperature manufactured solution.

m	N	L_1		L_2		L_∞	
		E	p	E	p	E	p
1	1000	0.6079	-	0.8072	-	1.746	-
2	4000	0.1354	2.167	0.1823	2.147	0.433	2.012
3	16000	0.0324	2.065	0.0442	2.045	0.106	2.031
4	64000	0.0079	2.024	0.0109	2.014	0.026	2.027

Table 2.2: Error norms (E) values and order of convergence (p) for the complex temperature profile manufactured solution.

m	N	L_1		L_2		L_∞	
		E	p	E	p	E	p
1	1000	0.2879	-	0.3338	-	1.258	-
2	4000	0.0709	2.021	0.0839	1.991	0.3671	1.777
3	16000	0.0184	1.948	0.0225	1.899	0.1055	1.798
4	64000	0.0043	2.108	0.0056	1.999	0.0257	2.039

As can be seen from these results, the correct solution is approached with an order of convergence around 2, when the mesh is refined, for both cases studies and the three error norms considered.This order of convergence was expected since all the governing equation terms were discretized using second order schemes (see Section 2.3.2). In conclusion, the results obtained allowed to verify the proper implementation of the energy equation.

2.4 Case studies

To assess the developed cod, and to evaluate the reliability of the proposed design methodology, two industrially relevant cases were considered:

i) Design/Optimization of a new extrusion die to produce a protection bar profile, aiming to achieve a balanced flow distribution at the die exit;

ii) Evaluating the feasibility of using the new code to improve the flow balance of an existing extrusion die, used to produce a swimming pool cover profile. In this case the objective is to improve the die performance by imposing different temperatures around its contour, as an economic alternative to the redesign and manufacture of a new die properly balanced.

In both cases the design procedure stages (illustrated in Figure 2.1) are followed, by focusing either on the geometry, for the first case, or on the modification of the boundary conditions, for the second case.

2.4.1 Material Characterization

The material used by the extrusion company to produce both profiles under study is a polycarbonate extrusion grade (TRIREX 3027U(M1)). The shear viscosity flow curves were obtained by using both parallel plate (ARG2, from TA Instruments) and capillary (Rosand RH7, from Malvern Instruments) rheometers, at three different temperatures (230° C, 250° C and 270° C).

The material is prone to thermal degradation and is also very rigid, turning difficult to obtain good quality results in the parallel plate experiments. i.e., at very low shear rates, due to the high residence times required to properly melt the material and those involved in testing. As a consequence, it was not possible to obtain reliable data for

the highest temperature used. On the other hand, the tests performed with the capillary rheometer were straightforward for all the test temperatures.

The intermediate temperature (250 ºC) was chosen as the reference one. Consequently, the experimental viscosity data obtained for 230°C and 270°C were shifted to that temperature using the shift factor a_T (Eq. 2.10). The activation energy (E), needed to calculate a_T, was determined in order to minimize the error between the experimental data and the model predictions. A fit of the master flow curve was then made with a Bird-Carreau model, resulting in the following parameters values: η_0 = 11731 Pa.s, η_∞ = 0 Pa.s, n = 0.524, λ = 0.1572 s and E/R = 16296 K. The master curve fit and experimental points are shown in Figure 2.8.

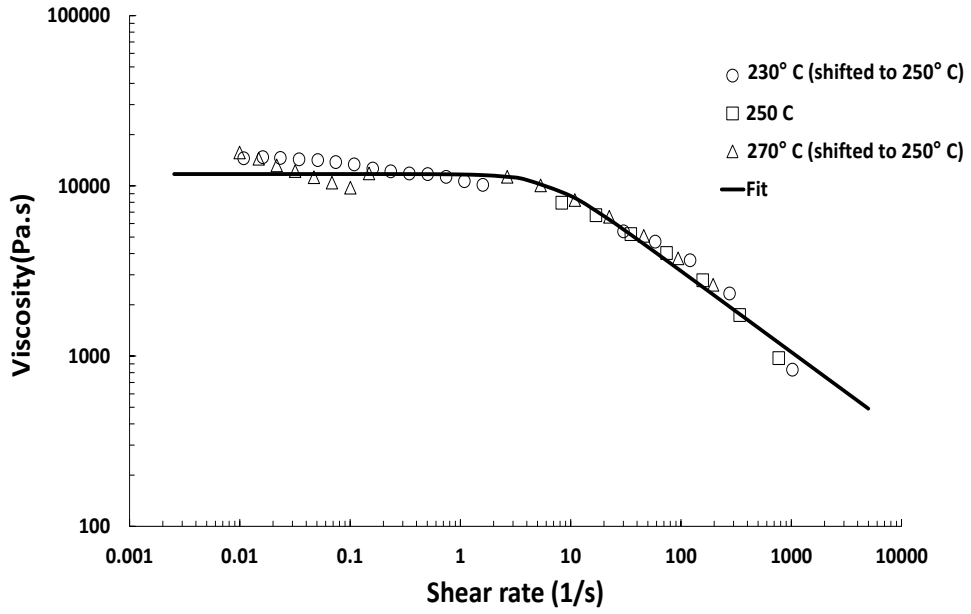

Figure 2.8: Polycarbonate extrusion grade (TRIREX 3027U (M1)) master flow curve: data obtained at three different temperatures and fitted with a Bird-Carreau model.

2.4.2 Case Study 1: Design of a new extrusion die

In this case, the proposed design methodology was used to optimize the flow channel geometry of the protection bar profile die, aiming to obtain a balanced flow

distribution. The required dimensions for the extrusion die flow channel outlet are shown in Figure 2.9. Due to symmetry reasons only half of the geometry is presented. The same geometry was used in the numerical studies.

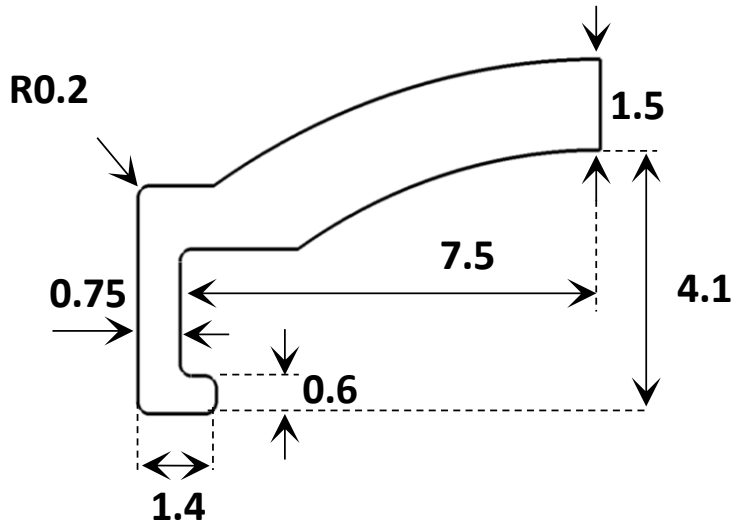

Figure 2.9: Cross section and required dimension for the protection bar profile (due to symmetry reasons only half of the geometry is shown; all dimension are in mm).

The length of the parallel zone was fixed to a minimum value of 20 mm to facilitate proper die assembly and machining, as requested by the company. A schematic representation of the die flow channel, and its partition in four main functional zones is shown in Figure 2.10.

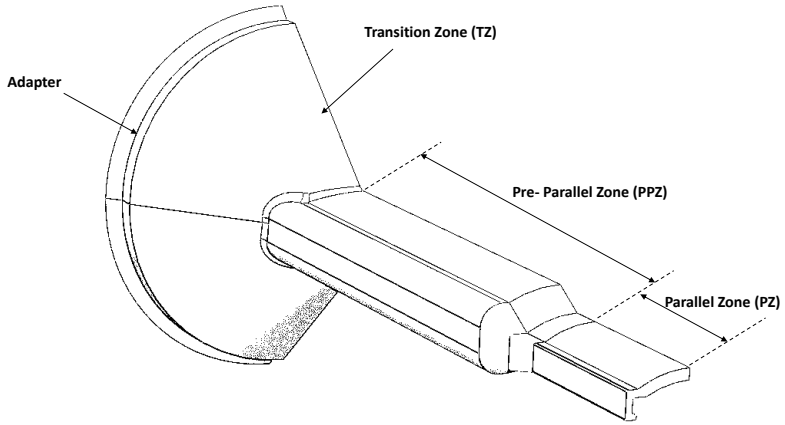

Figure 2.10: Protection bar profile extrusion die flow channel and its main zones (due to symmetry reasons only half of the geometry is presented).

As mentioned in Section 2.2, the geometry generation and the division of its outlet into Elemental Sections (ESs) and Intersection Sections (ISs) was done using the CAD software. The division of the external surface of the flow channel into subzones, where different boundary conditions should be applied and/or specific parameters have to be monitored (e.g. the outlet flow rate in each ES) for numerical simulation purposes, was done in Salome. The die outlet division is shown in Figure 2.11, encompassing four ESs and two ISs.

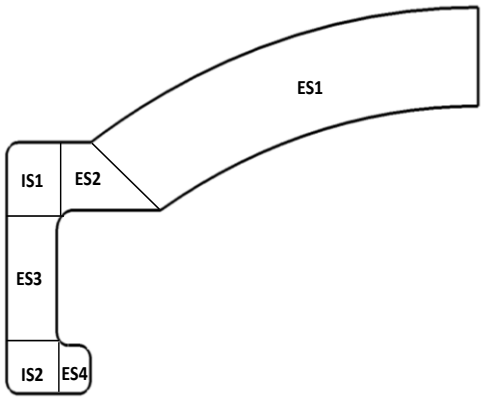

Figure 2.11: Division of the protection bar profile extrusion die outlet into ESs and ISs subsections.

The velocity boundary condition at the inlet was determined from the required extrusion line speed, which was expected to be close to 2.5 m/min. A zero gradient boundary condition is considered at the outlet, and a no slip boundary condition was imposed at the walls. For the pressure field we assumed zero pressure at the outlet and a zero gradient variation at the inlet and walls. Regarding the temperature, a value of 250 °C was imposed at the inlet, 245 °C at the walls (as prescribed by the company, based on its experience. This decrease in 5 °C, increases the melt viscosity by 17% (considering the rheological characterization described in Section 2.4.1), which contributes to stabilize the melt flow, avoids thermal degradation along the flow channel, and also facilitates the manipulation of the extrudate after die exit, thus providing a better quality product and simple line operation.

After generating the geometry and defining the required regions, the mesh generation and the numerical calculations were performed in the OpenFOAM® framework, as specified in the die-design procedure (Figure 2.1).

Before starting the numerical simulation trials, a mesh sensitivity study was performed to identify the refinement level required to obtain accurate results. This study was done with the flow channel presented in Figure 2.10, for three different mesh refinements with 26,282, 2,042,790 and 10,175,198 computational cells.

The field values obtained for each mesh, namely the pressure drop, the maximum temperature in the domain and the average velocity at each outlet section, were normalized with the reference field value obtained for the finer mesh used in the study. The results are shown in Figure 2.12, where the Mesh 2 predictions show a minor difference when compared to those obtained for Mesh 3 (the most refined mesh). Based on these results, all the subsequent numerical runs were made using Mesh 2 (see Figure 2.13).

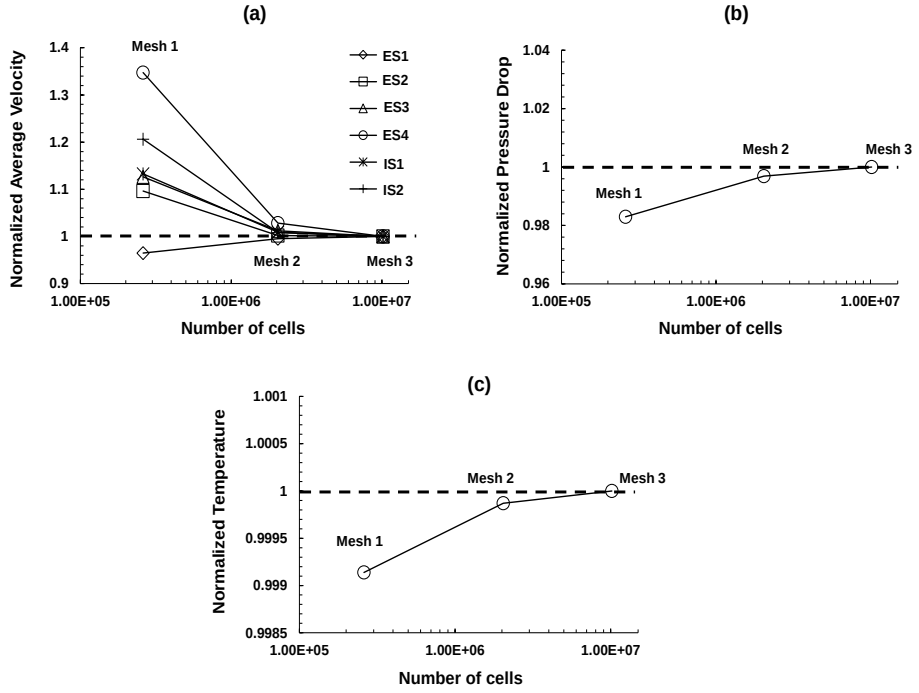

Figure 2.12: Results of the mesh sensitivity analysis, for the protection bar profile flow channel, normalized with those obtained with the finer mesh: (a) average velocity for all ESs; (b) pressure drop; (c) maximum temperature in the domain.

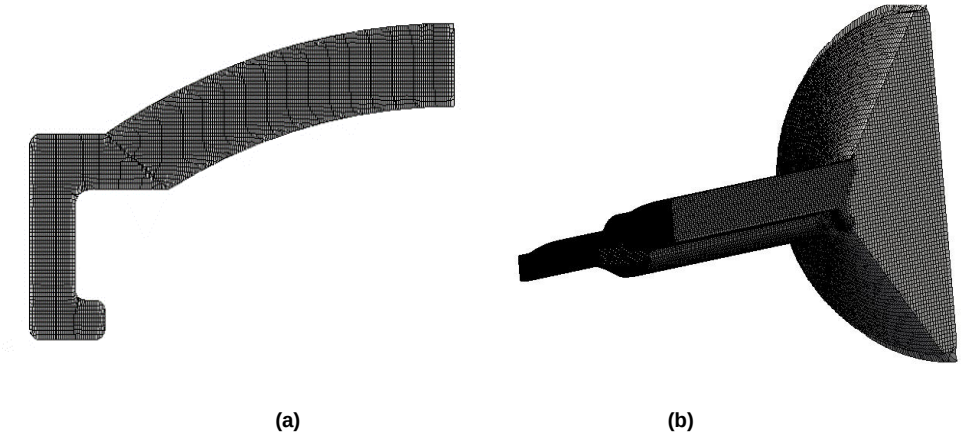

Figure 2.13: Selected mesh (Mesh 2) for the protection bar profile flow channel optimization study: (a) die exit cross section; (b) flow channel.

2.4.2.1 Numerical trials and results

In the first stage of this numerical study, several trials involving modifications of the PPZ cross section geometry were performed. To avoid data cluster only the Initial trial (Trial1) and the last two trials (Trial2 and Trial3) of this stage are discussed. A schematic representation of the cross section of PPZ and PZ for the last two trials is given in Figure 2.14, where the changes in the PPZ cross section performed on Trial3 (with respect to Trial2), are indicated with arrows. The corresponding $F_{obj,i,}$ results obtained for these cases are given in Figure 2.15. As one can see, the $F_{obj,i}$ of all the section show a small improvement from Trial1 to Trial2, but almost no improvement from Trial 2 to Trial 3, since the flow in ES1 (the thickest section, seeFigure 2.10) dominates the remaining.

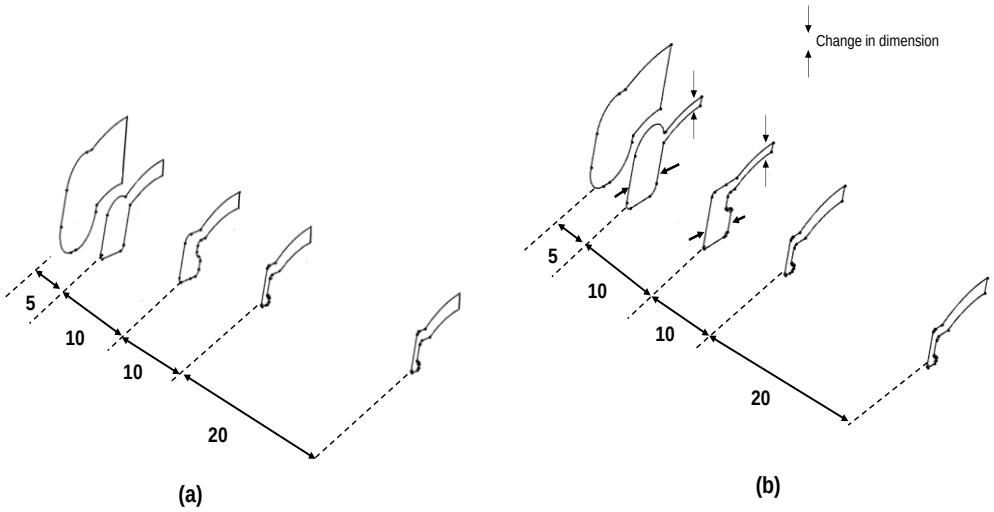

Figure 2.14: Cross sections used to build the flow channel PPZ and PZ zones (protection bar profile): (a) Trial2; (b) Trial3.

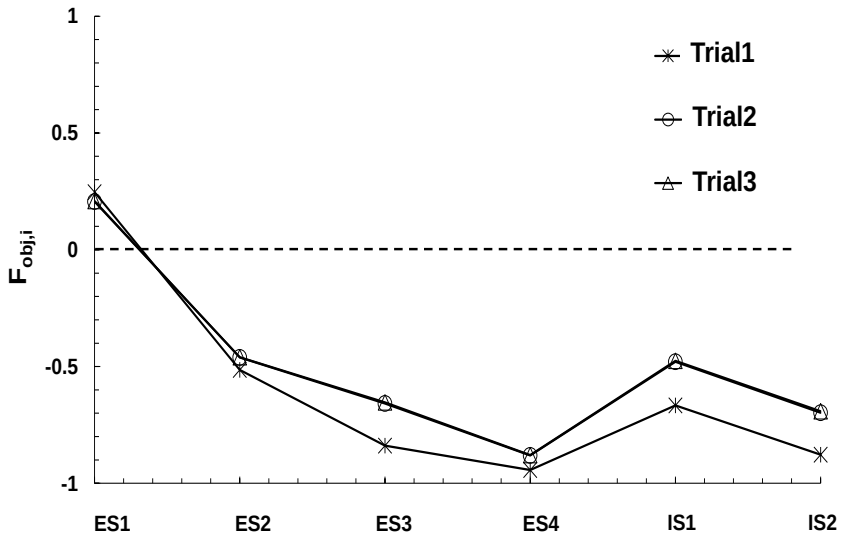

Figure 2.15: Fobj,i predicted for the different subsections of the die outlet for Trial1, Trial2 and Trial3.

Based on the knowledge obtained from from this initial set of trials, it was decided to use a flow separator (both at PPZ and PZ), located at the ES1-ES2 interface, allowing a more independent flow control in both regions (Nóbrega et al., 2003b). Also, the width of the thinnest Elemental Section (ES4) was doubled, to increase the flow in the most restricted ES. Slight adjustments were also made on the PPZ cross section geometry and length. Subsequently, a second set of numerical trials were done considering the above mentioned changes resulting in Trial4 and Trial5, shown in Figure 2.16. The corresponding $F_{obj,i}$ results are presented in Figure 2.17.

As can be seen, Trial4 presents a significant increase of flow in the more restrictive sections, when compared to Trial3, but still not satisfactory, with the larger Elemental section, ES1, still dominating the flow, with an average velocity 1.5 times higher than the global average one. For this reason, the PPZ cross section was further adjusted in Trial5 (see Figure 2.16 (b)), in which an almost balanced flow was reached (see Figure 2.17).

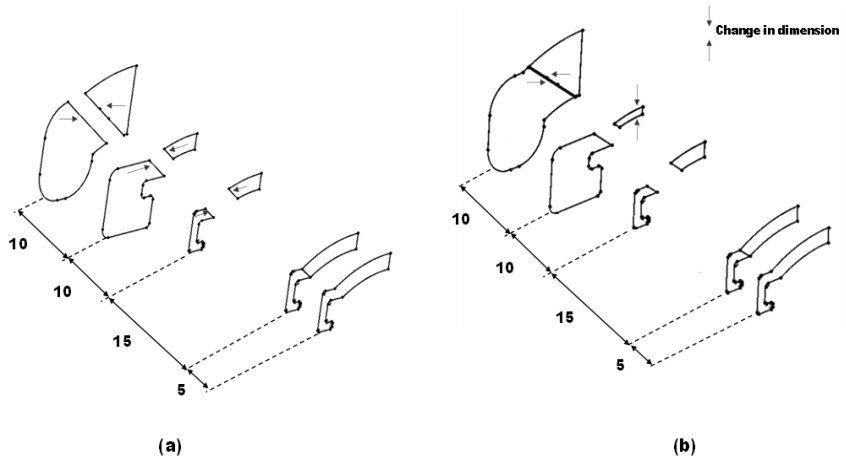

Figure 2.16: Cross sections used to build the flow channel PPZ and PZ zones (protection bar profile): (a) Trial4; (b) Trial5.

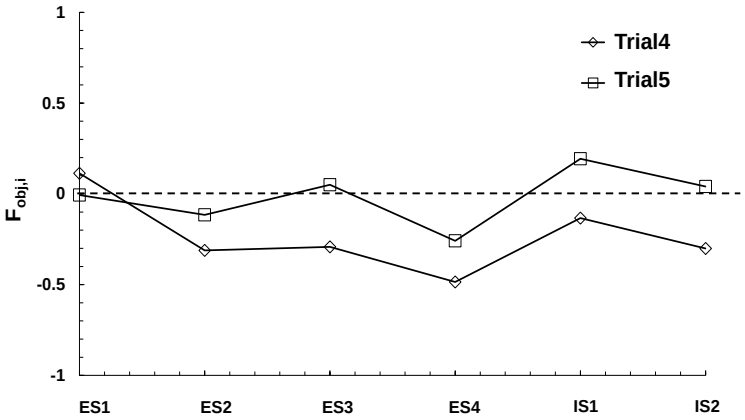

Figure 2.17: Fobj,i predicted for the different subsections of the die outlet for Trial4 and Trial5.

The global objective function, $F_{obj,}$ (computed with Eq. 2.2), are shown in Figure 2.18.

As one can observe, F_{obj} value drops in the consecutive trials, being the higher performance obtained in Trial5.

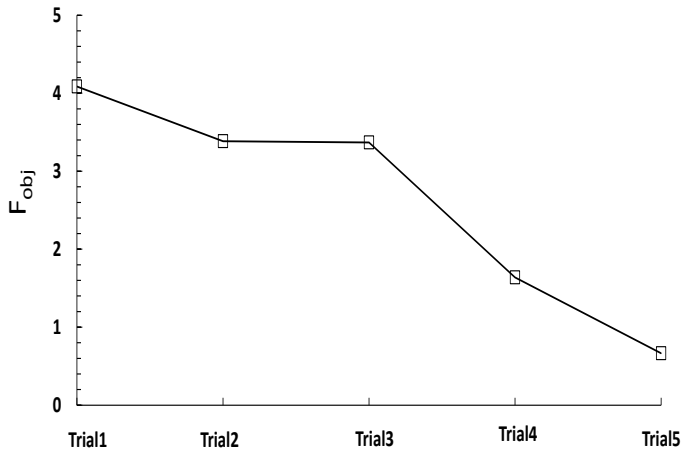

Figure 2.18: Fobj evolution along the design process (protection bar profile).

The exact dimensional details of the numerically optimized flow channel (corresponding to Trial5) were then used to build the extrusion die shown in Figure 2.19, which was used to produce the protection bar profile. Samples from the first production trial, also illustrated in Figure 2.19, were collected to assess the code predictions.

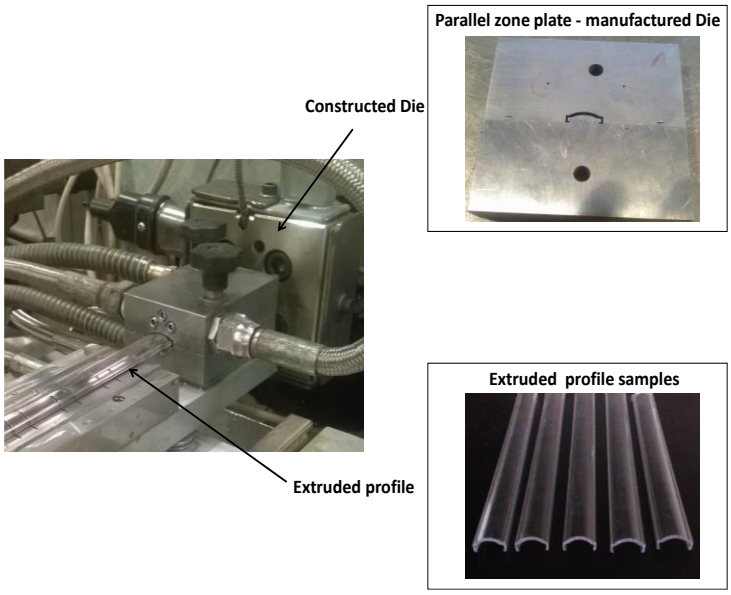

Figure 2.19: Extrusion of the protection bar profile: die constructed based on the numerical results and samples of extruded profiles.

2.4.2.2 Experimental Assessment

In-order to estimate the actual flow distribution in the manufactured extrusion die, the relative flow distribution was determined by measuring the profile relative area of each ESs, as suggested by Szarvasy et al. (2000). For this purpose, the cross section areas of the extruded profile samples were measured following the protocol described in a previous work (Nóbrega et al., 2004), using a digital microscope (Leica DMS 1000) and a proper software (Leica Application Suite).

The area of each subsection of the complete profile was measured in five samples. The image of one of the extruded profile samples measured, together with the area details, is shown in Figure 2.20.

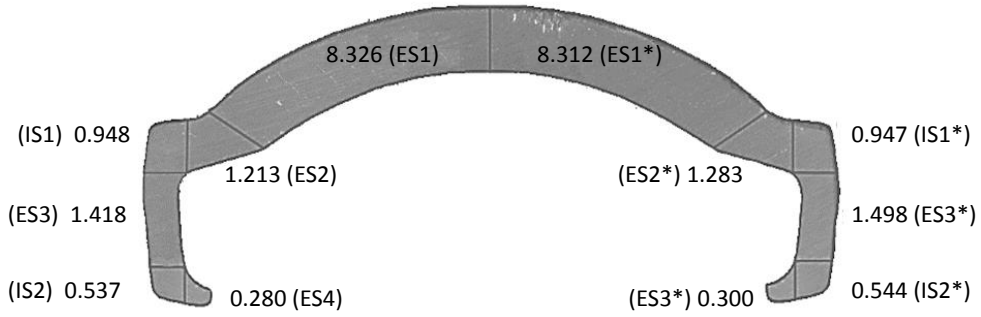

Figure 2.20: Cross sectional areas of the ESs and ISs of one of the extruded profile samples of the protection bar, measured at both left and right* sides (all the dimensions are in mm2).

The relative area ratios obtained from the extruded samples and those numerically predicted, are shown in Table 2.3. On accounting the limits provided by the standard deviation, the highest difference found between the two types of results is around 1%,

occurring in the thickest subsection (ES1), which is a very good result and thus allows to further validate the numerical code predictions.

Table 2.3: Relative area ratios for the numerical predictions and experimental results (average and standard deviation measured values) obtained for the protection bar profile.

Sections	Relative area ratio of the profile (%)	
	Predicted	Extruded
ES1	34.426	32.937 ± 0.485
ES2	4.545	4.598 ± 0.300
ES3	5.004	5.856 ± 0.244
ES4	1.198	0.940 ± 0.122
IS1	2.995	3.624 ± 0.162
IS2	1.832	1.809 ± 0.193

2.4.2.3 Remarks

It should be mentioned that before requesting our aid to design this extrusion die, the company tried it using an experimental trial-and-error approach. In their efforts, the shape and quality of the profile produced after twelve experimental trials were not as good as those obtained in the first trial production that used the numerical optimized die. Furthermore, the resources involved in each experimental trial included two labors to set the machine and to run the experiment for a 4 hours period, 25 kg of raw material and one labor to clean the die and to modify its flow channel (minimum duration of 2-3 hours per trial). As referred, using the numerical methodology the company managed to produce the profile at the first experimental trial, clearly reducing the development costs and the time to market.

2.4.3 Case Study 2: Effect of die heaters temperature on the flow distribution

The second industrial case study involves the production of a swimming pool cover profile. In this case, the extrusion die, already in tests in the company, had a poor flow distribution. This die had four heaters, one on each face of the forming tool PZ region, all controlled by the same thermocouple.

The polymer melt shear viscosity is substantially affected by temperature. Consequently, the local resistance to flow can be adjusted through controlled variations of the material temperature at specific locations. Thus, the main purpose of this study was to verify if there was advantage in having the four heaters controlled by independent thermocouples, in order to balance the flow.

The exact flow channel geometry of the existing die was replicated in the CAD software, and the flow channel wall was divided in PPZ, top, bottom, right, left and inner walls, as indicated in Figure 2.21 (a). The division in four outer regions allows imposing different temperatures in each zone.

The flow channel outlet geometry and its division into ESs and ISs, are shown in Figure 2.21 (b). The $F_{obj,i}$ will only be shown for the ESs, due to the large number of subsections involved, and also because the direct control of flow in the ISs is not possible, since the flow distribution in these ISs regions is a consequence of the flow from its neighboring ESs.

The boundary conditions employed in this case are as follows. The inlet velocity was determined from the required extrusion line speed, 1.28 m/min, considering zero gradient boundary condition at the outlet, and no slip boundary condition at the walls. Concerning the pressure field, the outlet was assumed with zero pressure and a zero gradient variation was considered at the inlet and walls. In terms of temperatures, different sets of values will be used in the die walls (top, bottom, right and left), the

inlet and the converging walls were assumed to have a value of 245°C (as prescribed by the company) and a zero gradient at the outlet and inner walls was considered.

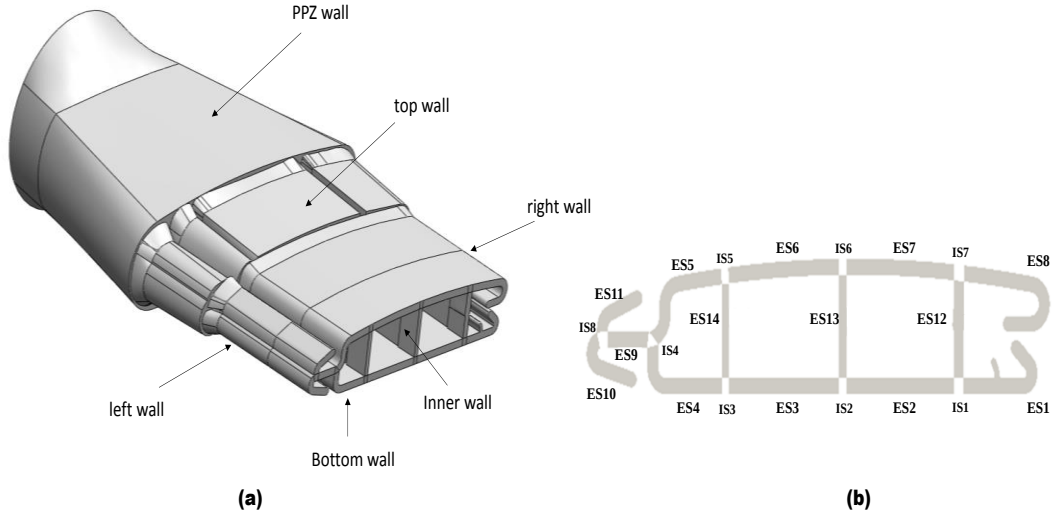

Figure 2.21: Swimming pool cover: (a) flow channel; (b) division of the die exit into ESs and ISs subsections.

As in the previous case study, a mesh sensitivity analysis was performed to identify the mesh refinement level required to obtain accurate results. Three different mesh refinements with 432,653, 3,336,519 and 26,254,523 computational cells were used to discretize the flow channel. The same fields used in the previous case mesh study, were employed here to perform the mesh sensitivity study. The results were normalized with the reference field value obtained for the most refined mesh, and are shown in Figure 2.22.

As one can see from the average velocity field (Figure 2.22 (a)), the predict values for all the ESs, using the Mesh2, converge to the value of the most refined one (Mesh3). Based on these results, and considering the computational times, Mesh2 was chosen to perform all the numerical simulations. A schematic representation of the cross

section and the complete flow channel of the selected mesh (Mesh2) is provided in Figure 2.23.

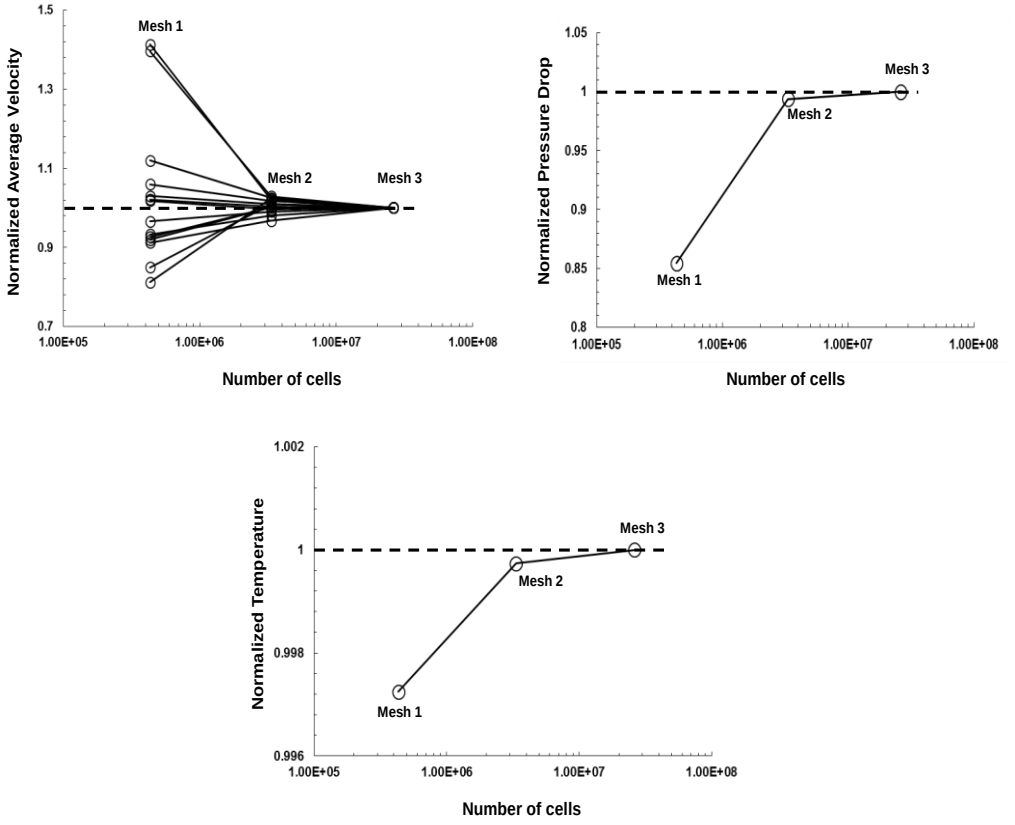

Figure 2.22: Results of the mesh refinement study, for the swimming pool cover profile flow channel, normalized with those obtained with the finer mesh: (a) average velocity for all ESs; (b) pressure drop; (c) maximum temperature in the domain.

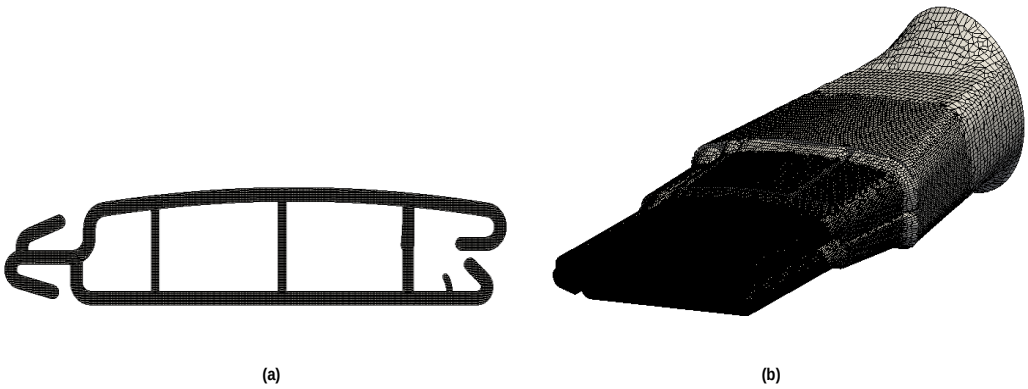

Figure 2.23: Selected mesh (Mesh 2) for the swimming pool cover profile flow channel optimization study: (a) die exit cross section; (b) flow channel.

2.4.3.1 Numerical study results

The initial numerical trial (Trial1) was performed setting 245 ºC for all the heaters, to mimic the previous extrusion runs performed at the company.The results obtained, shown in Figure 2.24, allow to conclude that the flow in ES10 and ES11 (located on the left side of the profile; see Figure 2.21(b)) is substantially higher than the required, whereas the opposite happens in ES12 to ES14 (the inner profile walls). In Trial2, and to compensate for the excessive flow verified on the left side of the profile, the temperature of this side heater was decreased from 245 ºC to 230 ºC (see Figure 2.25 (a)). As described in the beginning of the section, this action was intended to increase the local flow restriction, through an increase in the melt viscosity promoted by reduction of the local temperature.

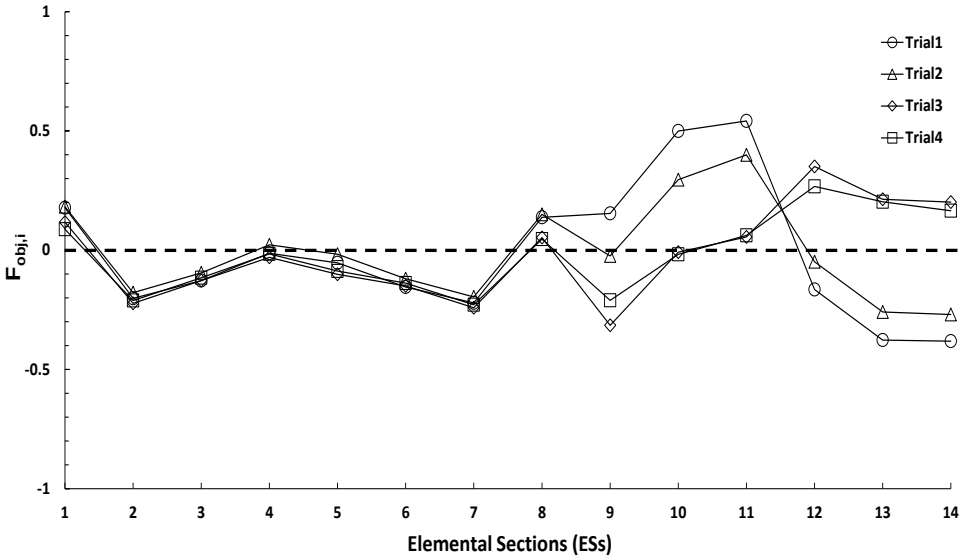

Figure 2.24: Fobj,i predicted at the die outlet (swimming pool cover profile).

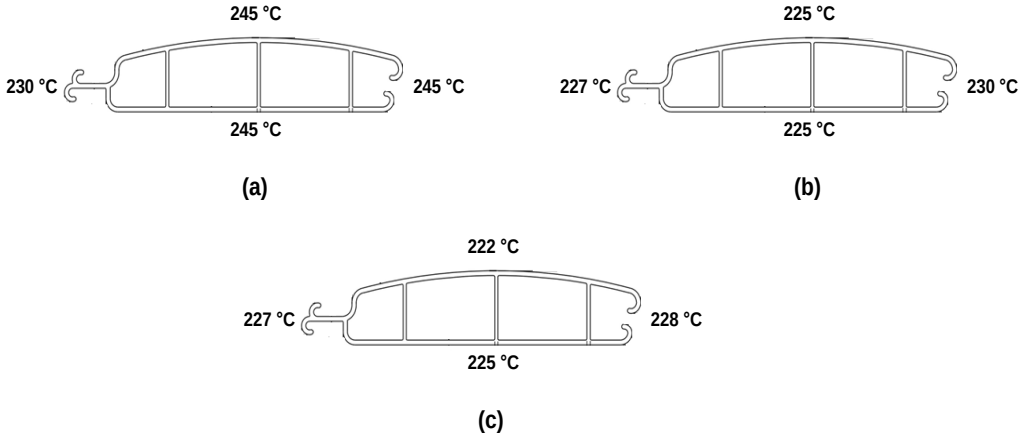

Figure 2.25: Die heaters temperature distribution: (a) Trial2; (b) Trial3; (c) Trial4.

The results (also illustrated in Figure 2.24), show an improvement of the flow distribution along the die, namely a decrease of the flow in ES10 and ES11, and an increase in ES12 to ES14, proving the potential of the strategy employed. However,

ES11 is still the most unbalanced region, showing a higher flow rate (with an average velocity 1.8 times higher than the global average one). Therefore, the temperature of the left side can be further decreased. The temperatures at the other sides can also be decreased to increase the flow rate in sections ES13 and ES14. As a consequence, Trial3 was performed with 225 ºC at the top and bottom heaters, 230 ºC at the right heater and 227 ºC at the left one, as indicated in Figure 2.25 (b). The results (see Figure 2.24) show a significant improvement, providing a much better flow distribution, with a decrease in flow for ES10 and ES11 and an increase for ES12, ES13 and ES14, as expected. However, it negatively affected the flow in ES9 (which is now 1.5 times lower than the global average) and in ES12 (that is now slightly higher).

Subsequent numerical trials were performed, adjusting the temperatures of the heaters. Trial4 (the last one), in which the temperatures illustrated in Figure 2.25 (c) were used, provided a satisfactory flow distribution. The $F_{obj,i}$ results for this last trial are also represented in Figure 2.24. Accordingly, a lower value for the global objective function F_{obj} is also obtained for this trial, as indicated in Figure 2.26.

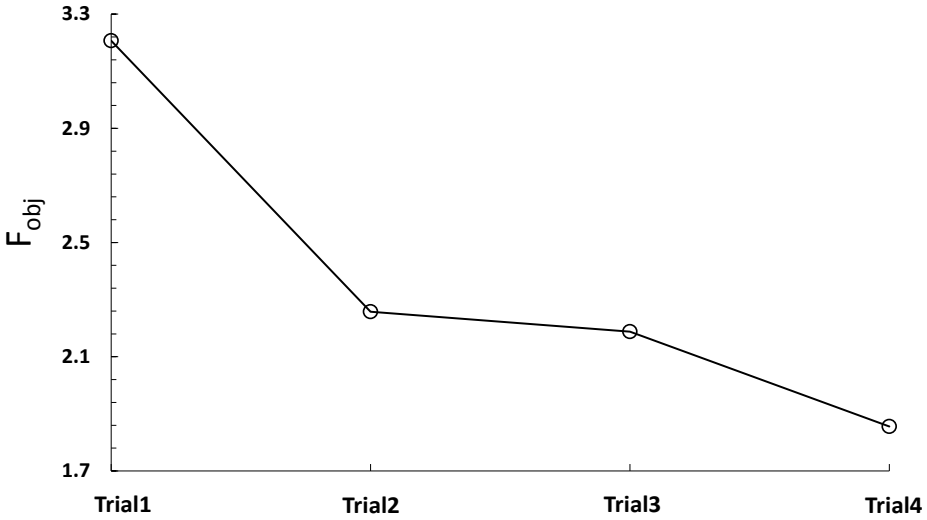

Figure 2.26: Fobj determined for the different numerical trials performed (swimming pool cover profile).

Based on the results obtained, the company decided to modify the extrusion die heating control system, enabling to test the proposed solution. This modification allowed them to extrude the profile with all the dimensions within the required tolerances. The production line and the extruded profile samples of the swimming pool cover obtained with the proposed solution (Trial4), are shown in Figure 2.27.

(a) (b)

Figure 2.27: Extrusion of the swimming pool cover profile: (a) extrusion line in service; (b) extruded samples.

2.4.3.2 Experimental Validation

Similarly to the experimental assessment of the previous case study (Section 2.4.2.2), the relative area of the ESs and ISs of the extruded samples were determined. In this case the cross section of the profile was imprinted and its soft copy image was imported to the Leica software. Three samples were used, being the schematic representation of one of them shown in Figure 2.28.

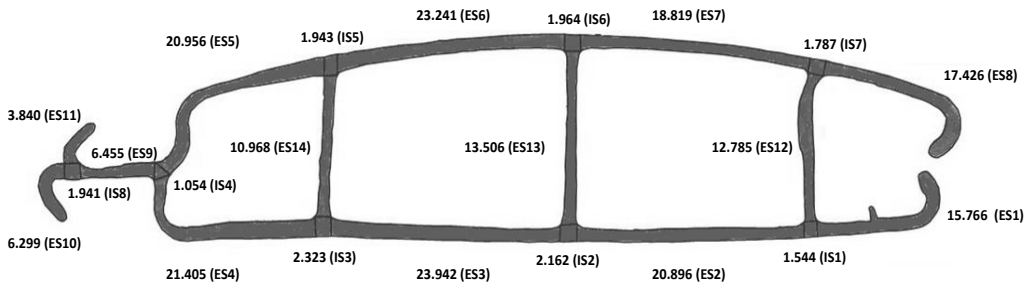

Figure 2.28: Cross sectional areas of the ESs and ISs of one of the extruded profile samples of the swimming pool cover (all the dimensions are in mm2).

The areas of the subsections were measured and the relative area ratio was calculated. The average of the relative areas and the corresponding standard deviation of the samples, and the numerically predicted relative area ratios are shown in Table 2.4.

Table 2.4: Relative area ratios for the numerical predictions and experimental results (average and standard deviation measured values) for the swimming pool cover profile.

Sections	Relative area ratio of the profile (%)	
	Predicted	Extruded
ES1	6.521	6.987 ± 0.309
ES2	10.502	8.968 ± 0.236
ES3	10.456	10.251 ± 0.230
ES4	8.624	9.074 ± 0.335
ES5	8.644	8.796 ± 0.354
ES6	10.562	10.212 ± 0.165
ES7	10.577	8.310 ± 0.268
ES8	8.282	7.655 ± 0.449
ES9	3.321	2.735 ± 0.084
ES10	2.634	2.703 ± 0.072
ES11	1.923	1.757 ± 0.131
ES12	4.782	5.582 ± 0.119
ES13	4.879	5.717 ± 0.233
ES14	4.258	4.846 ± 0.395
IS1	0.532	0.673 ± 0.046
IS2	0.482	0.875 ± 0.054
IS3	0.482	1.004 ± 0.022
IS4	0.298	0.439 ± 0.018
IS5	0.506	0.912 ± 0.134
IS6	0.484	0.843 ± 0.013
IS7	0.530	0.743 ± 0.062
IS8	0.722	0.916 ± 0.069

As can be seen, the experimental values and the numerical predictions are in very good agreement, being the largest difference 2%, for ES7, the thickest of all sections.

2.4.3.3 Remarks

The numerical approach allowed to propose a solution for a poorly designed existing die, successfully tested by the company. Moreover, it was shown that the differential heating of the die cancelled the negative effects of a deficient design, avoiding the machining of a new die.

2.5 Conclusion

In this work we present a computational framework, based in open source software, to aid the design of profile extrusion dies. The codes employed were FreeCAD (for geometry generation), Salome (for dividing the geometry boundary into sub regions), SnappyHexMesh (for Mesh generation) and OpenFOAM® (to perform the numerical calculations). Due to the process requirements, a new numerical code capable of dealing with non-isothermal flows of generalized Newtonian fluids was developed, and verified using the Method of Manufactured Solutions (Roache, 2002). A profile extrusion die design methodology, using the above mentioned open-source software packages, was proposed.

The computational framework and design methodology were experimentally assessed with two industrial case studies, comprising complex cross section geometry profiles, for which the use of experimental trial-and-error approaches showed to be inadequate.

In the first case study, a new extrusion die for the production of a protection bar profile was designed, machined and tested. The results provided were excellent, since it allowed the production of the desired profile shape, with good quality, at the first extrusion trial.

In the second case study, the differential heating of an existing die showed to be an economic alternative to compensate for a poor design. The results obtained confirmed the effectiveness of the strategy, which was implemented via independent temperature control of each die face.

In both case studies the relative profile cross section areas distribution, for all their different elemental sections, presented a very good correlation with the numerical predictions.

In conclusion, the developed computational framework and the proposed die design methodology proved to be a much better alternative to the usual experimental based trial-and-error procedure, currently employed in many companies, showing that it can significantly reduce the development costs and the time to market.

2.6 References

ANSYSPOLYFLOW (2016)
URL:.http://www.ansys.com/.

Carley, J. F. (1989). *Plastics extrusion technology handbook.* NewYork, Industrial Press Inc.

Carneiro, O. S. and Nóbrega, J. M. (2012). *Design of Extrusion forming Tools*, Smithers Rapra Technology Ltd.

DIEFLOW (2016).
URL: http://www.dieflow.com/.

Ettinger, H. J., Pittman, J. F. T. and Sienz, J. (2013). Optimization-driven design of dies for profile extrusion: Parameterization, strategy, and performance, *Polymer Engineering & Science* **53**(1): 189-203.

Ettinger, H. J., Sienz,J, Pittman, J. F. T. and Polynkin, A. (2004). Parameterization and optimization strategies for the automated design of uPVC profile extrusion dies, *Structural and Multidisciplinary Optimization* **28**(2-3): 180-194.

FLOW2000 (2016)
URL: http://www.futuresoft.net/F2k-ext.htm.

FreeCAD (2016).
URL: http://www.freecadweb.org/.

Gonçalves, N. D., Carneiro, O. S. and Nóbrega, J. M. (2013). Design of complex profile extrusion dies through numerical modeling, *Journal of Non-Newtonian Fluid Mechanics* **200**: 103-110.

Hristov, V. and Vlachopoulos, J. (2007). Thermoplastic silicone elastomer lubricant in extrusion of polypropylene wood flour composites, *Advances in Polymer Technology* **26**(2): 100-108.

Agassant, J.F. (2000). New Challenges in the Numerical Modelling of Polymer Processes. *3rd Esaform Conference on Material Forming*. Stuttgart, Germany.

Karadogan, C. (2005). Advanced methods in numerical modeling of extrusion processes, Technische Wissenschaften, Eidgenössische Technische Hochschule ETH, Zürich.

Kostic, M. and Reifschneider, L. (2006). Design of extrusion dies, *Encyclopedia of Chemical Processing DOI* **10**.

Koziey, B., Vlachopoulos, J., Vlcek J. and Svabik, J. (1996). Profile die design by pressure balancing and cross flow minimization, *Technical papers of the annual technical conference-society of plastics engineers incorporated*, society of plastics engineers .

Legat, V. and Marchal, J. M. (1993). Die design: an implicit formulation for the inverse problem, *International journal for numerical methods in fluids* **16**(1): 29-42.

Leica (2016).
URL:http://www.leica-microsystems.com/products/stereo-microscopes-macroscopes/macroscopes/details/product/leica-dms1000/.

Marchal, J. and Goublomme, A. (2000). Parametric optimization of extrusion dies through numerical simulation. *3rd Esaform Conference on Material Forming*.

Michaeli, W. (2003). *Extrusion Dies for Plastics and Rubber Design and Engineering Computations*, Carl Hanser Verlag GmbH & Co.

Nóbrega, J. M., Carneiro, O. S., Oliveira, P. J. and Pinho, F. T. (2003a). Flow balancing in extrusion dies for thermoplastic profiles- part I :Automatic design, *International Polymer Processing* **18 (3)** 225-235.

Nóbrega, J. M., Carneiro, O. S., Oliveira, P. J. and Pinho, F. T. (2003b). Flow Balancing in Extrusion Dies for Thermoplastic Profiles: Part II: Influence of the Design Strategy, *International Polymer Processing* **18**(3): 307-312.

Nóbrega, J. M., Carneiro, O. S., Oliveira, P. J. and Pinho, F. T. (2004). Flow Balancing in Extrusion Dies for Thermoplastic Profiles: Part III: Experimental Assessment, *International Polymer Processing* **19**(3): 225-235.

OpenFOAM® (2016).
URL:http://openfoam.org/version/2-3-0/.

Patankar, S. V. and Spalding, D. B. (1972). A calculation procedure for heat, mass and momentum transfer in three-dimensional parabolic flows, *International journal of heat and mass transfer* **15**(10): 1787-1806.

patchIntegrate (2016).
URL:http://www.cfdsupport.com/OpenFOAM-Training-by-CFD-Support/node79.html.

PROFILECAD (2016).
URL:http://www.polydynamics.com/profile.htm.

Roache, P. J. (2002). Code verification by the method of manufactured solutions, *Journal of Fluids Engineering* **124**(1): 4-10.

Roy, C. J. (2003). Grid convergence error analysis for mixed-order numerical schemes, *The American Institute of Aeronautics and Astronautics journal* **41**(4): 595-604.

Salome (2016).
URL:http://www.salome-platform.org/.

SimpleFOAM (2016).
URL:http://openfoamwiki.net/index.php/OpenFOAMguide/TheSIMPLEalgorithmin OpenFOAM.

SnappyHexMesh (2016).
URL:http://cfd.direct/openfoam/user-guide/snappyhexmesh/.

Szarvasy, I., Sienz, J., Pittman, J.and Hinton, E. (2000). Computer aided optimisation of profile extrusion dies: definition and assessment of the objective function *International Polymer Processing* **15**(1): 28-39.

Tadmor, Z. and Gogos, C. G. (2006). *Principles of polymer processing*, John Wiley & Sons.

Chapter 3

Design guidelines to balance the flow distribution in complex profile extrusion dies

Abstract

In this work a novel methodology to balance the flow distribution in complex extrusion dies is proposed. For this purpose, the profile cross section geometry is divided into simpler geometries (*L* and *T* shaped profiles), which are balanced with a surrogate model obtained by a detailed numerical study.

The numerical simulations are performed considering the non-isothermal flow of Bird-Carreau inelastic fluids, and, the numerical computations are performed with a solver implemented in OpenFOAM® computational library. The proposed methodology is assessed with some case studies.

This chapter was adapted from: A.Rajkumar, L. L. Ferrás, C.Fernandes, O. S.Carneiro, M.Becker, and , J.M. Nóbrega (2016). "Design guidelines to balance the flow distribution in complex profile extrusion dies." International Polymer Processing, XXXII, 1.

3.1 Introduction

Extrusion is one of the oldest and most common methods used in the production of plastic parts. In this process, polymer pellets are transported and melted along the extruder, the polymer melt is then forced to pass through an extrusion die that shapes the desired profile geometry. Finally, the cooling system is used to cool down the polymer profile (Carneiro and Nóbrega, 2012) .At the shaping stage, the polymer melt undergoes a deformation that leads to different flow restrictions along the flow channel cross section, making it difficult to obtain a homogeneous flow distribution at the die flow channel outlet. Therefore, one of the main challenges in the extrusion die design process is the achievement of a balanced flow distribution, i.e. obtaining similar average velocity in the die outlet contour.

The geometrical complexity of the common profiles, along with the rheological properties of the polymer melt and its dependence on the deformation rate and temperature, further complicates the extrusion die design process (Carneiro et al., 2004). Therefore, in order to obtain a balanced flow at the extrusion die outlet, adequate adjustments should be made in the flow channel geometry (FCG). In most cases an experimental trial-and-error practice is employed to attain an appropriate FCG, but this process consumes a huge amount of time and material resources, and it relies utterly on the designer's experience.

In the literature, one can easily find several experimental and numerical studies on the optimization of the extrusion die design process. For example, Michaeli (1984), presented a study on the flow balancing of each section of the extrusion die by modifying the land length and die entry angle, by using analytical flow computations and a trial-and-error method. The use of analytical relations for the die design process was also provided by Tadmor and Gogos(2006). Summers and Brown(1981), derived simplified equations to facilitate the die design of rigid PVC. Huneault et al.(1996), used a network approach, named FAN (flow analysis network), to analyze and optimize the flow inside extrusion dies.

In an another study by Hurez et al.(1996), a methodology based on a blend of the FAN approach (to describe the complex layout of flow channels in the die land) and the cross-section method (to compute the pressure drop in individual channels) was presented. The results of the study showed a good accordance with the experimental and theoretical results.

It is worth mentioning that neural networks were also used for die design optimization purposes, and, some improvements were made in order to reduce the computational time needed to obtain an optimized die (Mehta et al., 1999).

All the methods/works described before are useful for the balancing of simple flows, but they lack the full influence of the lateral flows, and therefore, may lead to poor results when designing extrusion dies to produce complex profiles.

With the significant and fast development of numerical tools, several numerical studies were done on the subject of extrusion die design. McKelvey and Ito(1971), provided a numerical method for analyzing the uniformity of flow in flat sheet dies, considering a power law model and isothermal flow conditions. They presented the procedures to follow in order to obtain the die dimensions for the uniform flow distribution at specific flow rates and pressure drops.

Using the Finite Element Method (FEM) Wortberg et al.(1982), presented the calculation of three dimensional flow patterns in Y and T shaped profiles extrusion dies. The main units of the extrusion process, namely the extruder, the die and the cooling were investigated in this study.

Many other researchers have performed numerical study analysis (based on the FEM) of the flow balance using different optimization techniques, like sensitivity analysis, genetic algorithms, polynomial network and constraint optimization algorithms (Yu and Liu, 1998 ; Ulysse, 1999; Ulysse, 2002; Wu and Hsu, 2002; Lehnhäuser and Schäfer, 2005; Lebaal et al., 2009; Sienz et al., 2010; Elgeti et al., 2012; Yilmaz et al., 2014)

An automatic optimization framework was proposed by Ettinger (Ettinger et al., 2004; Ettinger et al., 2013), where the main parameters and optimization strategies

needed to automatize the design of profile extrusion dies were identified using 2D models.

A series of studies using in-house numerical codes to optimize the extrusion die flow channel geometry were presented by Nóbrega (Nóbrega et al., 2003a; Nóbrega et al., 2003b; Nóbrega, 2004; Nóbrega et al., 2004b)

They identified the main steps needed for the automatic design (Nóbrega et al., 2003a) and the optimization design strategies used were based on changes performed in the pre-parallel and parallel zones of the extrusion die, dealing with simple profiles. Subsequently, a numerical code was developed to simulate complex geometries, based on unstructured meshes (Goncalves, 2013).

The large number of works on computer aided die design clearly indicates the ability to accurately predict and adjust the fluid flow distribution using numerical tools. These numerical tools are a better alternative to the usual experimental trial-and-error approach, with the advantage of reducing substantially the cost and resources consumed during the experimental trials. However, the ability to deal with any die geometry without the designer intervention is still far beyond our capabilities. Furthermore, the number of extrusion companies using numerical tools for the extrusion die design process is small, mainly due to the lack of adequate knowledge and/or financial resources. Considering these facts, it is of significant importance to provide useful design guidelines (that can help predicting the necessary die dimensions for obtaining a homogeneous flow distribution) for the extrusion die designers with no access to numerical modeling tools.

The aim of this work is then to establish useful design guidelines for obtaining a balanced flow distribution at the die outlet, which circumvent the limitation inherent to analytical approaches and do not demand the use of numerical codes. The proposed methodology consists on dividing a complex cross section into a combination of *L* and *T* shaped profiles, and to determine the relationship between the parallel zone length and the thickness of the different subsections that promote an adequate flow distribution. For this purpose, the two basic geometries, *T* and *L*, are studied in detail

numerically, aiming to identify a surrogate model for the conditions required to achieve a balanced flow distribution. Since a large number of profile cross sections can be decomposed into L and T subsections, the proposed methodology is expected to have a significant impact in the field of profile extrusion.

The rest of the chapter is organized as follows. In Section 3.2 the geometry manipulation used in this study is explained. In Section 3.3 the numerical code and the equations governing the fluid flow are described. In Section 3.4, the simulation strategy is presented and a flow balancing function is devised for simple extrusion dies used to produce L and T shaped profiles. In Section 3.5, two different die design methodologies are proposed. In Section 3.6, the proposed methodologies are tested for three different profile geometries and the results of the assessment are discussed. The chapter ends with the conclusions in Section 3.7.

3.2 Geometry

Since several complex extruded profile cross sections can be decomposed into *L* and *T*-shaped simpler geometries (Figure 3.1), these are the basic geometries studied in this work (Figure 3.2).

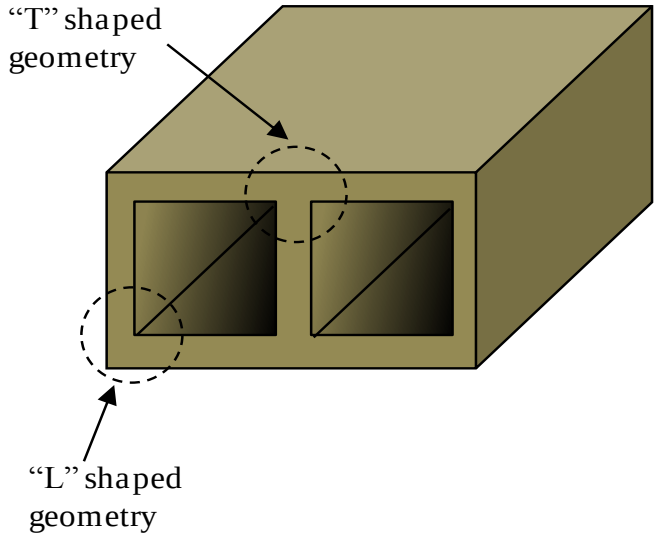

Figure 3.1: Typical profile geometry illustrating its decomposition into L and T shaped subsections.

In order to monitor the flow distribution in the different regions that compose the *L* and *T* shaped parts, their outlet cross section was divided into Elemental Sections (ESs) and Intersection Sections (ISs) [23], as shown in Figure 3.3. Both cross sections (*L* and *T*) comprise two elemental sections (ESi, i=1,2) with a parallel zone length L_i and width w_i (Figure 3.2 and Figure 3.3). The flow channel total length (L_t) was set to be L_2+15 mm, to assure fully developed flow conditions. The thickness of ES1 and ES2 is represented by t_1 and t_2 respectively, as shown in Figure 3.3.

The main purpose of the numerical based studies, described in Section 3.4, is to identify the flow channel length that allows to achieve a similar average velocity in all ESs, and how that is affected by the profile cross-section dimensions. Note that the

flow in the ISs cannot be controlled directly, since the flow distribution in these regions is a consequence of the flow in the neighboring ESs.

Due to symmetry reasons just half of the T shaped flow channel was considered for modelling purposes.

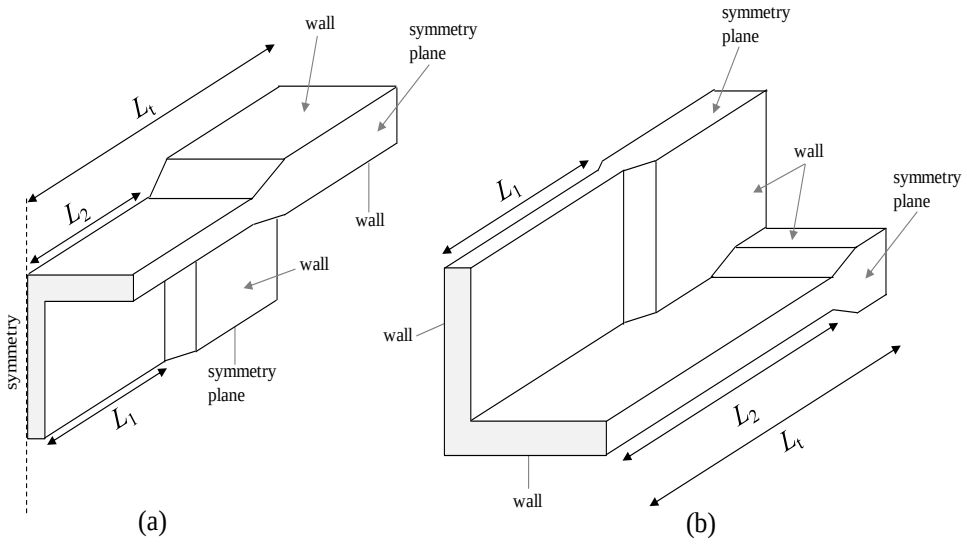

Figure 3.2: 3D Flow channel geometry and boundary conditions used: (a) T-die (for symmetry reasons only half of the geometry is considered); (b) L-die.

It should be noted that when merging several of these L and T shaped geometries to build a specific (more complex) profile die, the devised models do not consider the eventual existence of cross flows developing among them. If present, cross flow will diminish the effectiveness of the methodology developed. However, this problem cannot be solved through a methodology, such as the one developed in this work, which intends to be simple, and applicable without the need of a numerical modelling code.

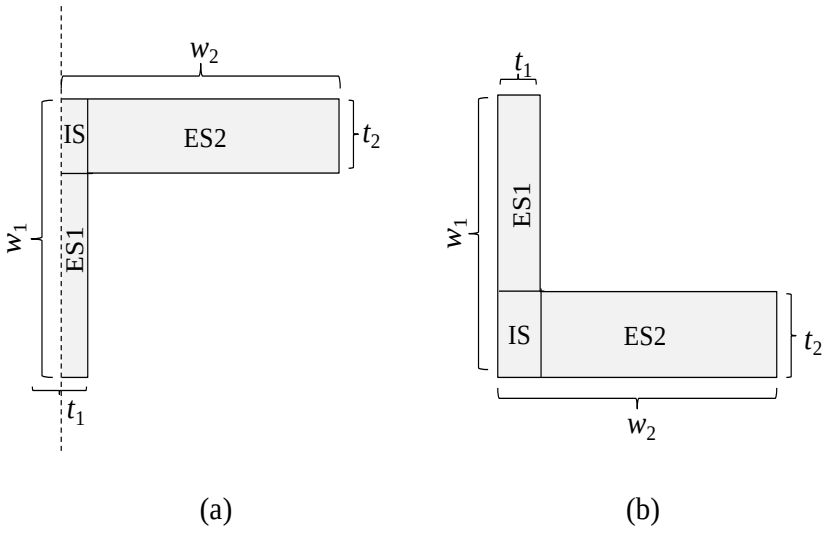

Figure 3.3: Division of the extrusion die outlet into Elemental Sections (ESs) and Intersection sections (ISs): (a) T-shaped die (T-die) (for symmetry reasons, only half of the profile is shown); (b) L-shaped die (L-die). Note that t_2 and ES2 always stand for the thickest elementary section.

3.3 Numerical Method

The Governing equation used in this study, to model the polymer fluid is given in the previous chapter (Chapter 2) Section 2.3.1. The rheological behavior of the fluid considered to devise the proposed methodology follows a non-isothermal inelastic generalized Newtonian constitutive model. Based on the number of successful numerical codes on the field of profile extrusion die design based on this class of models (Flow2000, Polycad), the inherent limitations do not seem to be relevant for the typical deformation rates to which the polymer melts are subjected in profile extrusion.

To solve this coupled system of equations (Eqs. 2.4 – 2.9 (Chapter 2)), the open source computational library OpenFOAM® was used. For this purpose, a new solver was implemented by inserting in the available SIMPLE calculation procedure the

solution of the energy conservation equation and the effects of temperature and shear rate in the shear viscosity.

In this new solver, the steady state, SIMPLE method was used to couple the pressure and velocity fields (Patankar and Spalding, 1972), and the solution of the energy equation was inserted in the sequence, as illustrated in Figure 3.4. At each iteration the shear viscosity is updated, with the temperature and velocity distributions obtained in the previous steps.

To check for convergence, the values of the residuals of all the variables involved were verified at the end of each iteration. When all the residuals are below a certain tolerance, the computations are stopped, assuming that the numerical solution obtained is sufficiently accurate.

For the interpolation of the linear momentum convective terms, the Minmod scheme (Harten, 1983) was used, whereas a linear scheme was employed for the energy convective ones. For the approximation of diffusive terms a second order linear scheme was used.

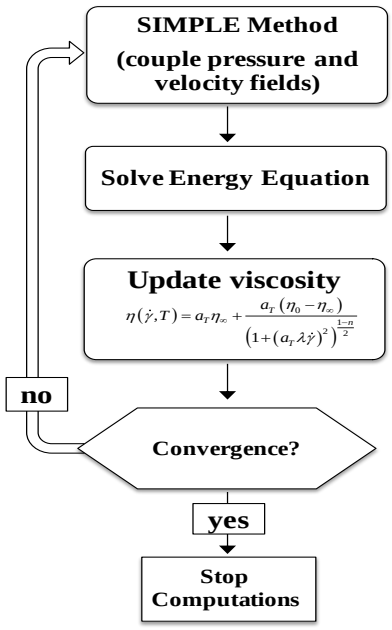

Figure 3.4: Iterative procedure used for the solution of Eqs. 2.4 – 2.9 (see Chapter 2).

For performing the numerical simulations, boundary conditions have to be provided. Therefore, we have imposed a fully developed velocity profile at the inlet. The extrusion linear speed employed is a typical value for profile extrusion.

The fully developed velocity profile was obtained by performing simulations in a constant section flow channel (equal inlet and outlet cross-sections). Using mapped boundary conditions, the outlet profile was mapped as the initial profile of the next iteration, until convergence was achieved.

At the outlet, a zero gradient boundary condition was considered for the velocity field, and for the walls a usual no slip boundary condition was used. For the pressure, we have assumed zero pressure at the outlet and a zero gradient variation at the inlet and walls. For the temperature, a constant value was considered at the wall and inlet, and a zero gradient boundary condition was considered at the outlet.

3.4 Surrogate flow balance models

3.4.1 Case studies

The purpose of these numerical studies is to devise surrogate models for the flow distribution in profile extrusion dies used to produce *L* and *T* shaped profiles, described in Section 3.2. These models should be sufficiently general to cover all the relevant geometrical possibilities. Considering this, the geometries to be studied will have the following characteristics (see Figure 3.2 and Figure 3.3):

- Thickest ES thickness t_2 = 1, 2 and 4 mm;
- ES thickness ratio t_1/t_2 = [0.25, 0.875];
- Thickest ES length/thickness ratio L_2/t_2=15, 10 and 5.

For each case study, several numerical runs will be done aiming to identify the thinnest ES length/thickness ratio (L_2/t_2) that will promote a balanced flow

distribution. In these studies the width parameters (see Figure 3.3) employed were $w_1=t_2+10$ mm and $w_2= t_1+10$ mm.

All the numerical runs performed are summarized in

Table 3.1. As shown, for some geometries (e.g. $L_2/t_2=15$) a large number of t_1/t_2 ratios were analyzed, while for other (e.g. $L_2/t_2=5$ and 10*)* fewer studies were performed, due to the acquaintance gained with the initial results obtained.

In order to provide an idea of the number of numerical runs involved in these studies, one can say that more than 400 simulations were performed.

Table 3.1: Problems studied to obtain the surrogate flow balance models.

L_2/t_2	t_2 [mm]	L_2 [mm]	t_1/t_2	t_1 [mm]
15	1	15	[0.25; 0.875]	[0.25; 0.875]
	2	30		[0.5; 1.75]
	4	60		[1; 3.5]
10	1	10	{0.375;0.625; 0.875}	{0.325;0.675; 0.875}
	2	20		{0.75;1.25; 1.75}
	4	40		{1.5;2.5; 3.5}
5	1	5	{0.375;0.625; 0.875}	{0.325;0.675; 0.875}
	2	10		{0.75;1.25; 1.75}
	4	20		{1.5;2.5; 3.5}

The studies were performed for a polypropylene homopolymer extrusion grade that was previously characterized (Nóbrega et al., 2003a) The rheological parameters obtained considering a Bird-Carreau model (Eq. 2.9 (Chapter 2)) were as follows: η_0 = 55800 Pa.s, η_∞ = 0 Pa.s, n = 0.3014, and λ = 3.21 s. The parameters obtained for the Arrhenius law (Eq. 2.10 (Chapter 2)) were E/R = 2900 K and T_{ref} = 230˚ C (these parameters were obtained from a rheological characterization performed at 210 ºC, 230 ºC and 250 ºC (Nóbrega et al., 2003a)).

In order to obtain mesh independent results, a mesh refinement study was performed to determine the appropriate mesh refinement level. This study was performed for the *T*-die geometry, with t_2 = 2 mm, t_1 = 1 mm, L_1/t_1 and L_2/t_2 equal to

15, considering four different meshes with 4214, 30616, 250432 and 2086016 computational cells (each mesh refinement level was obtained by doubling the number of cells, of the previous one, in each coordinate direction).

To assess the numerical code predictions accuracy, the average velocity at both ESs and IS, the maximum temperature in the domain, and the total pressure drop were calculated and normalized with the reference value obtained with the finer mesh, as shown in Figure 3.5.

Since the difference between the results obtained for the third mesh refinement and for the finest mesh is very small, a mesh refinement similar to the one employed on the third mesh (250432 cells) was used on all the runs done for the undertaken studies. A typical mesh employed is illustrated in Figure 3.6 for a *T*-die.

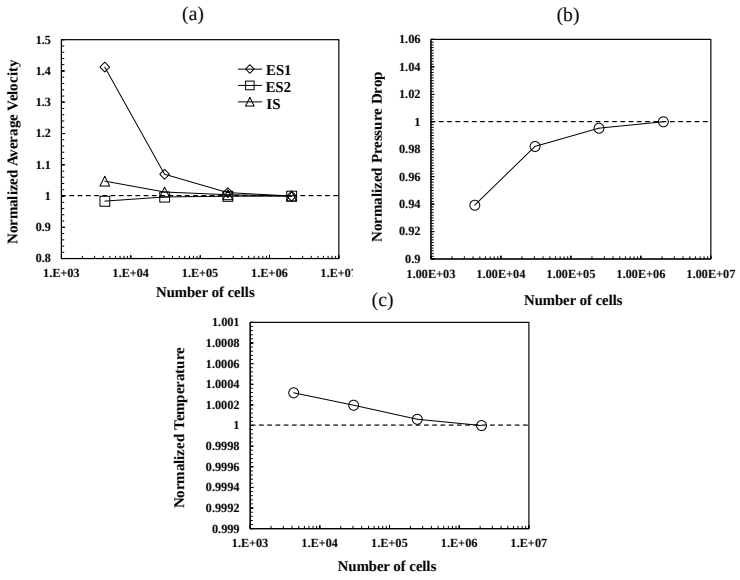

Figure 3.5: Results of the mesh refinement study for the T-die geometry normalized with the results obtained for the finer mesh: (a) Average velocity; (b) pressure drop; (c) maximum temperature in the domain.

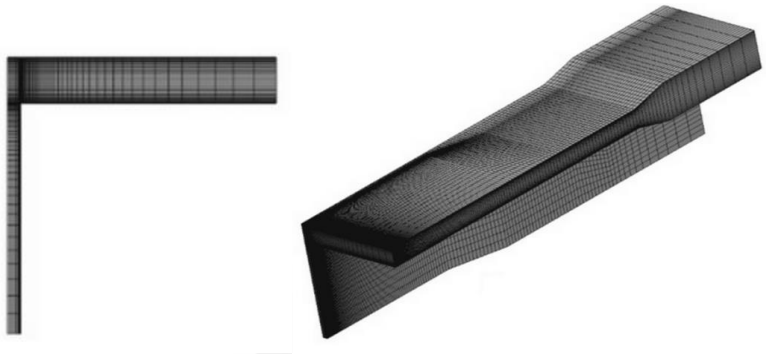

(a) (b)

Figure 3.6: Typical Mesh used for the T-die geometry: (a) cross section of the outlet profile; (b) flow channel.

3.4.2 Results and discussion

Based on what was said before, we have performed numerical simulations in order to find the ideal length (for the different thicknesses combinations) that provides a balanced flow distribution. In order to avoid the cluttering of figures we have only presented the graphical results for the case L_2 =15.

Figure 3.7 and Figure 3.8 show the variation of the velocity ratio (Vi/V) (V is the expected global average velocity at the outlet), as a function of the L_1/t_1 ratio, for the *T* and *L* die geometries, respectively. The results are shown for different values of t_1/t_2 so that for each case, we can monitor the intersection of the different curves. Note that the intersection point (obtained by linear interpolation) represents the value of L_1/t_1 for which a balanced flow is obtained.

As expected, we observe that the L_1/t_1 component of the intersection point increases with the increase of the ratio t_1/t_2, for both *T* and *L* shaped dies.

Ideally we would like to obtain the intersection of the three curves in the same point. But, as explained before, the flow at the intersection sections (ISs) cannot be directly controlled. For example, for the case of the *T*-die, Figure 3.7 (f) we can see

that the intersection between ES1 and IS is obtained for a value of L_1/t_1 around 2, while the intersection of ES1 and ES2 is obtained for a value of L_1/t_1 around 9.

Regarding the *L*-die, the velocity ratio at the IS is smaller (near 1 (see Figure 3.8)) when compared to the results obtained for the *T*-die, meaning that, this geometry is better for obtaining a balanced flow. This happens because the IS is mostly influenced by the ES2 section, and the restriction suffered from the presence of a wall, is also shared with ES2.

We can see (Figure 3.8) that for a higher ratio of t_1/t_2, the intersection of the three curves is possible, and, an almost fully balanced flow is obtained.

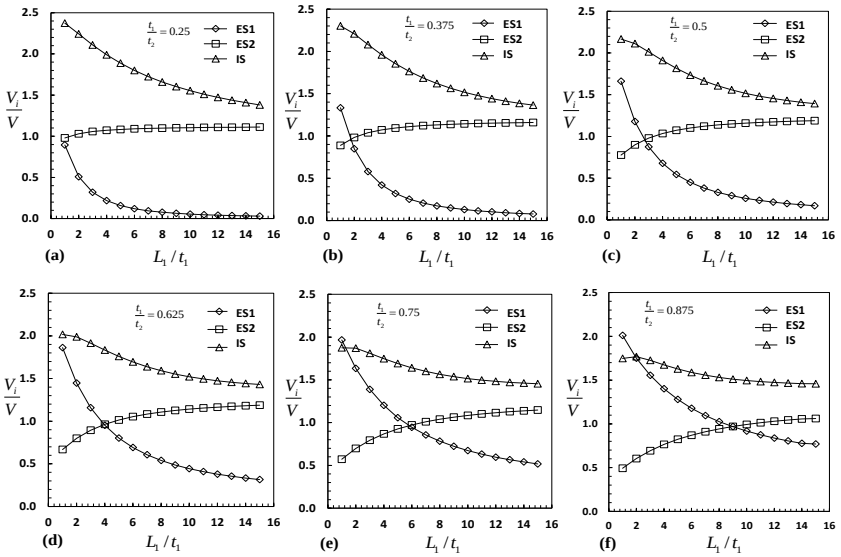

Figure 3.7: Effect of length/thickness ratio of ES1 on the average velocity ratio (Vi/V) for the T-die. (a) t1/t2=0.25; (b) t1/t2=0.375; (c) t1/t2=0.5; (d) t1/t2=0.625; (e) t1/t2=0.75; (f) t1/t2=0.875.

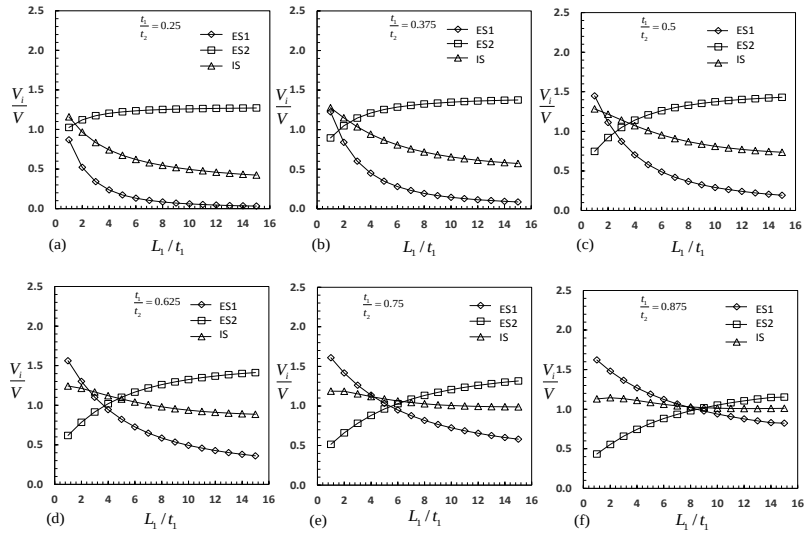

Figure 3.8: Effect of length/thickness ratio of ES1 on the average velocity ratio (Vi/V) for the L-die: (a) t1/t2=0.25; (b) t1/t2=0.375; (c) t1/t2=0.5; (d) t1/t2=0.625; (e) t1/t2=0.75; (f) t1/t2=0.875.

After collecting the balancing data points for all the *T* and *L* shaped die geometries, the results were compiled and plotted (Figure 3.9 for L_2/t_2=15, 10 and 5), to verify the existence of a behavior trend in both geometries (T and L).All the curves present a similar trend, with L_1/t_1 exhibiting a quadratic growth. Therefore, we have devised a fitting formula (Eq. 3.1) for the dependence of the balanced flow point (L_1/t_1) on the thickness ratio (t_1/t_2), that follows a quadratic relationship,

$$\frac{L_1}{t_1} = a(t_2, L_2/t_2)\left[\frac{t_1}{t_2}\right]^2 + b\,(t_2, L_2/t_2)\left[\frac{t_1}{t_2}\right] + c\,(t_2, L_2/t_2) \qquad (3.1)$$

where $a(t_2, L_2/t_2)$, $b(t_2, L_2/t_2)$ and $c(t_2, L_2/t_2)$, are fitting polynomials that are given in appendix.

In order to fit the data, we have used different solvers to minimize the difference between the numerical simulation data and the results obtained by the fitting function. The final results for the fitting function are shown in Figure 3.9, and the mean relative error is presented in

Table 3.2.

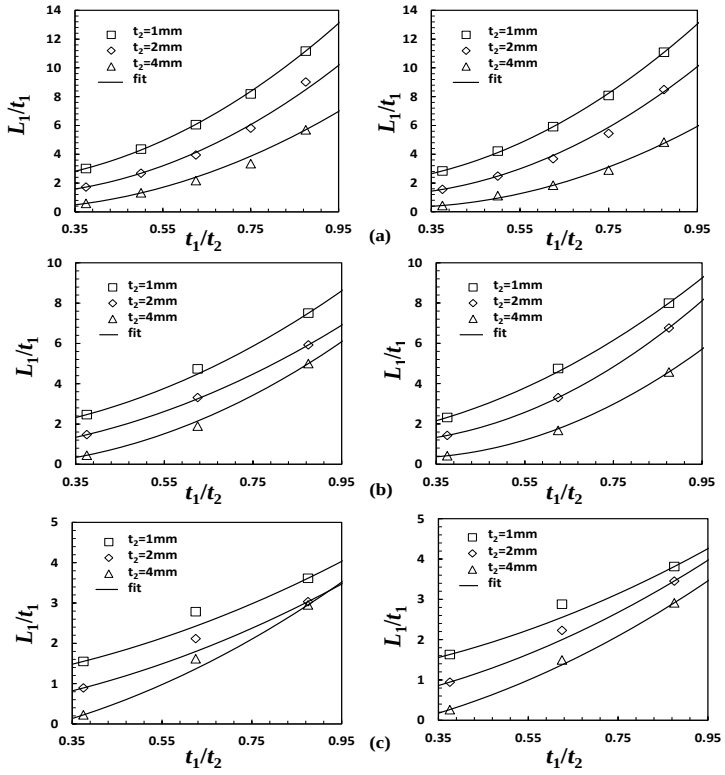

Figure 3.9: Dependence of the balanced flow point (L_1/t_1) on the thickness ratio (t_1/t_2) for the T-die (left) and L-die (right), for different thicknesses (t_2): (a) L_2/t_2=15; (b) L_2/t_2=10; (c) L_2/t_2=5.

Table 3.2: Mean relative errors, obtained with the fitting functions for the L and T die geometries.

		Mean Relative Error [%]		
	L_2/t_2	t_2=1mm	t_2=2mm	t_2=4mm
***L*-die**	5	3.801	3.478	2.744
	10	1.150	0.001	1.654
	15	0.853	3.131	4.784
***T*-die**	5	4.306	5.038	5.163
	10	1.822	0.638	4.506
	15	0.794	2.942	5.496

Note that the relative error tends to increase for low values of L_2/t_2 since in this case very small values of L_1/t_1 are obtained

3.5 Die Design Methodology

In this section, the die design methodology that makes use of the models (Eq. 3.1) obtained in the previous section, is presented. Since in a typical problem there are more restrictions than variables (for example, conflicting values of lengths of neighboring ESs), it is impossible to generate a flow channel having all its ESs lengths provided by the model.

Having this limitation in mind, two different optimization methods were devised to guide the design of profile extrusion dies based on the information provided by the model: one based on averaging the lengths of each section, **Average Method** (Figure 3.10), and another one based on the minimization of the differences between the length values given by the fitting functions applied to each ES and the actual length imposed, **Minimum Method**.

In order to facilitate the design methodology description, the design of the flow channel to produce the profile given in Figure 3.11 (a), was used for illustration purposes.

For the sake of clarity, the sequence of stages to be adopted is described in more detail in the following text, referring, whenever applicable, the numbered steps identified in Figure 3.10.

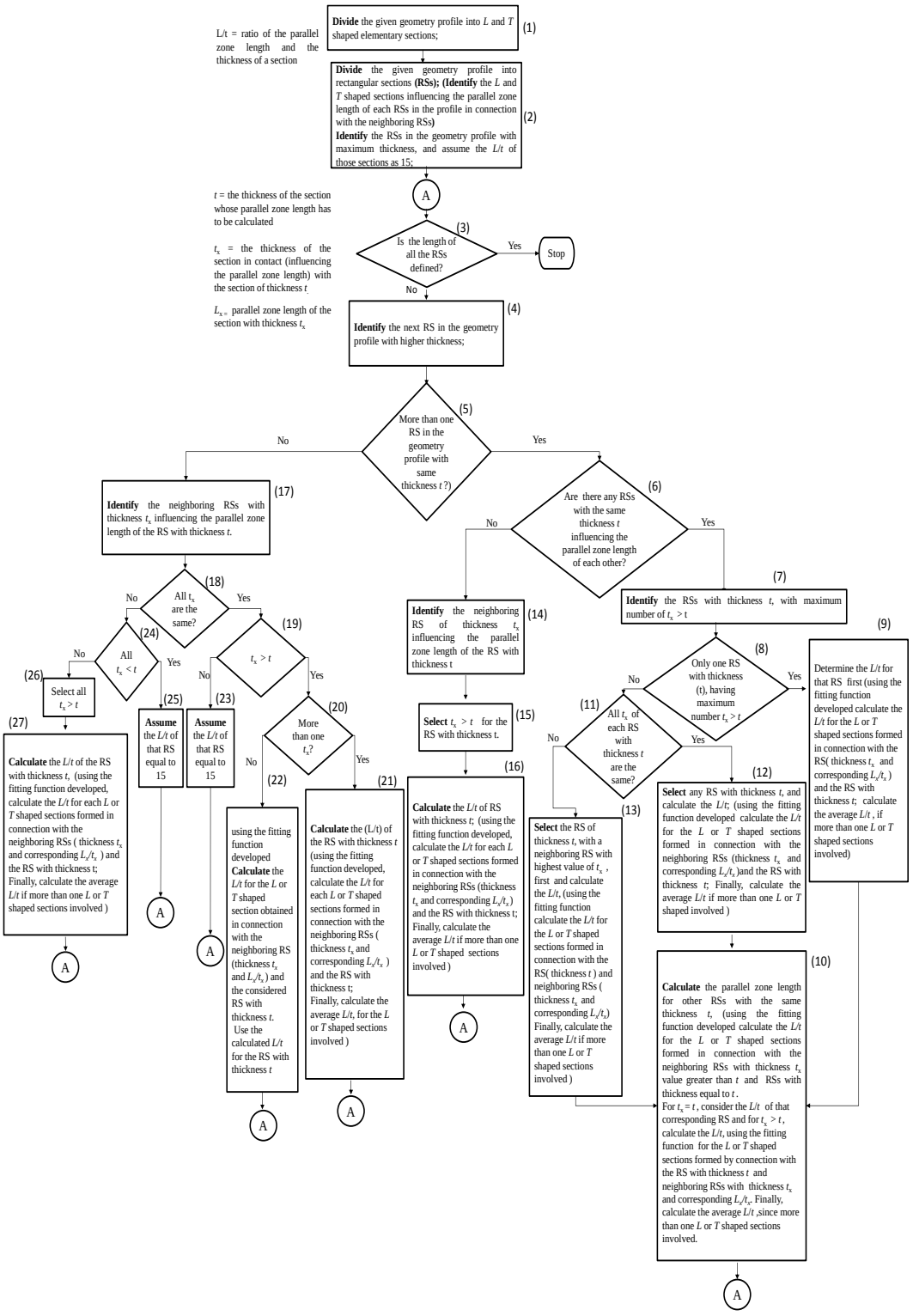

Figure 3.10: Flowchart of the optimization procedure using the Average Method.

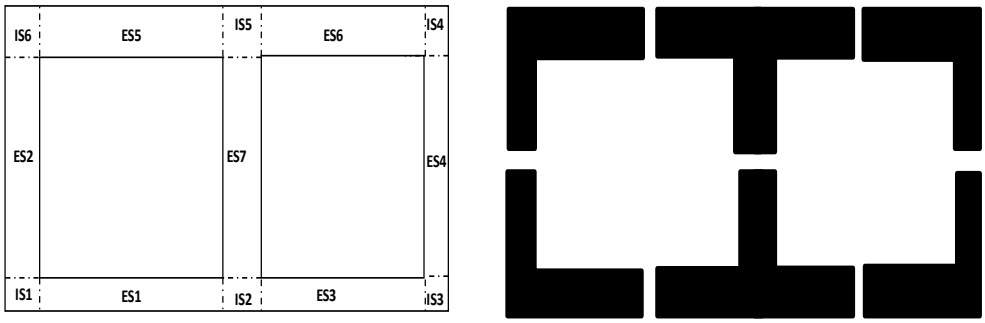

Figure 3.11: Complex geometry used in the simulations: (a) division into IS and ES; (b) partition into L and T shaped geometries.

Average Method (stages):

Although the algorithm presented in Figure 3.10 seems to be complex, its application is relatively straightforward, as can be seen from the following example.

1 Given the parallel zone cross section geometry, divide it into L and T shaped sections, as shown in Figure 3.11 (b) (Figure 3.10, step 1).

2 Divide the die outlet cross section into rectangular sections (RSs) (Figure 3.10, step 2). Each RS holds either one or more ES (due to machining requirements, we cannot have two ESs belonging to the same RS, having different thicknesses and/or lengths). The division of the parallel zone cross section into RSs is shown in Figure 3.12, where, for example, RS1 holds two elemental sections (ES5 and ES6) and RS2 holds only one elemental section (ES2).

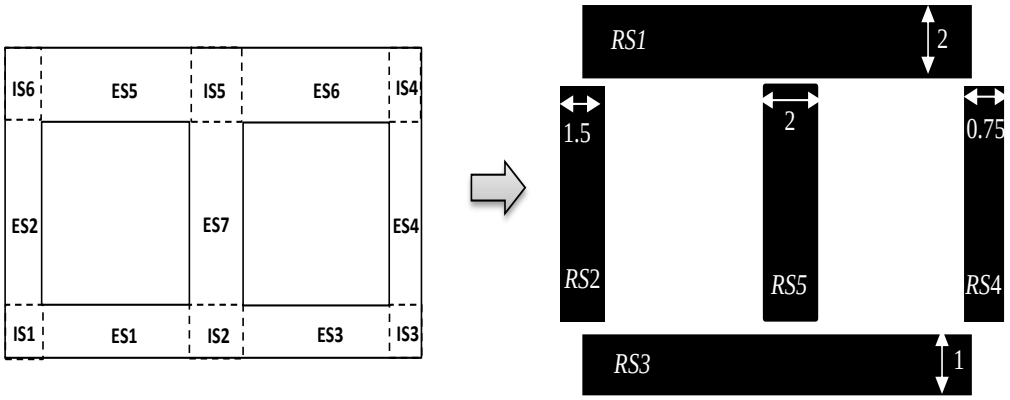

Figure 3.12: Example of the geometry used in the optimization process.

3 Identify the rectangular sections with the largest thickness and assume the ratio of the parallel zone length and thickness (L/t) of those sections as 15 (Figure 3.10, step 2). This value is the largest typical one used in profile extrusion dies (Nóbrega et al., 2004b).

In the example below (*Figure 3.12) there are five RSs, and RS1 and RS5 are those that have the largest thickness (2 mm). Therefore, we assume the L/t for these RSs is 15.*

4 Select the next rectangular section with the largest thickness.

In our example, the next section with highest thickness, after sections RS1 and RS5, is RS2. Therefore, we select RS2, with a thickness of 1.5 mm (Figure 3.10, step 4).

5 For the selected rectangular section, identify the neighboring RSs forming *L* or *T* shaped geometries, as indicated in flow chart (Figure 3.10, step 6 or 17, based on the condition given in step 5)

In the provided example, RS2 is connected to RS1 and RS3, as shown below in Figure 3.13, forming two L-shaped geometries (Figure 3.10, step 17).

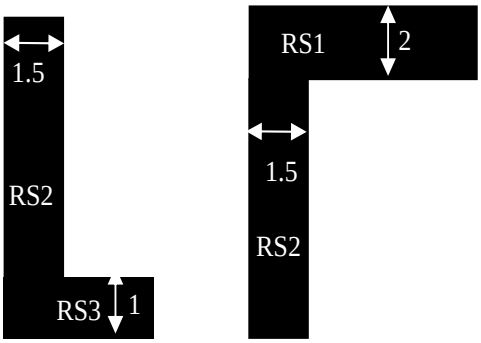

Figure 3.13: L-shaped geometries.

6 Using the model presented before (Eq. 3.1), determine the *L*/*t* ratio for the *L* or *T* shaped geometries identified in the previous stage. If the RS selected in stage 5 is connected to more than one RS, calculate the mean value of the L/t ratios obtained from the various *L* or *T* shaped geometries formed by the chosen RS (Figure 3.10, follow the branch of step 6 or 17, based on the condition given in step 5).

In the example provided, we use the model (Eq.3.1) to calculate the L/t ratio of RS2, from the two L shaped geometries shown in Figure 3.13. The L geometry formed by connecting RS2 and RS3 is not considered since the thickness of RS3 is smaller than that of RS2 (Figure 3.10, step 26). The L/t ratio obtained from the model (Eq.3.1) for the L shaped geometry formed by RS2 and RS1 is used as the L/t ratio of RS2.

7 Go to stage 4, to identify the next RS with larger thickness and proceed with stages 5 and 6 to define the *L/t* ratio for that RS using the model (Eq.3.1).

See in the example provided that the next RS with larger thickness is RS3, with a thickness of 1mm (Figure 3.12). The L or T geometries formed by RS3 are shown in Figure 3.14.

The L shaped geometry formed by RS3 and RS4 is not considered since the thickness of RS4 is smaller than that of RS3 (Figure 3.10, step 26). The L/t ratio is determined for the L shaped geometry formed by RS2 and RS3, and, for the T-shaped geometry formed by RS5 and RS3, using Eq.3.1. Then the average of the

two L/t ratios is calculated and used as the L/t ratio for RS3 (see flow chart in Figure 3.10 for more details).

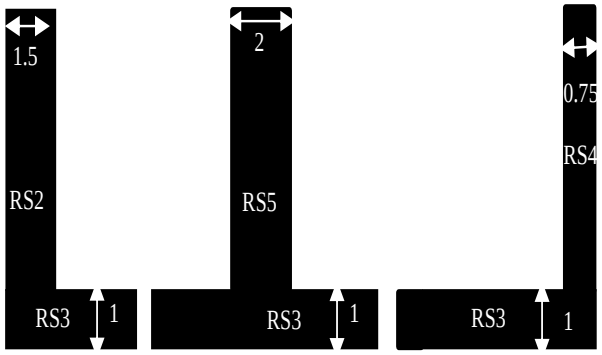

Figure 3.14: L and T shaped geometries forming RS3 and their neighboring RSs.

8 Go to stage 4 and repeat stages 4, 5 and 6, until all RSs lengths are defined.

For the alternative optimization method, the Minimum Method, the sequence of stages is the following.

Minimum Method (stages):

1 Given the parallel zone cross section geometry, divide it into L and T shaped sections, as shown in Figure 3.11 (b).

2 Divide the geometry into rectangular sections, and, assign a length variable to each one of these RSs (see Figure 3.12).
In the example of Figure 3.12 we have five rectangular sections and five length variables {RS1, RS2, RS3, RS4, RS}

3 Define an equation for each L and T shaped sections identified in Step 1, using the surrogate models devised in Section 3.4.

4 The system of equations obtained is implicitly solved using a minimum least squares method, as the *minimize* function from Mathematica software. This function minimizes the differences between the length values given by the model (Eq. 3.1) applied to each *L* and *T* geometries and the actual length imposed.

The solution provided allows to calculate the lengths for all RS. Note that sometimes we may only find a local minimum, thus for verification purposes the problem should be initiated with different starting solutions.

3.6 Die Design Methodology Assessment

The two simplified design methods, presented in the previous section, will now be tested for three different geometries, similar to that shown in Figure 3.11, considering three different sets of thicknesses for the different ESs. The initial trial geometry dimensions was assumed to have L/t =15 for all the sections, as recommended (Nóbrega et al., 2004b). For assessment purposes, numerical runs were performed for the initial trial geometry and the ones provided by both design methods

The ESs thicknesses are presented in Figure 3.15. On the left of this figure, one can see the initial trial lengths and the final ones obtained with the two design methods presented in Section 3.5. On the right, an objective function $F_{obj,i}$ is given for each ES,

$$F_{obj}(V_i) = \frac{\frac{V_i}{V_{obj}} - 1}{max\left(\frac{V_i}{V_{obj}}, 1\right)} \tag{3.2}$$

where, V_i stands for the numerically obtained average velocity for ESi and V_{obj} is the objective average velocity at the outlet. The objective function was developed in such a way that equal importance is given to the ratio $\frac{V_i}{V_{obj}}$ $(V_i < V_{obj})$ and $\frac{V_{obj}}{V_i}$ $(V_i > V_{obj})$.

For example, when we have a ratio $\frac{V_i}{V_{obj}} = 0.5$ the absolute $F_{obj}(V_i)$ value obtained is the same as for the case $\frac{V_i}{V_{obj}} = 2$. Defined in this way the flow distribution improves when $F_{obj}(V_i)$ approaches 0, being the ideal scenario when the $F_{obj}(V_i)$ are equal to zero for all ES.

Geometry 1

		Initial dimensions		Average method Final dimensions		Minimum method Final dimensions	
Elemental Sections	**Thickness of ESs (mm)**	**L_1/t_1**	**L_1**	**L_1/t_1**	**L_1**	**L_1/t_1**	**L_1**
ES4	0.75	15	11.25	1.53	1.15	1.5	1.125
ES1,ES3	1	15	15	2.77	2.77	2.73	2.73
ES2	1.5	15	22.5	5.87	8.81	5.58	8.37
ES7	2	15	30	15	30	16.73	37.19
ES5,ES6	2	15	30	15	30	12.91	25.82

(a)

Geometry 2

		Initial dimensions		Average method Final dimensions		Minimum method Final dimensions	
Elemental Sections	**Thickness of ESs (mm)**	**L_1/t_1**	**L_1**	**L_1/t_1**	**L_1**	**L_1/t_1**	**L_1**
ES4	0.75	15	11.25	1.53	1.15	1.43	1.07
ES7	1	15	15	2.68	2.68	2.61	2.61
ES1,ES3	1	15	15	2.77	2.77	3.1	3.1
ES2	1.5	15	22.5	5.87	8.81	5.9	8.85
ES5,ES6	2	15	30	15	30	17.36	34.72

(b)

Geometry 3

		Initial dimensions		Average method Final dimensions		Minimum method Final dimensions	
Elemental Sections	**Thickness of ESs (mm)**	**L_1/t_1**	**L_1**	**L_1/t_1**	**L_1**	**L_1/t_1**	**L_1**
ES4	0.75	15	11.25	1.81	1.36	1.46	1.095
ES7	1	15	15	3.12	3.12	2.21	2.21
ES2	1.5	15	22.5	6.9	10.35	4.74	7.1
ES1,ES3	1.8	15	27	15	27	7.12	12.82
ES5,ES6	2	15	30	15	30	9.742	19.48

(c)

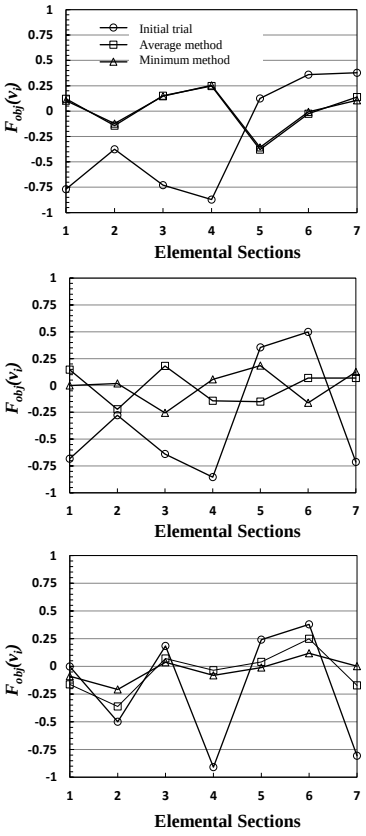

Figure 3.15: (left) Geometry dimensions used as initial solution, together with the final dimensions obtained using the Average and Minimum methods. (right) F_obj (V_i) obtained at each section, for the three different geometries and design method. (a) Geometry 1; (b) Geometry 2; (c) Geometry 3.

By looking at Figure 3.15, an obvious conclusion is that both methods (**Average** and **Minimum**) allow a significant improvement of the flow distribution, when compared with the initial trial, where *L*/*t*=15 was considered for all ESs. As shown in Figure 3.15 when considering *L*/*t*=15, an unbalanced flow is always obtained,

especially at the thinner ES (ES1, 3 and 4 in Geometry 1; ES1, 3, 4 and 7 in Geometry 2; ES4 and 7 in Geometry 3).

When the proposed design methods are applied, a significant improvement on the flow distribution is achieved. For example, in Geometry 1 we have an initial objective function value of approximately -0.9 for ES4, while using the optimization methods, a value of 0.25 is obtained. The same happens for the other two geometries. In general, the high oscillations of the objective function obtained with the initial trials were suppressed by both design methods when applied to the three geometries tested. Also, a good flow balancing was obtained for all the optimized geometries.

In Geometry 1 the Average and Minimum methods provide similar results, but, when some of the thicknesses are changed, the methods tend to provide different optimized solutions. For example, in Geometry 2 we have two rectangular sections with the same thickness, and, depending on the method, the path for an optimized solution is different. Even though, the absolute value results are similar for both methods, except at ES1 and ES2 where the Minimum Method provide better results (the objective function gives a value of approximately 0), and ES6 where the Average Method shows a better balancing of the flow. For Geometry 3 both methods show the same tendency, with the Minimum Method providing the best results.

The improvements obtained, which implies a more uniform velocity distribution, can also be observed in Figure 3.16, Figure 3.17 and Figure 3.18 where the velocity contours are shown for the three versions of all the Geometries used in the assessment (initial and optimized with the two design methods).

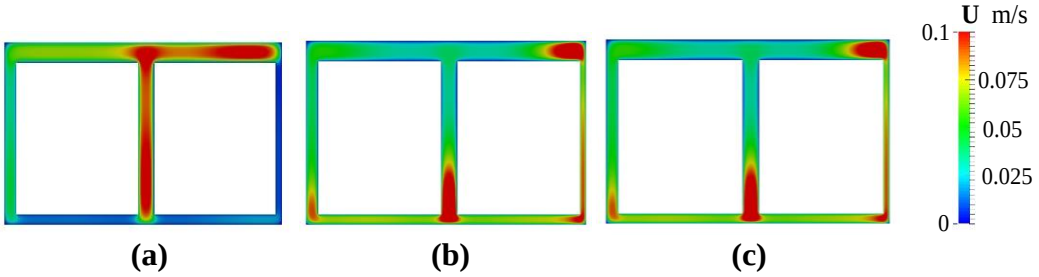

Figure 3.16: Velocity contour plots corresponding to Geometry 1: (a) initial; final obtained using the (b) Average Method and (c) the Minimum Method.

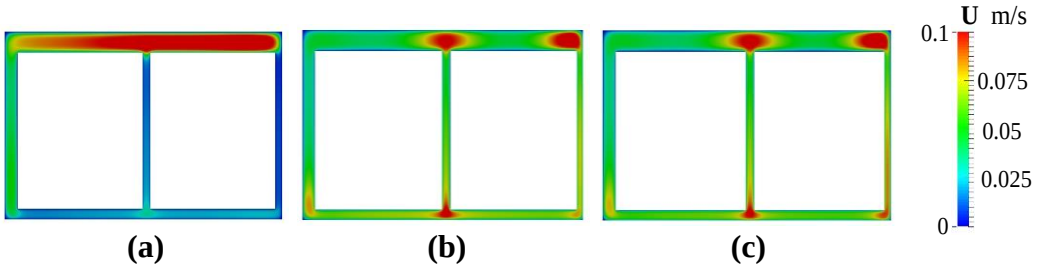

Figure 3.17: Velocity contour plots corresponding to Geometry 2: (a) initial; final obtained using the (b) Average Method and (c) the Minimum Method.

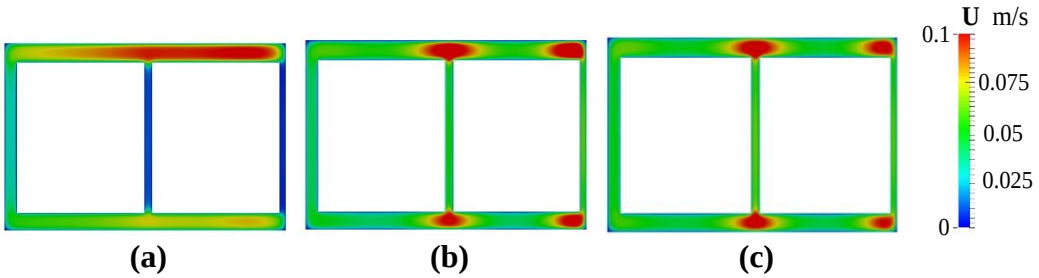

Figure 3.18: Velocity contour plots corresponding to Geometry 3: (a) initial; final obtained using the (b) Average Method and (c) the Minimum Method.

In order to quantify the differences between the two methods, we have measured the error on each ES, for the three geometries studied. First we have created the error vector, *error*=(V_1-1, V_2-1,…,V_7-1), and, we have calculated the L_2 norm of the error, obtaining a value of 1.654 for the trial geometry, 0.592 for the Average Method and

0.562 for the Minimum Method. These are the results obtained for Geometry 1. For the same purpose we have also computed the $L\infty$ norm. A compilation of these results is shown in Table *3.3*

It can be seen that the Minimum Method provides the smallest error (highlighted values in Table *3.3*). As expected, the coupled solution of the equations influencing each ES, inherent to this method, provides better results since the overall influence of one section over the other is taken in to account. However, the results obtained with the Average Method also show a good flow distribution. Moreover, this method is much simpler and self-contained, when compared to the Minimum Method that requires specific software to perform the minimization process.

Table 3.3: Error obtained for the different methods.

Geometry 1	L_2	L_∞
Initial trial	1.654	0.872
Average Method	0.592	0.379
Minimum Method	0.562	0.357

Geometry 2	L_2	L_∞
Initial trial	1.863	0.993
Average Method	0.427	0.223
Minimum Method	0.413	0.255

Geometry 3	L_2	I_∞
Initial trial	1.499	0.908
Average Method	0.553	0.362
Minimum Method	0.278	0.208

3.7 Conclusions

The main objective of this work was to provide simplified guidelines to aid the design of complex profile extrusion dies that do not depend on the use of numerical

modelling codes. For this purpose, we have derived a new methodology that used results of detailed numerical studies to devise surrogate models for the behavior of extrusion dies used to produce L and T-shaped profiles. As a large quantity of profiles can be decomposed into those more basic (L and T) shapes, the devised surrogate models were employed to develop an innovative die design procedure, for which two alternative approaches were proposed: the Average Method and Minimum Methods.

The proposed methods were assessed with a complex geometry considering three different case studies. The significant improvements, when compared to the usual initial trial used in industry, obtained for the flow distribution at the extrusion die outlet confirmed the efficiency of the proposed design methodologies.

The results provided by both methods (Average and Minimum) were similar, but the Minimum Method proved to be slightly more efficient. Moreover, the Average Method is self-contained, while the Minimum Method requires the use of a software (in our case Mathematica) to find the solution of a system of equations. Consequently, the most appropriate method for each case will depend on the software available to support the design tasks.

3.8 References

Carneiro, O. S., Nóbrega, J. M., Oliveira, P. J., and Pinho, F. T. (2004). Accounting for temperature-dependent properties in viscoelastic duct flows, *International journal of heat and mass transfer* **47**(6): 1141-1158.

Carneiro, O. S. and. Nóbrega J. M. (2012). *Design of Extrusion forming Tools*, Smithers Rapra Technology Ltd.

Elgeti, S., Probst, M., Windeck, C., Behr, M., Michaeli, W., and Hopmann, C. (2012). Numerical shape optimization as an approach to extrusion die design, *Finite Elements in Analysis and Design* **61**: 35-43.

Ettinger, H., Sienz, J., Pittman, J., and Polynkin, A. (2004). Parameterization and optimization strategies for the automated design of uPVC profile extrusion dies, *Structural and Multidisciplinary Optimization* **28**(2-3): 180-194.

Ettinger, H., Pittman, J., and Sienz, J. (2013). Optimization-driven design of dies for profile extrusion: Parameterization, strategy, and performance, *Polymer Engineering & Science* **53**(1): 189-203.

Flow2000 (2016).
URL: http://www.futuresoft.net/F2k-ext.htm.

Goncalves, N. D. F. (2013). *Computer aided design of extrusion forming tools for complex geometry profiles*, Ph.D Thesis, University of Minho.

Harten, A. (1983). High resolution schemes for hyperbolic conservation laws, *Journal of computational physics* **49**(3): 357-393.

Huneault, M., Lafleur, P. and Carreau, P. (1996). Evaluation of the FAN technique for profile die design, *International Polymer Processing* **11**(1): 50-57.

Hurez, P., Tanguy, P. and Blouin, D. (1996). A new design procedure for profile extrusion dies, *Polymer Engineering & Science* **36**(5): 626-635.

Lebaal, N., Schmidt, F.and Puissant, S. (2009). Design and optimization of three-dimensional extrusion dies, using constraint optimization algorithm, *Finite Elements in Analysis and Design* **45**(5): 333-340.

Lehnhäuser, T. and Schäfer M. (2005). A numerical approach for shape optimization of fluid flow domains, *Computer methods in applied mechanics and engineering* **194**(50): 5221-5241.

Mathematica (2016).

URL: http://www.wolfram.com/mathematica/source=nav

McKelvey, J. M. and Ito, K. (1971). Uniformity of flow from sheeting dies, *Polymer Engineering & Science* **11**(3): 258-263.

Mehta, B. V., Ghulman, H. and Gerth, R. (1999). Extrusion die design: a new methodology of using design of experiments as a precursor to neural networks, *Journal of Materials* **51**(9).

Michaeli, W. (1984). *Extrusion Dies Design and Engineering Computations*, Hanser Publishers.

Nóbrega, J. M. (2004). *Computer aided design of forming tools for the production of Extruded profiles*, Ph.D Thesis, University of Minho.

Nóbrega, J. M., Carneiro, O. S. Oliveira, P. J. and Pinho,F. T. (2003a). Flow Balancing in Extrusion Dies for Thermoplastic Profiles Part I : Automatic Design, *International Polymer Processing* **vol. XVIII**.

Nóbrega, J. M., Carneiro, O. S. Oliveira, P. J. and Pinho,F. T. (2003b). Flow Balancing in Extrusion Dies for Thermoplastic Profiles: Part II: Influence of the Design Strategy, *International Polymer Processing* **18**(3): 307-312.

Nóbrega, J. M., Carneiro, O. S. Oliveira, P. J. and Pinho,F. T. (2004b). Flow Balancing in Extrusion Dies for Thermoplastic Profiles: Part III: Experimental Assessment, *International Polymer Processing* **19**(3): 225-235.

OpenFOAM® (2016).
URL: http://openfoam.org/version/2-3-0/.

Patankar, S. V. and Spalding, D. B. (1972). A calculation procedure for heat, mass and momentum transfer in three-dimensional parabolic flows, *International Journal of Heat and Mass Transfer* **15**(10): 1787-1806.

Polycad (2016).
URL: http://www.polydynamics.com.

Sienz, J., Goublomme, A.and Luege, M. (2010). Sensitivity analysis for the design of profile extrusion dies, *Computers & structures* **88**(9): 610-624.

Summers, J. and Brown, R. (1981). Practical principles of die design—a simplified procedure, in table form, for rigid PVC, *Journal of Vinyl Technology* **3**(4): 215-218.

Tadmor, Z. and Gogos, C. G. (2006). *Principles of polymer processing*, John Wiley & Sons.

Ulysse, P. (1999). Optimal extrusion die design to achieve flow balance, *International journal of machine tools and manufacture* **39**(7): 1047-1064.

Ulysse, P. (2002). Extrusion die design for flow balance using FE and optimization methods, *International Journal of Mechanical Sciences* **44**(2): 319-341.

Wortberg, J., Haberstroh, E., Lutterbeck, J., Masberg, U., Schmidt, J. and Targiel, G. (1982). Designing of extrusion lines, *Advances in Polymer Technology* **2**(2): 75-106.

Wu, C.Y. and Hsu, Y. C. (2002). Optimal shape design of an extrusion die using polynomial networks and genetic algorithms, *The International Journal of Advanced Manufacturing Technology* **19**(2): 79-87.

Yilmaz, O., Gunes,H., and Kirkkopru, K. (2014). Optimization of a profile extrusion die for flow balance, *Fibers and Polymers* **15**(4): 753-761.

Yu, Y. W. and Liu, T. J. (1998). A simple numerical approach for the optimal design of an extrusion die, *Journal of Polymer Research* **5**(1): 1-7.

3.9 Appendix

The fitting function, or model, is given by:

$$\frac{L_1}{t_1} = a(t_2, L_2/t_2)\left[\frac{t_1}{t_2}\right]^2 + b\,(t_2, L_2/t_2)\left[\frac{t_1}{t_2}\right] + c\,(t_2, L_2/t_2).$$

For the *L*-die, the coefficients are given as follows, $a=x_1(t_2)^2+y_1(t_2)+z_1$, $b=x_2(t_2)^2+y_2(t_2)+z_2$ and $c=x_3(t_2)^2+y_3(t_2)+z_3$.

For the *T*-die, the coefficients are given by $a=u_1(t_2)^2+v_1(t_2)+w_1$, $b=u_2(t_2)^2+v_2(t_2)+w_2$ and $c=u_3(t_2)^2+v_3(t_2)+w_3$,

***L*-die**

	Parameters	Quadratic equations
a	x_1	$0.03734510(L_2/t_2)^2 - 0.80169016\,(L_2/t_2) + 2.93937832$
	y_1	$-0.24939070(L_2/t_2)^2 + 5.08338350(L_2/t_2) - 18.26560500$
	z_1	$0.23746280(L_2/t_2)^2 - 3.38520534(L_2/t_2) + 12.91528668$
b	x_2	$-0.04051703(L_2/t_2)^2 + 0.91053283(L_2/t_2) - 3.54060001$
	y_2	$0.27547970(L_2/t_2)^2 - 6.07985350(L_2/t_2) + 23.52837000$
	z_2	$-0.30383447(L_2/t_2)^2 + 6.00266366(L_2/t_2) - 21.44919999$
c	x_3	$0.01189827(L_2/t_2)^2 - 0.25518200(L_2/t_2) + 1.11254833$
	y_3	$-0.07780220(L_2/t_2)^2 + 1.65860100(L_2/t_2) - 7.51204500$
	z_3	$0.08473653(L_2/t_2)^2 - 1.65247800(L_2/t_2) + 8.05443667$

_T_-die

	Parameters	Quadratic equations
a	u_1	$-0.03283900(L_2/t_2)^2 + 0.60375660(L_2/t_2) - 2.09687500$
	v_1	$0.12601310(L_2/t_2)^2 - 2.43891870(L_2/t_2) + 8.89061200$
	w_1	$-0.04083970(L_2/t_2)^2 + 2.16125150(L_2/t_2) - 7.21692400$
b	u_2	$0.03474026(L_2/t_2)^2 - 0.60500330(L_2/t_2) + 2.17478900$
	v_2	$-0.14470624(L_2/t_2)^2 + 2.42773880(L_2/t_2) - 8.60696400$
	w_2	$0.05018524(L_2/t_2)^2 - 1.12527240(L_2/t_2) + 5.42178600$
c	u_3	$-0.00788694(L_2/t_2)^2 + 0.14490350(L_2/t_2) - 0.44020200$
	v_3	$0.03579614(L_2/t_2)^2 - 0.65609770(L_2/t_2) + 1.45577200$
	w_3	$-0.02011246(L_2/t_2)^2 + 0.49551710(L_2/t_2) - 0.30281100$

Chapter 4

Guidelines for balancing the flow in extrusion dies: the influence of the material rheology

Abstract

In this work we present improved design guidelines to support the die designer activity, when searching for the flow channel geometry that allows the achievement of a balanced flow distribution, in complex profile extrusion dies.

The proposed methodology relies on surrogate models, obtained through a detailed and extensive numerical study, carried out with the open source computational library OpenFOAM®in which an appropriate numerical solver for the problems under study was implemented.

The main contribution of this work is to further enlarge the applicability of the simplified design methodology proposed by this group for similar purposes in the previous Chapter 3, by considering the effect of processing parameters and material rheology.

The sensitivity analyses performed showed that, among the studied parameters, the power-law exponent was the only one that affected the system behavior. Thus, the previous proposed surrogate models were modified to include the effect the material power-law exponent.

Verification studies performed for three geometries and different rheological and process parameters, evidenced the effectiveness of the proposed simplified design methodology.

This chapter was adapted from: A. Rajkumar, L.L. Ferrás, C. Fernandes, O. S. Carneiro and , J.M. Nóbrega (2016). "Guidelines for balancing the flow in extrusion dies: the influence of the material rheology", submitted to The Journal of Polymer Engineering, January 2017.

4.1 Introduction

From all the difficulties encountered in the design of profile extrusion dies, flow balancing (i.e. obtaining similar average velocity in all the sections of the die exit (Michaeli and Kaul, 2004; Carneiro and Nóbrega, 2012)) remains a major challenge, whose success is highly dependent on the experience of the tool designer.

Several parameters may influence the distribution of the flow at the die exit, namely, the material behavior, the processing conditions, such as temperature and flow rate, the geometry of the die flow channel, etc. The rheological properties of the polymer melt play a major role in the flow distribution, demanding a tailored design for each material (Rauwendaal, 2014).

The approaches proposed in the literature to solve this problem can be grouped into analytical, numerical and experimental, but, most of them are only related to specific materials and processing conditions.

Due to their intrinsic limitations, just a few studies are supported by analytical methods, and, based on its potentialities, a relatively larger number of works report numerical approaches that take into account the influence of the rheological parameters and processing condition on the flow balancing of extrusion dies.

For example, a study on the use of analytical flow computations and trial-and-error methods to balance the flow in each section of the extrusion die, by modifying the land length and die entry angle, was given by Michaeli (1984).Tadmor and Gogos (2006), proposed a similar approach to improve the die design process, comprising the combination of analytical calculations along with the practical rules obtained from experimental practice.

In a research study by Hurez et al. (1996), a design procedure for complex profile extrusion dies based on a blend of the Flow Analysis Network approach was developed. This method was applied for flow balancing of multiple channel dies, allowing to obtain

the channel topology that endorses a uniform flow distribution at the flow channel outlet. The proposed approach showed very good results for all the cases considered.

Reid et al. (2003), studied analytically the influence of the material rheology on the flow distribution in coat hanger dies using a 1-D design equation. The study concluded that the power-law index *n* has a small effect over the flow uniformity, but they did not consider the influence of cross lateral flows. The use of analytical models allow the creation of a better initial die geometry, but, since most of the works based on these models can only consider 1D or 2D flows (Wu et al., 2006), significant simplifications must be undertaken, which may lead to poorly designed dies in practice.

Nowadays, numerical modeling codes are becoming more powerful, due to the availability of faster processors and the possibility of performing parallel computations, allowing more accurate simulations of the fluid flow in complex extrusion dies in a reasonable timeframe.

Regarding studies carried out with the support of numerical tools, (McKelvey and Ito, 1971), analyzed the flow uniformity on sheeting dies, considering the power-law model for capturing the polymer non-Newtonian behavior. By using a uniformity index, the method allowed the calculation of new extrusion die dimensions (for a specific flow rate and pressure drop), leading to a uniform flow distribution. Contrarily to Reid et al. (2003), they concluded that the power law index *n* plays a key role in the flow distribution.

Proctor (1972), studied the flow of a power-law fluid under isothermal conditions in spiral-mandrel dies. The results obtained allowed to evidence a clear influence of the power-law index on the flow distribution. Chen et al. (1997), studied the optimization of a coat hanger profile using the Taguchi method, which allowed them to conclude that the velocity distribution at the outlet of the die was influenced by the material rheology, processing conditions and die geometry.

A global optimization approach based on numerical methods for the design of profile extrusion dies was proposed by Carneiro et al. (2001). The methodology presented in their study could deal with rheological defects, flow balancing and post-extrusion phenomena. A numerical code to optimize the extrusion die flow channel geometry was developed by Nóbrega (2004), however the code was limited to simple geometry profiles, because it was able to cope just with structured computational meshes. Considering this restriction, Goncalves (2013) prepared a novel numerical code able to deal with complex profiles based on unstructured meshes.

Elgeti et al. (2012), presented a novel design procedure which encompass two steps, systematic design of initial geometry, and numerical shape optimization of the flow channel. The examples used in their study are a slit profile and a floor skirting. The study also compared the results predicted from two different rheological models, namely Newtonian fluid and non-Newtonian inelastic fluid modelled by the Carreau model, and the results indicate that the Carreau model shows a significant impact on the predictions accuracy. The influence of the rheological parameters and operating conditions on the flow channel outlet velocity distribution was discussed numerically by several other researchers Lebaal et al. (2012). Their main conclusions were that the parameters flow rate and the zero-shear viscosity have no significant influence on the flow distribution, while the power-law index shows a strong effect (Nóbrega et al., 2003b).

Moreover, there are many commercially available softwares that can be used to support the extrusion die design process, namely, ANSYSPolyflow, Dieflow, Compuplast, and Polydynamics. ANSYSPolyflow, provides solutions for companies in the polymer, glass, metals and cement processing industries. Dieflow has applications in design of flat extrusion dies for film, sheet and coating processes, annular dies for tube and sheet applications, flat and annular dies for foam applications and profile dies. Compuplast and Polydynamics Inc. provide softwares that can be used to support the design of profile and spiral die, among several others.

In what concerns to experimental investigations on the flow uniformity at the exit of an extrusion die, we may refer the work of Zolfaghari et al. (2010) that considered different polyethylene/wood flour formulations and an U-shaped extrusion die. Their results indicate that the increase of wood flour content endorse plug flow with enhanced slip, making the flow balancing process less critical. In another experimental based study, Grieß and Münstedt (2012) concluded that the power-law index n has a significant influence on the velocity distribution in a coat-hanger die, in agreement with some theoretical results referred above.

In conclusion, it is consensual that the most accurate approach to deal with the complex task of designing a complex geometry die is to do it with the support of numerical modelling codes. However, a problem faced by several companies is that they do not have a specialist in numerical modeling able to take advantage of the available tools. Moreover, the cost of commercial modelling codes licenses is usually prohibitive for small to medium size companies. Thus, most of currently employed die design methodologies, in industrial practice, are still based on experimental trial-and-error approaches, whose success is highly dependent on the accumulated experience, which clearly limits the design process efficiency.

Having those restrictions in mind, we devised, in a previous work explained in Chapter 3, simple design guidelines to aid the design of relatively complex profile extrusion dies, for die designers with no access to numerical modeling tools. Those guidelines are based on surrogate analytical models obtained by detailed numerical modelling studies, but can be applied just for a narrow range of materials, with similar rheological properties to the ones used in Chapter 3. Therefore, the aim of the present work is to expand the applicability of the previously proposed simplified design guidelines, by considering the influence of the material rheological parameters (power law Index (n), zero shear rate viscosity (η_0), and the relaxation time (λ)) and some processing conditions (extrusion velocity (V) and temperature (T)).

The remainder of this chapter is organized as follows. In Section 4.2 we describe the methodology, the geometry, the boundary conditions, the numerical code employed, and, present the mesh sensitivity study performed. In Section 4.3 we study the influence of the material rheology and processing conditions on the flow distribution, to select the most relevant parameters to be included in the improved models. In Section 4.4 the new surrogate models developed to mimic the flow distribution in profile extrusion dies, are presented, taking into account the parameters identified in the previous section. The accuracy of the new developed models is assessed in Section 4.5. The chapter ends with the main conclusions.

4.2 Methodology

Several complex profile geometries can be composed by a combination of *L* and *T*-shaped simpler geometries, as illustrated in Figure 4.1. Therefore, aiming the development of surrogate models with a similar methodology to the ones proposed in Chapter 3, in this work we study the fluid flow inside simple L and T shaped extrusion dies. The studies performed to devise the surrogate models aim to identify the flow channel geometry dimensions that promote a balanced flow distribution at the flow channel outlet. The models obtained should allow the optimization of relatively complex (combination of *L* and *T*-shaped simpler geometries) profile extrusion dies.

The aim of this study is then to enlarge the applicability of the surrogate models proposed in Chapter 3 to a wide range of material properties and processing conditions.

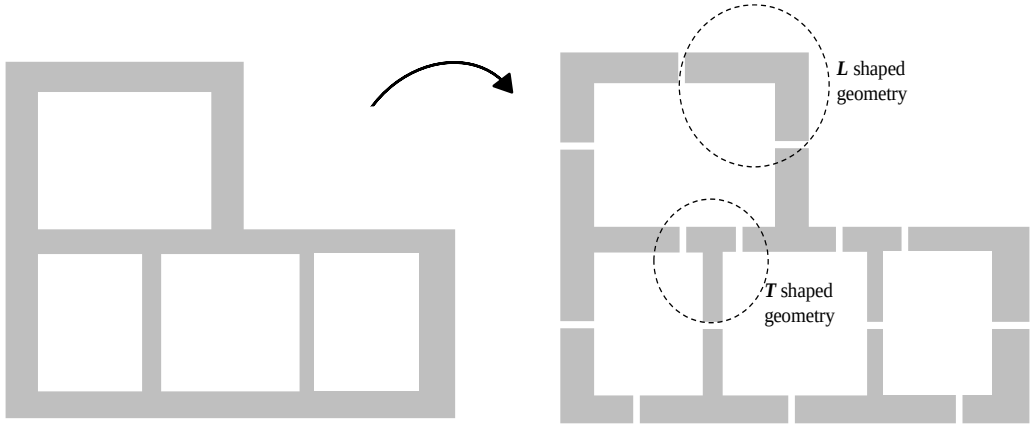

Figure 4.1: Complex profile geometry illustrating its decomposition into L and T shaped subsections.

4.2.1 Geometry and boundary conditions

The parameterized geometry of both *L* and *T* shaped dies studied in this work is illustrated in Figure 4.2. To monitor the flow distribution, the flow outlet cross sections were divided into elemental sections (ESs) and intersection Sections (ISs), as presented in Figure 4.3. In this way each ESi (with i=1,2) has two parameters that define the geometry, the length, L_i, and the thickness, t_i. Notice that assuming the flow channel outlet cross section cannot be modified (i.e. the ES thicknesses, t_i, cannot be changed), the flow distribution is mainly determined by the ESs lengths (L_i). Moreover, the IS flow rate cannot be controlled directly, since it does not have any geometrical parameter associated, thus the flow rate in these regions is a consequence of the flow in the neighboring ESs. Based on the above, the detailed numerical based studies were performed to identify the ESs that allows to balance the flow at the die exit (i.e., to achieve an equal average velocity in both ESs), for a wide range of geometries, materials properties and processing conditions.

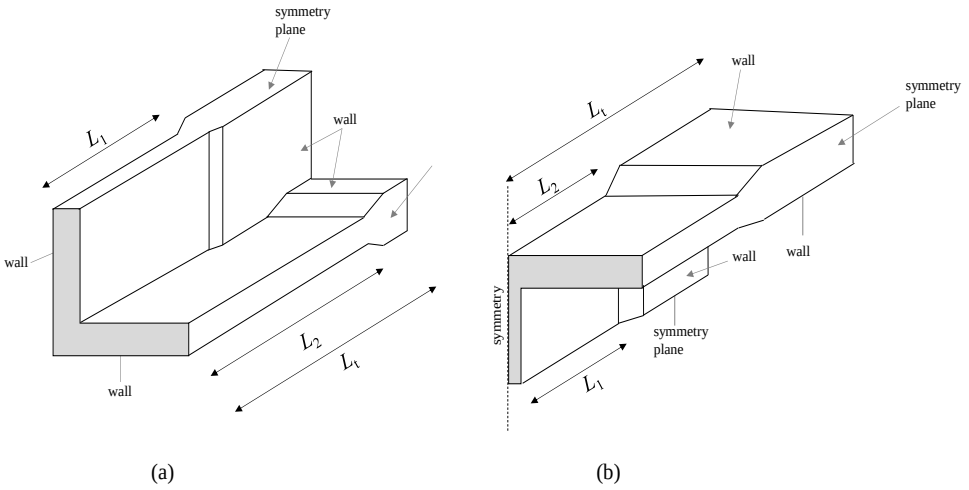

Figure 4.2: Flow channel geometry and respective boundary conditions: (a) L-die; (b) T-die (only half of the geometry is shown due to symmetry reasons).

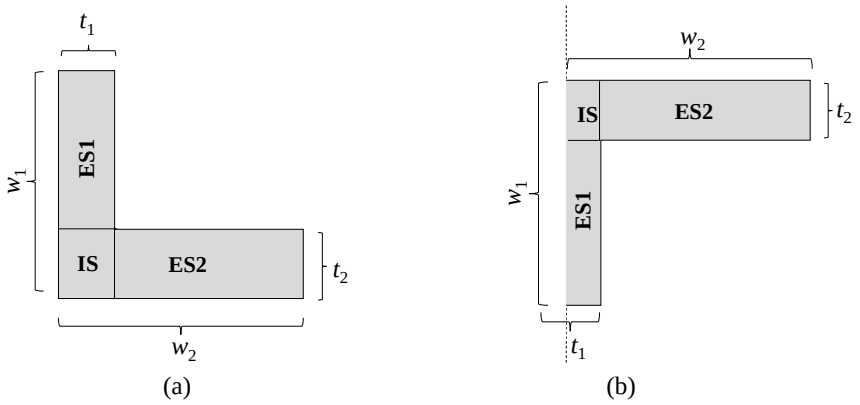

Figure 4.3: Division of die outlet into ESs and Intersections ISs: (a) L-shaped die; (b) T-shaped die (only half of the profile is shown due to symmetry).

For the numerical runs a fully developed velocity profile was imposed at the flow channel inlet. This velocity profile was obtained by performing simulations in a constant (and equal to that of the full extrusion die flow channel inlet) cross-section flow channel, using cyclic outlet-inlet boundary, same as the one used in Chapter 3.

For the velocity at the flow channel outlet, a zero gradient boundary condition was used, and at the wall the usual no slip boundary condition was considered. For the pressure, at the inlet and walls, a zero gradient boundary condition was assumed and a

null pressure was imposed at the outlet. For the temperature, a Dirichlet boundary condition was considered at the flow channel walls and inlet, and, a zero gradient boundary condition was assumed at the outlet.

4.2.2 Numerical procedure

The open source computational library OpenFOAM® was used to solve the coupled system of differential governing equations that was provided in Chapter 2 (Section 2.3.1). This numerical code uses the Finite Volume Method to perform the discretization for those set of governing equations. The non-isothermal solver and the library for modeling the Bird-Carreau model coupled to the Arrhenius temperature law used in Chapter 2, were also employed on this chapter.

The SIMPLE method was used to couple the pressure and velocity, with the energy equation being solved at the end of each iteration, after updating velocity the pressure fields. The momentum convective terms were discretized using the Minmod scheme. A Gauss linear scheme was employed to discretize all the diffusion terms and the advective term of the energy conservation equation.

4.2.3 Mesh sensitivity studies

In order to identify the most adequate mesh refinement level to use in the numerical studies, we followed a similar procedure to the one presented in the previous Chapter (Chapter 3) for the same purpose. The *L* shaped extrusion die with t_2 = 2 mm, t_1= 1.5mm, L_1/t_1 and L_2/t_2 equal to 15, was used for the mesh sensitivity studies. To evaluate the calculation accuracy, the average of the outlet velocity, maximum temperature in the flow channel, and pressure drop, were computed for different meshes with increasing density. The consecutive meshes were obtained by doubling the number of cells in each domain edge, resulting in different meshes with computational cells 5760, 48144,

418880 and 3453312. As shown in Figure 4.4, the value of the monitored quantities (normalized with the reference value obtained for the finer mesh) predicted by the third mesh already present a good level of accuracy, with a maximum difference of circa 0.5% to the fourth mesh. These results allowed to conclude that the meshes with a refinement level of the one presented in Figure 4.5 (with circa 420000 computational cells), provided an adequate calculation accuracy, within an acceptable computation time. Thus this mesh refinement level was employed for all the numerical studies performed.

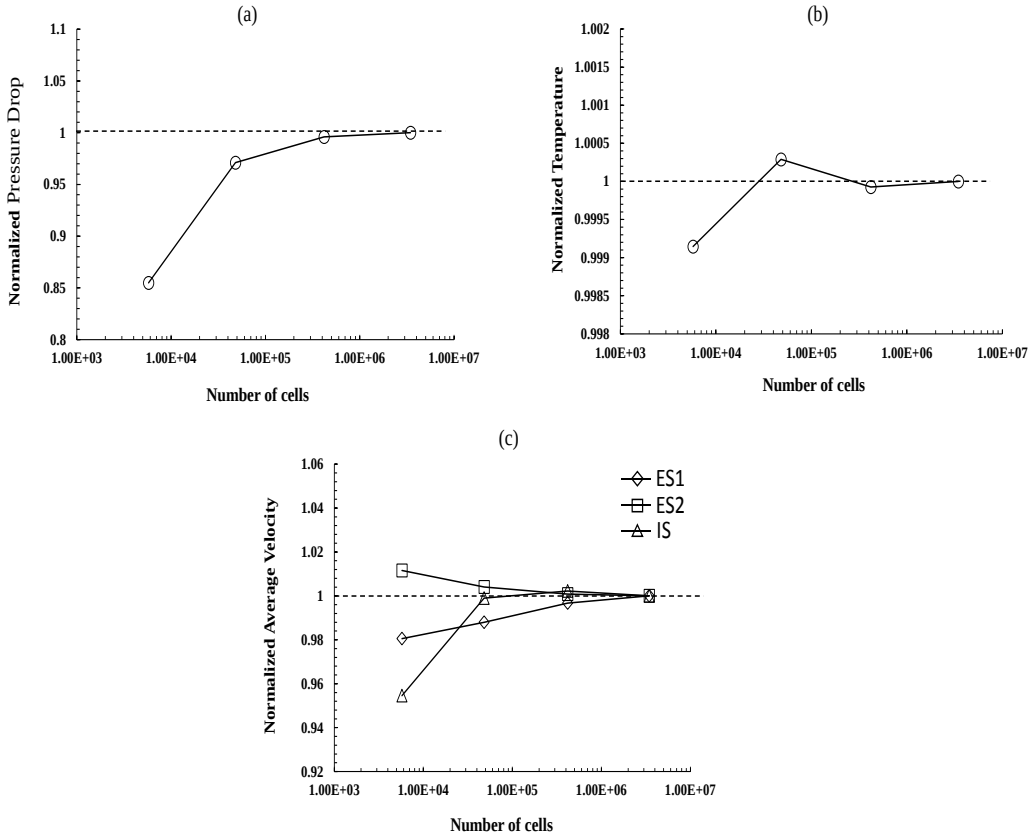

Figure 4.4: Results for the mesh refinement study with L-shaped extrusion die: (a) pressure drop, (b) maximum temperature in the domain, and (c) average velocity. The results are normalized with the results obtained for the finer mesh (mesh 4).

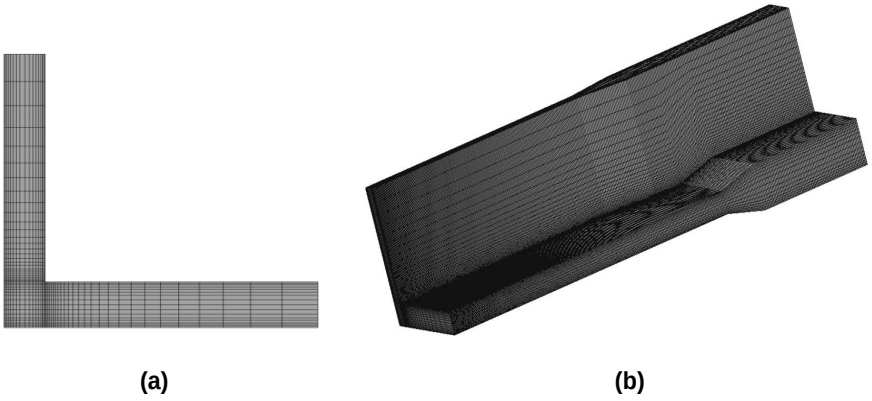

Figure 4.5: Selected mesh for the L-die geometry: (a) cross section of the die exit; (b) flow channel 3D view.

4.3 The influence of rheological parameters and processing conditions on flow distribution

The improved surrogate models to be devised should consider the most relevant material and process parameters influencing the flow distribution in profile extrusion dies. In order to identify those parameters, several numerical runs were performed for the *L* and *T* shaped extrusion dies already described, considering different rheological parameters and processing conditions and evaluating their effect on the geometry that promoted a balanced flow distribution. The rheological parameters of the reference material used in the study were: η_0 = 55800 Pa.s, η_∞ = 0 Pa.s, n = 0.3014, and λ = 3.21 s, and the parameters obtained for the Arrhenius law (see Chapter 2 (Eq. 2.10)) were E/R = 2900 K and T_{ref} = 230 ˚C (these parameters were obtained from a rheological characterization performed at 210 ºC, 230 ºC and 250 ºC (Nóbrega et al., 2003a)). The reference outlet average velocity considered for the polymer profile was 3 m/min.

To test the influence of the rheological parameters and processing conditions on the flow distribution, we have used the same geometry and respective parameters t_2, t_1, L_2/t_2 of the one used in the mesh refinement studies, except for L_1/t_1, which now varies from 1 to 15. The effect of each parameter was evaluated by performing simulations for three different values (the reference value and a ±20% variation), while keeping the remaining

parameters constant (with the reference values). Hence, the study was performed for an outlet velocity, V, values of 2.4, 3.0 and 3.6 m/min, temperature, T, values of 210, 230 and 250 °C, relaxation time, λ, of 2.57, 3.21 and 3.85 s, zero shear rate viscosity, η_0, of 44640, 55800 and 66960 Pa.s, and power law index, n, of 0.24, 0.3 and 0.36.
In all the cases, a search for L_1/t_1 value that provides a balanced flow distribution was performed (i.e. the L_1/t_1 value that provides the same average velocity for ES1 and ES2, which is equal to the expected outlet average velocity), aiming to identify the influence of the parameter under study on the geometry that promotes an even flow distribution.

As an Overview, the results obtained in the study performed on both L and T dies, to determine the effect of various process parameters are presented in the radar chart shown in Figure 4.6. In which the L_1/t_1 value predicted for each case study is normalized with the L_1/t_1 value obtained for the reference one. The graph comprises four curves, two for each die (L and T), corresponding to the L_1/t_1 value obtained for the ±20% variation of all the studied parameters.

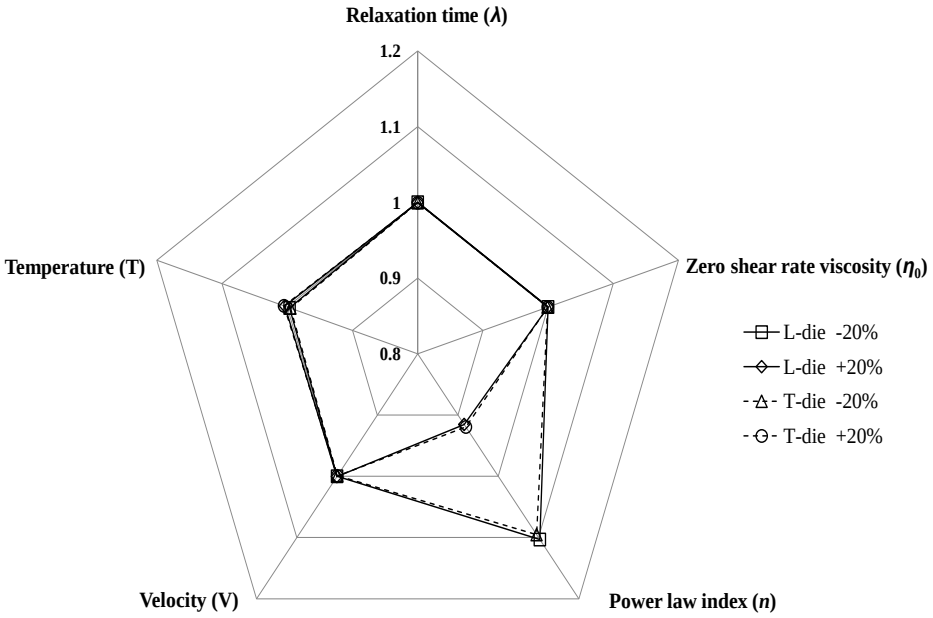

Figure 4.6: The influence of the rheological parameters and processing conditions on the L_1/t_1 value required to obtain and even flow distribution. All L_1/t_1 values are normalized with the ones obtained for the reference case study.

The results obtained in this study, shown in Figure 4.6, clearly indicate that the flow rate and the rheological parameters λ and η_0 and T show a negligible/slender effect on the geometry required to achieve a balanced flow distribution. Therefore, the result to be provided to the surrogate models to be developed, i.e. the L_1/t_1 ratio that promotes the same velocity ratio for ES1 and ES2, remains unaffected for the different values of the processing conditions V and T and rheological parameters λ and η_0 tested. On the other hand, the parameter *n* clearly influences the flow distribution, since the change in *n* value by ±20% affects the L_1/t_1 value that promotes a balanced flow distribution in a range of ±10%.

Based on these results, we concluded that it is relevant to enlarge the representativeness of the previously developed surrogate models explained in Chapter 3, by including the effect of *n*.

4.4 New surrogate flow balance models (taking into account the influence of n)

The studies presented in this section aim to further extend the previous surrogate models from Chapter 3, by considering the effect of the power law exponent *n*, which was the only parameter whose influence was identified to be relevant on the sensitivity studies described in Section 4.3. For this purpose, we have studied the behavior of L and T dies with different geometries (characterized by L_2/t_2, where t_2 is the largest thickness, and t_1/t_2) and values of the power law exponent *n* in the range [0.2 , 1], which covers all the actual values thermoplastic melts, and identified the required L_1/t_1 that promotes a balanced flow distribution at the flow channel outlet, i.e. the value of L_1/t_1 for which induces the same average velocity in ES1 and ES2.

Similarly to the procedure employed in the previous Chapter (Chapter 3), the numerical runs on *L* and *T* shaped dies were performed considering different thickness

ratios (t_1/t_2), ranging from 0.375 to 0.825, different values for t_2 {1, 2, 4} mm and for the ratio L_2/t_2 {5, 10, 15}. The geometrical parameters and the *n* values considered in these studies are provided in Table 4.1.

Table 4.1: Geometrical dimensions (length and thickness) of the different elemental sections, and n values used in the cases studied to obtain the surrogate models.

L_2/t_2	t_2 [mm]	L_2 [mm]	t_1/t_2	t_1 [mm]	n
5	1	5	[0.375;0.875]	[0.375; 0.875]	{0.2; 0.4; 0.6; 0.8; 1}
	2	10		[0.75; 1.75]	
	4	20		[1.5; 3.5]	
10	1	10	[0.375;0.875]	[0.375; 0.875]	{0.2; 0.4; 0.6; 0.8; 1}
	2	20		[0.75; 1.75]	
	4	40		[1.5; 3.5]	
15	1	15	[0.375;0.875]	[0.375; 0.875]	{0.2; 0.4; 0.6; 0.8; 1}
	2	30		[0.75; 1.75]	
	4	60		[1.5; 3.5]	

According to the information provided in Table 4.1, more than 2000 numerical runs were used to generate the surrogate models.

In order to avoid the cluttering of figures, the results showing the variation of the velocity ratio V_i/V V (where V_i is the outlet average velocity numerically obtained for ES1, ES2 and IS, with i =1, 2, 3, respectively, and V is the global outlet average velocity), as a function L_1/t_1 ratio, are only presented for the *L* and *T* shaped geometries with t_2=2 mm, t_1/t_2 ratio from 0.375 to 0.875, L_2/t_2 = 15 and for the minimum (0.2) and maximum (1) *n* values considered in the studies (see Figure 4.7 to Figure 4.10).

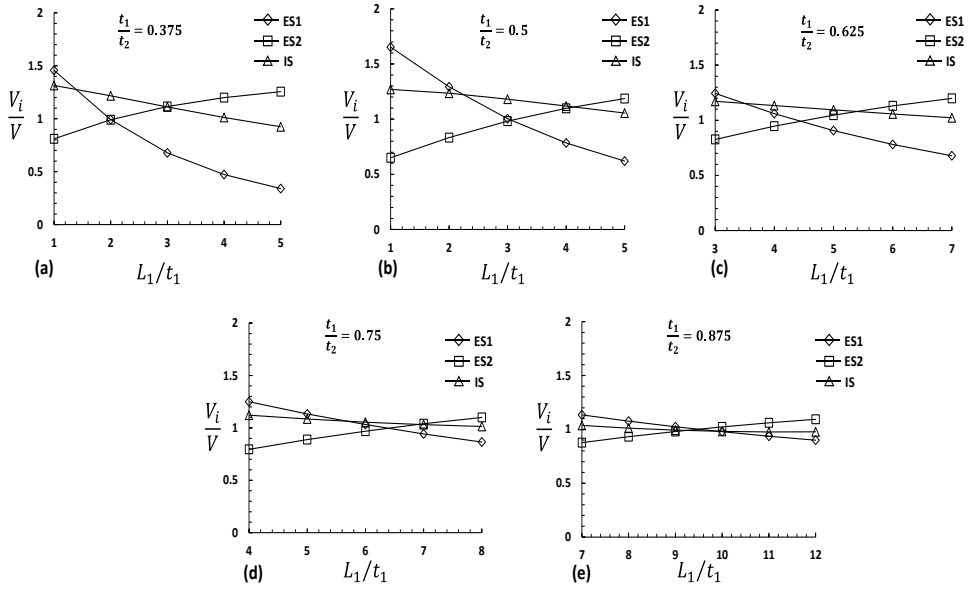

Figure 4.7: Variation of the average velocity (V_i/V) with L_1/t_1 for the L-die case with n= 0.2: (a) t_1/t_2 = 0.375; (b) t_1/t_2 = 0.5; (c) t_1/t_2 = 0.625; (d) t_1/t_2 = 0.75; (e) t_1/t_2 = 0.875.

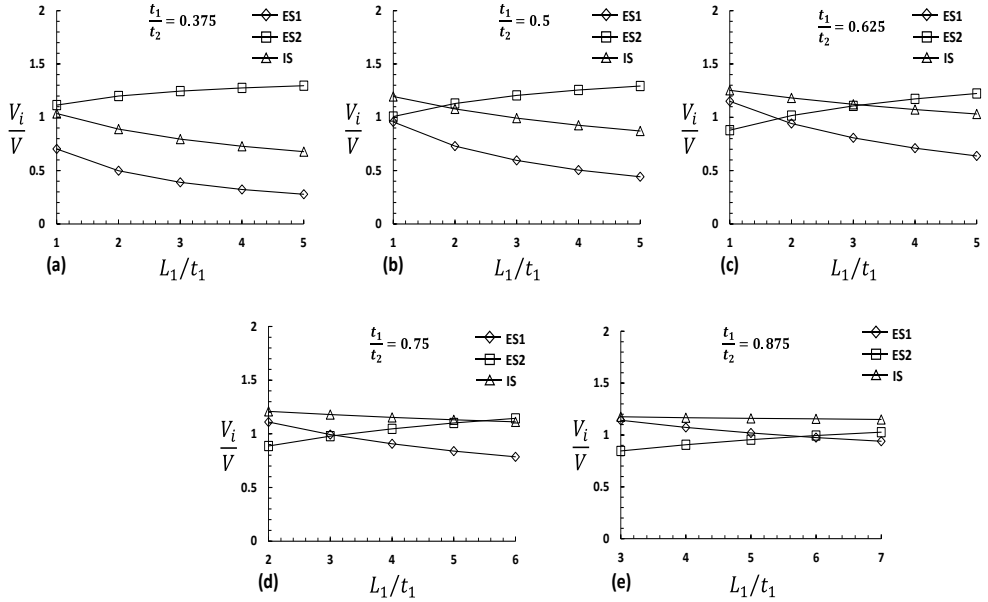

Figure 4.8: Variation of the average velocity (V_i/V) with L_1/t_1 for the L-die case with n= 1: (a) t_1/t_2 = 0.375; (b) t_1/t_2 = 0.5; (c) t_1/t_2 = 0.625; (d) t_1/t_2 = 0.75; (e) t_1/t_2 = 0.875.

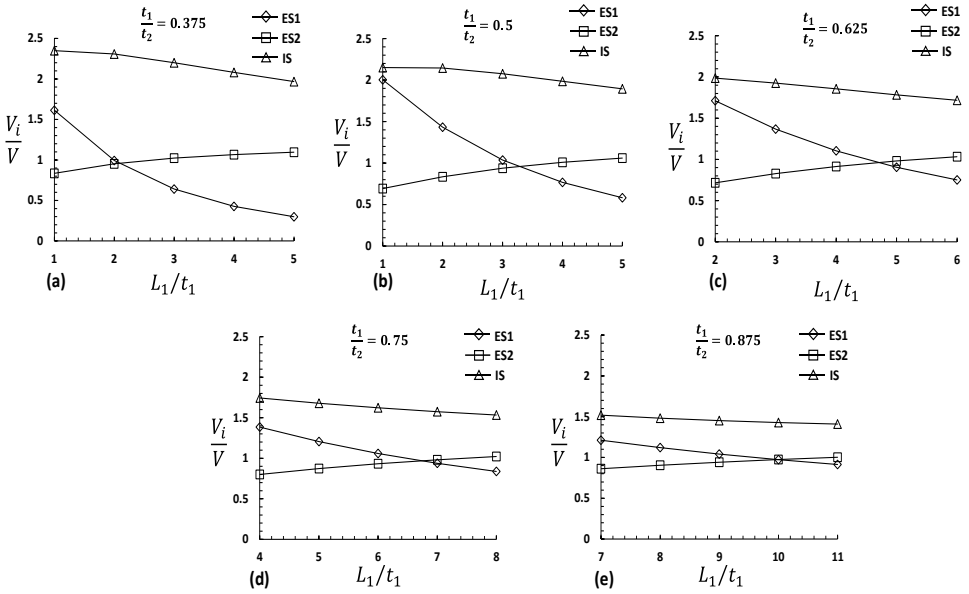

Figure 4.9: Variation of the average velocity (V_i/V) with L_1/t_1 for the T-die case with n= 0.2: (a) t_1/t_2 = 0.375; (b) t_1/t_2 = 0.5; (c) t_1/t_2 = 0.625; (d) t_1/t_2 = 0.75; (e) t_1/t_2 = 0.875.

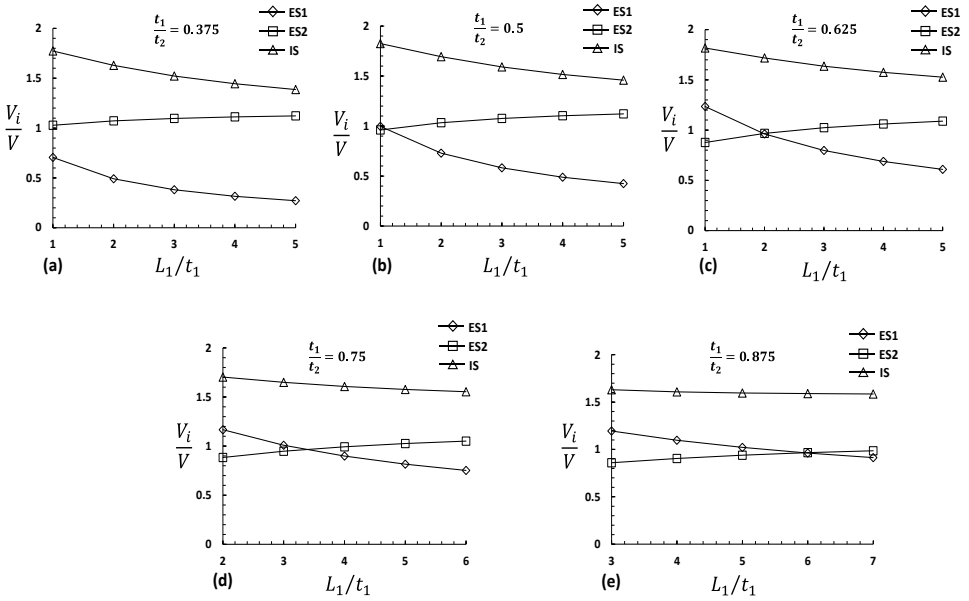

Figure 4.10: Variation of the average velocity (V_i/V) with L_1/t_1 for the T-die case with n= 1: (a) t_1/t_2 = 0.375; (b) t_1/t_2 = 0.5; (c) t_1/t_2 = 0.625; (d) t_1/t_2 = 0.75; (e) t_1/t_2 = 0.875.

In all the cases, the exact length over thickness ratio (L_1/t_1) for which the velocity ratio on ES1 and ES2 is the same, is obtained by interpolation of the two closest cases tested, before and above the intersection.

As can be concluded from the results obtained (see Figure 4.7 to Figure 4.10) the intersection value of L_1/t_1 increases with the increase of t_1/t_2, which can be explained by a progressive lower difference in the flow restriction promoted by the two sections as their thickness becomes similar (notice that t_1 is in all the cases the smallest thickness). Moreover, the intersection L_1/t_1 ratio decreases with increasing n value, as can be observed comparing the graphs corresponding to the same thickness ratio. For example, for the *L*-die case and t_1/t_2 = 0.75, the value of L_1/t_1 ratio that balances the flow is circa 6.4 for n=0.2 (see Figure 4.7 (d)) and circa 3.2 for n=1 (see Figure 4.8 (d)). A similar relationship was observed for the different thicknesses, t_2, and L_2/t_2 considered in the study, not shown here. The relationship between the rheological parameter n and the length of the thinnest elemental section (ES1), predicted by the numerical studies, has the expected trend, since it is in accordance with the analytical of the pressure drop (ΔP) in rectangular (parallel plate) cross section channels (Tadmor and Gogos, 2006):

$$\Delta P = \frac{2KL}{t^{2n+1}}\left(\frac{6Q}{W}\right)^n \tag{4.1}$$

where t, W and L are the thickness, width and length of the channel, respectively, K and n are the parameters of the power-law model, and Q is the volumetric flow rate. This equation has limited application since it is only adequate to deal with unidimensional flows (discarding, therefore, the lateral flow between adjacent ESs), it neglects the effect of temperature and is valid for a simpler generalized Newtonian fluid model, but it can be used to assess the trend of the numerical results obtained. Using this expression, to balance the flow in the geometry shown in Figure 4.11 the pressure drop in both ESs must be equal ($\Delta P_1=\Delta P_2$) when the average velocity is the same ($V_1=V_2$, or, equivalently, $Q_2=2Q_1$, since the cross section area ratio between ES2 and ES1 is 2). Applying Eq. 4.1 to each ES under those conditions, and computing the pressure drop ratio, we get

$$\frac{\Delta P_1}{\Delta P_2} = \frac{L_1}{L_2}\left(\frac{t_2}{t_1}\right)^{2n+1}\left(\frac{6Q_1}{12Q_1}\right)^{n} = 1 \qquad (4.2)$$

Having in mind that t_2/t_1 is equal to 2,

$$L_1 = \frac{L_2}{2^{n+1}}. \qquad (4.3)$$

Eq. 4.3 shows that a shorter length is required for ES1 with increasing *n* value, similarly to what was obtained for the numerical computations.

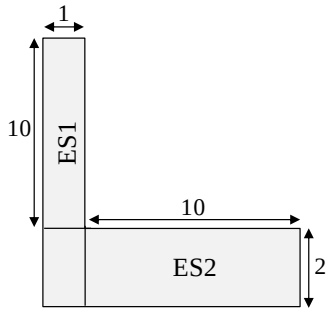

Figure 4.11: Geometry used to illustrate the effect of "n" in the flow distribution using Eq. 4.1.

The intersection points (values of L_1/t_1 ratio required to balance the flow) obtained for the *T* and *L* shaped dies (considering different parameters) were gathered and the trends obtained (illustrated in Figure 4.12) were fitted to Eq.4.4: a quadratic relationship, for the dependence of the balanced flow point (L_1/t_1) on the thickness ratio (t_1/t_2),

$$\frac{L_1}{t_1} = a(n, t_2, L_2/t_2)\left[\frac{t_1}{t_2}\right]^2 + b\,(n, t_2, L_2/t_2)\left[\frac{t_1}{t_2}\right] + c\,(n, t_2, L_2/t_2) \qquad (4.4)$$

where a(n, t_2, L_2/t_2), b(n, t_2, L_2/t_2) and c(n, t_2, L_2/t_2), are the fitting polynomials given in Appendix A. For the fitting a least squares method was employed.

In order to avoid the cluttering of figures, only the final results of the fitting function for t_2 =2 and for different values of L_2/t_2 are shown in Figure 4.12.

The mean relative error obtained for the fitting function, i.e. the difference between the fitting functions and the points obtained in the numerical studies, for all the studies performed is presented in

Table 4.2.

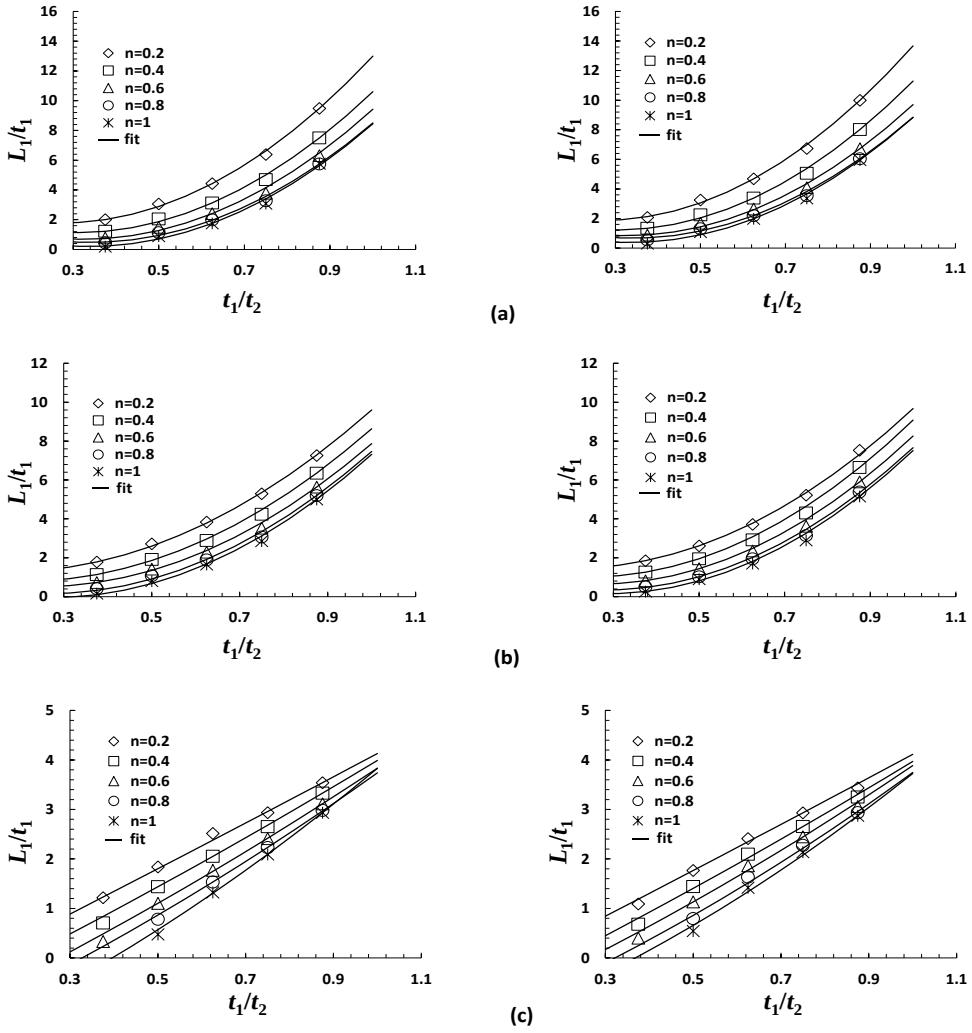

Figure 4.12: Dependence of the balanced flow point (L_1/t_1) on the thickness ratio (t_1/t_2) for the L-die (left) and T-die (right), for t_2 = 2 mm: (a) L_2/t_2=15; (b) L_2/t_2=10; (c) L_2/t_2=5.

Table 4.2: Mean relative errors, obtained with the fitting functions for the L and T die geometries.

		Mean Relative Error [%]														
		t2 =1mm					*t2* =2mm					*t2* =4mm				
	L2/t2	n=0.2	n=0.4	n=0.6	n=0.8	n=1	n=0.2	n=0.4	n=0.6	n=0.8	n=1	n=0.2	n=0.4	n=0.6	n=0.8	n=1
L-die	5	1.3359	0.9409	2.7797	4.7090	1.1423	1.8698	4.0238	9.4712	2.8627	5.3862	7.7335	7.3497	4.3384	0.3261	3.1983
	10	1.1068	0.5886	0.8274	1.4754	2.3893	1.4512	2.2067	3.3597	9.5379	13.1827	4.4356	5.8489	8.0997	8.1159	13.1442
	15	1.6136	1.1335	2.0408	3.0453	4.6719	1.9206	3.1619	6.3641	7.8623	11.1205	4.8477	14.0673	5.6663	3.2476	3.3146
T-die	5	1.2154	1.0216	2.3567	6.6501	3.5475	2.8397	5.1878	7.6227	4.7147	7.2226	5.5643	1.5347	1.6061	8.5632	3.5235
	10	0.7597	0.7425	1.0107	1.4604	2.3578	1.3905	2.7242	3.1744	4.1065	5.7866	3.6747	5.8566	12.6730	13.8539	20.0760
	15	1.4723	1.0868	1.7330	2.4619	3.1334	2.4084	3.2283	4.8114	9.3200	12.5862	2.9091	11.5586	9.0899	9.2690	15.6728

It is important to note that the majority of the relative errors are small but they tend to increase for higher values of *n*, since in this case very small values of L_1/t_1 are required to balance the flow, thus the relative errors are larger for similar absolute differences. Hence, we can conclude that the derived model fits adequately the behavior of a wide range of materials with different rheology, and thus provides the appropriate die dimensions required to obtain a balanced flow at the flow channel outlet, for typical polymeric materials: *n* values in the range (0.2 to 0.8).

4.5 Surrogate model assessment

To apply the model similar to the one presented in Section 4.4 to a profile extrusion die that can be decomposed into a combination of *L* and *T* subsections, as happens for the geometry shown in Figure 4.1, two different methods were proposed in a previous work Chapter 3: the Average and the Minimum methods. The Average Method is based on averaging the lengths of each section and the flow chart used to guide this process is given in the previous work Chapter 3; the Minimum Method uses the minimization of the differences between the fitting functions length values applied to each ES and the

actual length imposed. Both methods were also used in the assessment case studies presented in this section.

In order to assess the new model, we performed optimization tests considering three die geometries with different sets of thicknesses for the different ESs, all similar to the one illustrated in Figure 4.13 (same geometries were used in Chapter 3 for similar purposes), and each case geometry with three different *n* values (0.2, 0.4 and 0.6) were considered, since this represents the range of the major polymer melts found in practice (Tadmor and Gogos, 2006).

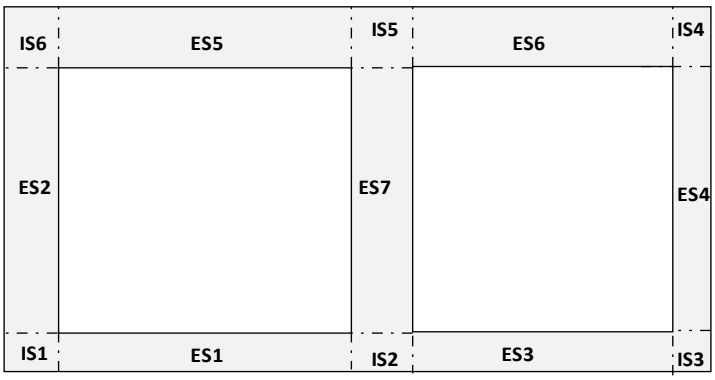

Figure 4.13: Cross section of the extrusion die flow channel outlet used for assessment purposes.

For the initial trial geometry, the length to thickness ratio (L/t) for all elemental sections was considered to be 15, a typical approach used in industrial practice (Nóbrega et al., 2004) to promote an even flow restriction to all ESs. The initial trial dimensions and the final ones obtained by the design methods for different *n* values, are given in Table 4.3, Table 4.4 and
Table 4.5.

To quantify the flow distribution in each ES the objective function, $F_{obj}(V_i)$, given by

$$F_{obj}(V_i) = \frac{\frac{V_i}{V_{obj}} - 1}{max\left(\frac{V_i}{V_{obj}}, 1\right)} \quad (4.5)$$

was used. In Eq. 4.5 V_i stands for the numerically obtained average velocity for ESi and V_{obj} is the objective average velocity at the outlet. Defined in this way, if $F_{obj}(V_i)$ is zero for all ESs, then the ideal flow distribution is achieved, i.e. the flow is fully balanced. Therefore, the better the results obtained, the lower will be the $F_{obj}(V_i)$ value (closer to 0).

The numerical results obtained from considering both the Average and Minimum methods, were compared with the results obtained for the initial trial geometry, as illustrated in Figure 4.14.

Table 4.3: First assessment case study: dimensions of the initial trial geometry and final geometries obtained using the Average and Minimum methods (dimensions in mm).

Geometry 1

Elemental Sections	Thickness of ESs	Initial trial dimensions		Average method final dimensions						Minimum method final dimensions					
				n = 0.2		n = 0.4		n = 0.6		n = 0.2		n = 0.4		n = 0.6	
		L_1/t_1	L_1	L_1/t_1	L_1	L_1/t_1	L_1	L_1/t_1	L_1	L_1/t_1	L_1	L_1/t_1	L_1	L_1/t_1	L_1
ES4	0.75	15	11.25	2.066	1.55	1.176	0.882	0.658	0.4935	1.697	1.273	1.0205	0.7654	0.5081	0.381
ES1,ES3	1	15	15	3.321	3.321	2.268	2.268	1.685	1.685	2.779	2.779	2.078	2.078	1.498	1.498
ES2	1.5	15	22.5	6.624	9.936	5.004	7.51	4.147	6.221	4.9316	7.397	4.001	6.002	2.933	4.399
ES5,ES6	2	15	30	15	30	15	30	15	30	8.928	17.86	8.2912	16.58	6.4317	12.863
ES7	2	15	30	15	30	15	30	15	30	11.379	22.76	13.44	26.88	12.54	25.08

Table 4.4: Second assessment case study: dimensions of the initial trial geometry and final geometries obtained using the Average and Minimum methods (dimensions in mm).

Geometry 2

Elemental Sections	Thickness of ESs	Initial trial dimensions		Average method final dimensions						Minimum method final dimensions					
				n = 0.2		n = 0.4		n = 0.6		n = 0.2		n = 0.4		n = 0.6	
		L_1/t_1	L_1	L_1/t_1	L_1	L_1/t_1	L_1	L_1/t_1	L_1	L_1/t_1	L_1	L_1/t_1	L_1	L_1/t_1	L_1
ES4	0.75	15	11.25	2.066	1.55	1.176	0.882	0.658	0.4935	1.4366	1.0775	0.9484	0.7113	0.3538	0.2654
ES7	1	15	15	3.059	3.059	2.037	2.037	1.439	1.439	2.968	2.968	2.892	2.892	2.462	2.462
ES1,ES3	1	15	15	3.321	3.321	2.268	2.268	1.685	1.685	2.221	2.221	1.775	1.775	1.024	1.024
ES2	1.5	15	22.5	6.624	9.936	5.004	7.51	4.147	6.221	4.4748	6.712	4.3839	6.576	3.074	4.611
ES5,ES6	2	15	30	15	30	15	30	15	30	8.2572	16.514	10.556	21.112	7.622	15.244

Table 4.5: Third assessment case study: dimensions of the initial trial geometry and final geometries obtained using the Average and Minimum methods (dimensions in mm).

	Elemental Sections	Thickness of ESs	Initial trial dimensions		Average method final dimensions						Minimum method final dimensions					
					n = 0.2		n = 0.4		n = 0.6		n = 0.2		n = 0.4		n = 0.6	
			L_1/t_1	L_1	L_1/t_1	L_1	L_1/t_1	L_1	L_1/t_1	L_1	L_1/t_1	L_1	L_1/t_1	L_1	L_1/t_1	L_1
Geometry 3	ES4	0.75	15	11.25	2.2365	1.677	1.413	1.0597	0.893	0.6698	1.9699	1.477	1.1948	0.8961	0.7739	0.5804
	ES7	1	15	15	3.5345	3.5345	2.4615	2.4615	1.815	1.815	2.885	2.885	1.9799	19799	1.4963	1.4963
	ES2	1.5	15	22.5	7.747	11.62	6.056	9.0833	5.1565	7.735	5.8665	8.7998	4.1672	6.251	3.4148	5.1222
	ES1,ES3	1.8	15	27	15	27	15	27	15	27	8.3491	15.028	6.4055	11.5299	5.6992	10.259
	ES5,ES6	2	15	30	15	30	15	30	15	30	11.689	23.38	9.021	18.042	8.347	16.694

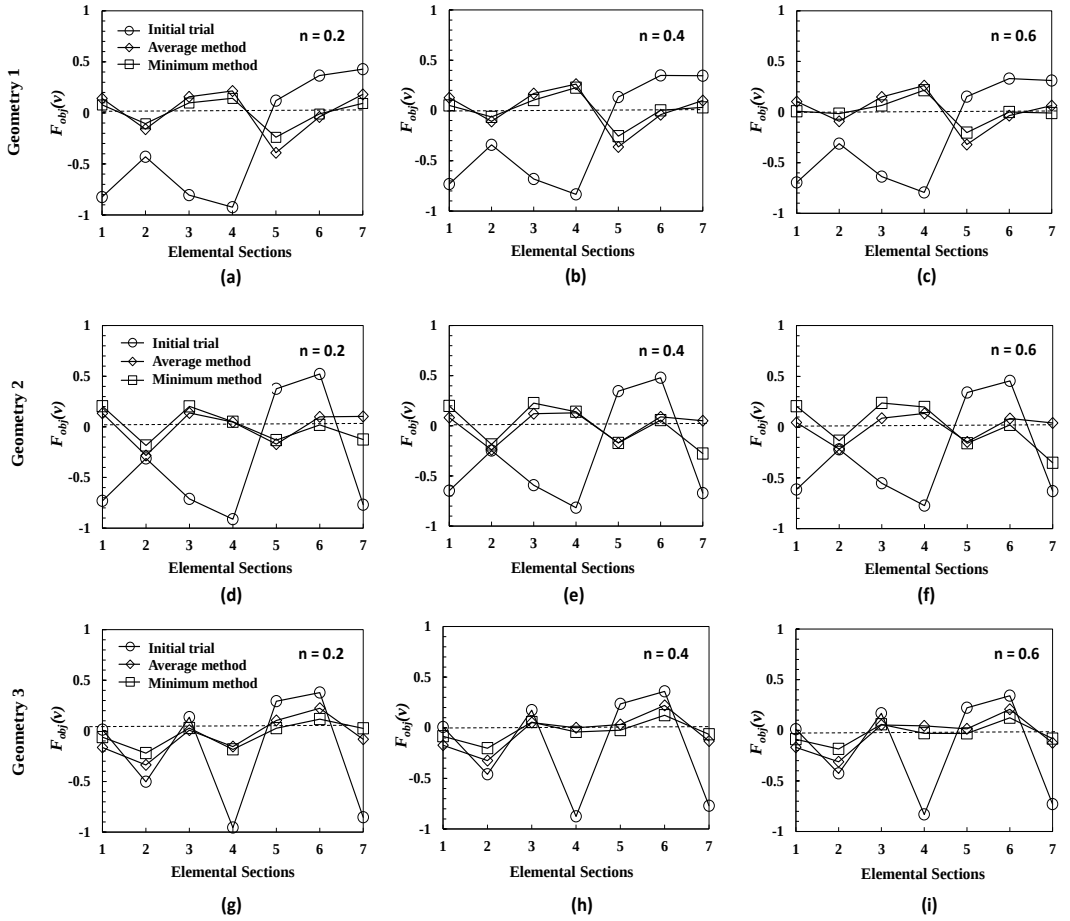

Figure 4.14: Fobj(V_i) obtained for each elemental section of the initial trial geometry and final geometries obtained using the Average and Minimum methods, for all the cases considered: Geometry1 (a,b,c); Geometry2 (d,e,f); Geometry3 (g,h,f); n=0.2 (a,d,g); n=0.4 (b,e,h) and n=0.6 (c,f,i).

By analyzing Figure 4.14, we can see that the initial trial always shows always a poorly balanced flow distribution, with high differences in the average velocities (quantified by $F_{obj}(V_i)$) over the different ES. Higher flow rates are obtained in the thicker sections and a significant reduced flow in the thinnest ones. On the other hand, the final geometries predicted using the Average and Minimum methods, reveal a huge enhancement in flow distribution when compared to the initial trials, for all the *n* values considered.

For instance, for Geometry1 initial trials, the thinnest elemental sections (ES1, 3 and 4), show a high flow restriction for all the *n* values (see Figure 4.14 (a) (b) and (c)). Similarly, this happens in ES1, ES3, ES4 and ES7 for Geometry2 (see Figure 4.14 (d) (e) and (f)) and in ES4 and ES7 for Geometry3 (see Figure 4.14 (g) (h) and (i)). As mentioned above this differences were significantly reduced in the geometries obtained with the proposed models.

The flow distribution improvements can also be observed in Figure 4.15, Figure 4.16 and Figure 4.17 where the velocity contours are provided for the three geometries and the different *n* values used in the assessment studies. In all the cases, the initial trial shows a low velocity (light color) in the thinnest ESs, indicating a reduced flow, whereas the geometries given by both the design methods show clear improvements on the flow distribution in all ESs.

In order to clearly enumerate the significant difference between the design methods, we determined the error norms namely the L_1, L_2 and L_∞ (Burden and Faires, 2001) for the $F_{obj}(V_i)$) on each ES, for the all the assessment case studies. The norms calculated were indicated by $F_{obj}\_L_1$, $F_{obj}\_L_2$ and $F_{obj}\_ L_\infty$, and the complete set of results is given in Table 4.6. These results evidence again the improvements obtained from the initial trial to the optimized geometries. Moreover, it is shown that the Minimum Method provides smaller values in all the error norms calculated, for the *n* values studied, for

Geometries 1 and 3. For Geometry2, the Average Method provides smaller error norms values for the *n* values of 0.4 and 0.6.

As an overall consideration, the Minimum Method gives better results since the influence of all the sections is considered simultaneously, while the Average Method comprises a sequential calculation. Nevertheless, the Average Method is also an excellent method, with the advantage of being simpler to apply as explained in Chapter 3. As discussed in Chapter 3, the Minimum Method relies on specific software to perform the minimization process, whereas the Average one does not. Thus, the Minimum Method should be the preferred one if the designer has access to the required minimization software, whereas the Average one can be used without significant losses in performance when that condition is not verified.

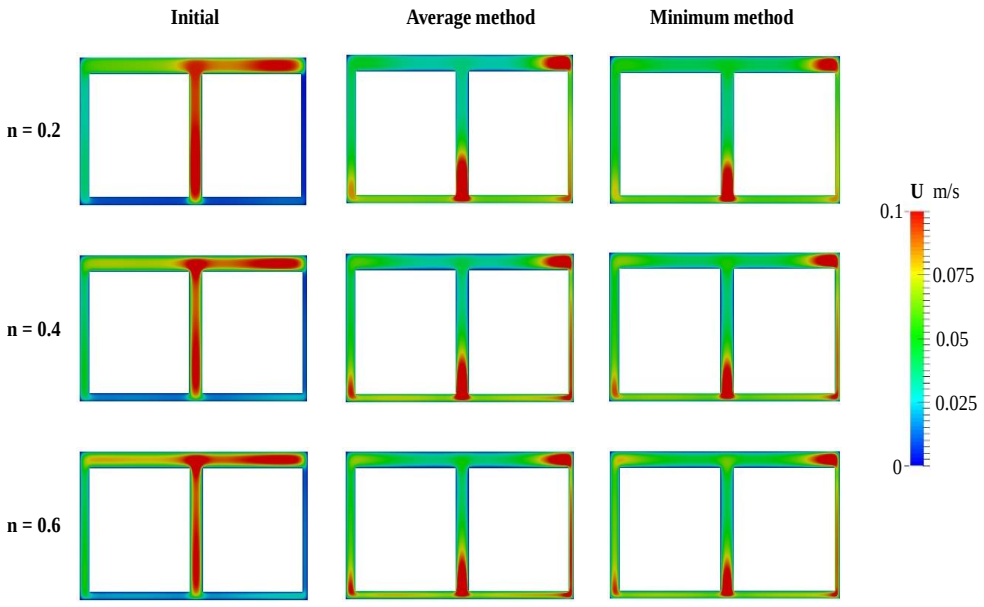

Figure 4.15: Velocity contour plots corresponding to Geometry1, containing the results of Initial, Average method and Minimum method for different n values (n =0.2, 0.4 and 0.6) studied.

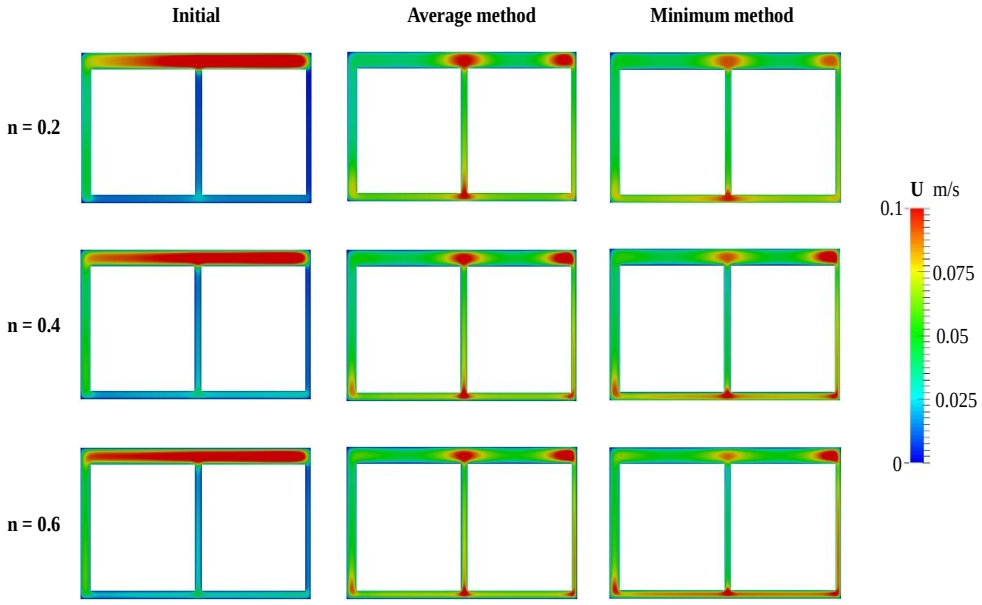

Figure 4.16: Velocity contour plots corresponding to Geometry2, containing the results of Initial, Average method and Minimum method for different n values (n =0.2, 0.4 and 0.6) studied.

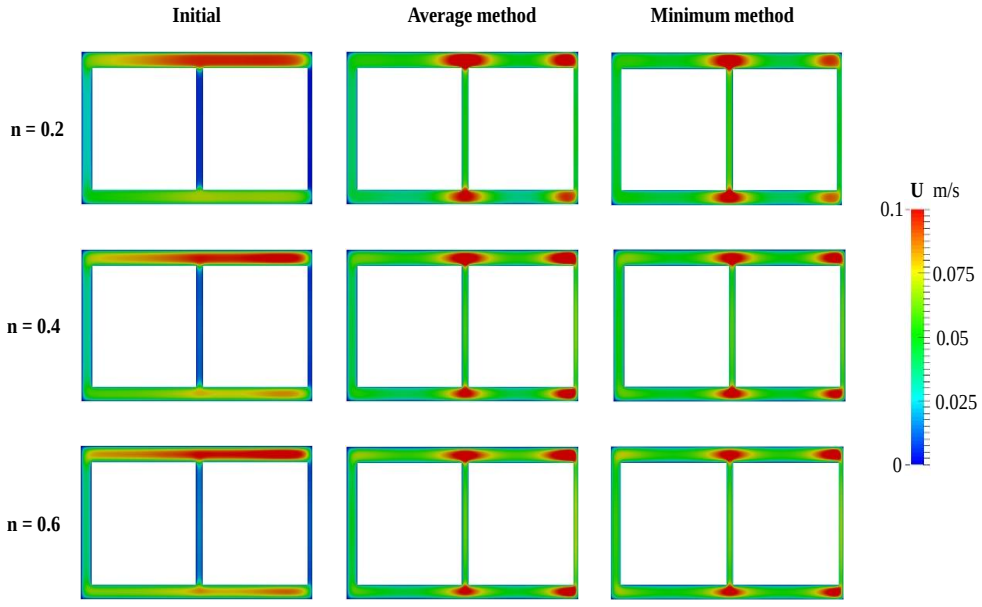

Figure 4.17: Velocity contour plots corresponding to Geometry3, containing the results of Initial, Average method and Minimum method for different n values (n =0.2, 0.4 and 0.6) studied.

Table 4.6: L_1, L_2 and L_∞ errors norms for the $F_{obj}(V_i)$) obtained from different methods.

Geometry1	**n = 0.2**			**n = 0.4**			**n = 0.6**		
	$F_{obj}\_L_1$	$F_{obj}\_L_2$	$F_{obj}\_L_\infty$	$F_{obj}\_L_1$	$F_{obj}\_L_2$	$F_{obj}\_L_\infty$	$F_{obj}\_L_1$	$F_{obj}\_L_2$	$F_{obj}\_L_\infty$
Initial trial	3.8954	1.6422	0.9236	3.4181	1.4396	0.8341	3.2326	1.3585	0.7932
Average Method	1.2841	0.5505	0.3905	1.1708	0.5178	0.3616	1.0226	0.4659	0.3201
Minimum Method	0.7653	0.3355	0.2378	0.7325	0.3675	0.2550	0.5187	0.3042	0.2159
Geometry2	**n = 0.2**			**n = 0.4**			**n = 0.6**		
	$F_{obj}\_L_1$	$F_{obj}\_L_2$	$F_{obj}\_L_\infty$	$F_{obj}\_L_1$	$F_{obj}\_L_2$	$F_{obj}\_L_\infty$	$F_{obj}\_L_1$	$F_{obj}\_L_2$	$F_{obj}\_L_\infty$
Initial trial	4.3330	1.7247	0.9123	3.8005	1.5162	0.8169	3.5891	1.4331	0.7737
Average Method	0.9757	0.4112	0.2833	0.8817	0.3672	0.2399	0.7566	0.3246	0.2171
Minimum Method	0.9151	0.3896	0.2035	1.2554	0.5039	0.2766	1.3078	0.5525	0.3522
Geometry3	**n = 0.2**			**n = 0.4**			**n = 0.6**		
	$F_{obj}\_L_1$	$F_{obj}\_L_2$	$F_{obj}\_L_\infty$	$F_{obj}\_L_1$	$F_{obj}\_L_2$	$F_{obj}\_L_\infty$	$F_{obj}\_L_1$	$F_{obj}\_L_2$	$F_{obj}\_L_\infty$
Initial trial	3.1293	1.4632	0.9550	2.8802	1.3363	0.8754	2.7285	1.2647	0.8316
Average Method	1.0714	0.4812	0.3367	0.9318	0.4524	0.3251	0.9217	0.4345	0.3117
Minimum Method	0.6593	0.3183	0.2195	0.5969	0.2701	0.2022	0.6022	0.2643	0.1853

4.6 Conclusions

This work proposes improvements on the simplified design guidelines presented in a previous Chapter (Chapter 3), through the inclusion of additional parameters in the surrogate models developed, which were previously focused just on the geometrical variables.

For this purpose, several numerical studies were performed to identify the most relevant parameters affecting the flow distribution in profile extrusion dies, among the material rheological properties and processing conditions. As a result, only the power law exponent '*n*' showed relevant effects on the conditions required to achieve a balanced flow distribution. Thus, several detailed numerical studies were done to add this parameter to the previously developed surrogate models.

The new surrogate models were derived from the results obtained from 3D non-isothermal numerical simulations on elementary geometries (*L* and *T* shaped extrusion dies), covering a wide and representative range of geometrical dimensions and fluid rheology. These models provide the extrusion die flow channel dimensions to obtain a balanced flow distribution at the die outlet, as function of the outlet cross section and the material rheological parameters

The usefulness of the model was tested in different geometries using two alternative optimization methods, the Average and the Minimum methods, which showed similar performance.

The results obtained, namely the improvements from the initial trial geometries (derived using design rules used in industrial practice) to the optimized ones, allowed to conclude that the proposed methodology is a very useful tool to support die designers' activity, with the advantage of dispensing the use of numerical modelling codes.

4.7 References

ANSYS Polyflow (2016).
URL: *http://www.ansys.com/*

Burden, R. L. and Faires, J. (2001). *Numerical Analysis*, Brooks/Cole, Vol **206**: 432- 438.

Carneiro, O. S. and Nóbrega, J. M. (2012). *Design of Extrusion forming Tools*, Smithers Rapra Technology Ltd.

Carneiro, O. S., Nóbrega, J.M., Pinho, F.T. and Oliveira, P.J. (2001). Computer aided rheological design of extrusion dies for profiles, *Journal of materials processing technology* **114**(1): 75-86.

Chen, C., Jen, P. and Lai, F. (1997). Optimization of the coathanger manifold via computer simulation and an orthogonal array method, *Polymer Engineering & Science* **37**(1): 188-196.

Compuplast (2016).
URL: *http://www.compuplast.com/product*

Die flow (2016).
URL: *http://www.dieflow.com*

Elgeti, S., Probst, M., Windeck, C., Behr, M., Michaeli, W. and Hopmann C. (2012). Numerical shape optimization as an approach to extrusion die design, *Finite Elements in Analysis and Design* **61**: 35-43.

Goncalves, N. D. (2013). *Computer aided design of extrusion forming tools for complex geometry profiles*, Ph.D Thesis, University of Minho.

Grieß, H. J. and Münstedt, H. (2012). Flow behavior of polypropylenes with different molecular structures in a coat-hanger die, *Polymer Engineering & Science* **52**(10): 2253-2259.

Hurez, P., Tanguy, P. and Blouin, D. (1996). A new design procedure for profile extrusion dies, *Polymer Engineering & Science* **36**(5): 626-635.

Lebaal, N., Puissant, S., Schmidt, F. and Schläfli, D. (2012). An optimization method with experimental validation for the design of extrusion wire coating dies for a range of different materials and operating conditions, *Polymer Engineering & Science* **52**(12): 2675-2687.

McKelvey, J. M. and Ito, K. (1971). Uniformity of flow from sheeting dies, *Polymer Engineering & Science* **11**(3): 258-263.

Michaeli, W. (1984). *Extrusion Dies Design and Engineering Computations*, Hanser Publishers.

Michaeli, W. and Kaul, S. (2004). Approach of an automatic extrusion die optimization, *Journal of polymer engineering* **24**(1-3): 123-136.

Nóbrega, J. M. (2004). *Computer aided design of forming tools for the production of Extruded profiles*, Ph.D Thesis, University of Minho.

Nóbrega, J. M., Carneiro, O. S, Oliveira, P. J. and Pinho, F. T. (2003). Flow Balancing in Extrusion Dies for Thermoplastic Profiles: Part I: Automatic Design, *International Polymer Processing* **18**(3): 298-306.

Nóbrega, J. M., Carneiro, O. S, Oliveira, P. J. and Pinho, F. T. (2003). Flow Balancing in Extrusion Dies for Thermoplastic Profiles: Part II: Influence of the Design Strategy, *International Polymer Processing* **18**(3): 307-312.

Nóbrega, J. M., Carneiro, O. S, Oliveira, P. J. and Pinho, F. T. (2004). Flow Balancing in Extrusion Dies for Thermoplastic Profiles: Part III: Experimental Assessment. *International Polymer Processing* **19**(3): 225-235.

OpenFOAM® (2016).
URL: *http://openfoam.org/version/2-3-0/*

Polydynamics (2016).
URL: *http://www.polydynamics.com/index.html*

Proctor, B. (1972). Flow analysis in extrusion dies, *SPE Journal, 28*: 34-41.

Rauwendaal, C. (2014). *Polymer extrusion*, Carl Hanser Verlag GmbH Co KG.

Reid, J., Campanella, O., Corvalan, C. and Okos, M. (2003). The influence of power-law rheology on flow distribution in coathanger manifolds, *Polymer Engineering & Science* **43**(3): 693-703.

Tadmor, Z. and Gogos, C. G. (2006). *Principles of polymer processing*, John Wiley & Sons.

Wu, T., Jiang, B., Xu, S. and Bi, C. (2006). Nonisothermal comprehensive 3D analysis of polymer melt flow in a coat-hanger die, *Polymer Engineering & Science* **46**(4): 406-415.

Zolfaghari, A., Behravesh, A., Shakouri E. and E. Soury (2010). Flow balancing in die design of wood flour/HDPE composite extrusion profiles with consideration of rheological effect. *Polymer Engineering & Science* **50**(3): 543-549.

4.8 Appendix

The fitting function, or model, is given by:

$$\frac{L_1}{t_1} = a(n, t_2, L_2/t_2)\left[\frac{t_1}{t_2}\right]^2 + b\,(n, t_2, L_2/t_2)\left[\frac{t_1}{t_2}\right] + c\,(n, t_2, L_2/t_2).$$

For the *L*-die and *T*-die, the coefficients are given as follows,

$a = x_1(n)^4 + x_2(n)^3 + x_3(n)^2 + x_4(n) + x_5$, $b = u_1(n)^4 + u_2(n)^3 + u_3(n)^2 + u_4(n) + u_5$
and $c = v_1(n)^4 + v_2(n)^3 + v_3(n)^2 + v_4(n) + v_5$

$\mathbf{x_1 = w_1(t_2)^2 + y_1(t_2) + z_1}$	$\mathbf{u_1 = o_1(t_2)^2 + p_1(t_2) + q_1}$	$\mathbf{v_1 = e_1(t_2)^2 + f_1(t_2) + g_1}$
$\mathbf{x_2 = w_2(t_2)^2 + y_2(t_2) + z_2}$	$\mathbf{u_2 = o_2(t_2)^2 + p_2(t_2) + q_2}$	$\mathbf{v_2 = e_2(t_2)^2 + f_2(t_2) + g_2}$
$\mathbf{x_3 = w_3(t_2)^2 + y_3(t_2) + z_3}$	$\mathbf{u_3 = o_3(t_2)^2 + p_3(t_2) + q_3}$	$\mathbf{v_3 = e_3(t_2)^2 + f_3(t_2) + g_3}$
$\mathbf{x_4 = w_4(t_2)^2 + y_4(t_2) + z_4}$	$\mathbf{u_4 = o_4(t_2)^2 + p_4(t_2) + q_4}$	$\mathbf{v_4 = e_4(t_2)^2 + f_4(t_2) + g_4}$
$\mathbf{x_5 = w_5(t_2)^2 + y_5(t_2) + z_5}$	$\mathbf{u_5 = o_5(t_2)^2 + p_5(t_2) + q_5}$	$\mathbf{v_5 = e_5(t_2)^2 + f_5(t_2) + g_5}$

L-die

$\mathbf{x_1}$	$w_1 = -0.71348000(L_1/t_1)^2 + 10.72920000(L_1/t_1) - 43.79010000$	$\mathbf{u_1}$ $o_1 = -0.34820868(L_1/t_1)^2 + 8.86852560(L_1/t_1) - 32.39351100$
	$y_1 = 3.74858400(L_1/t_1)^2 - 57.48760000(L_1/t_1) + 244.67840000$	$p_1 = 1.90033132(L_1/t_1)^2 - 49.31356140(L_1/t_1) + 188.32292400$
	$z_1 = -2.95297800(L_1/t_1)^2 + 43.36475000(L_1/t_1) - 206.10020000$	$q_1 = -1.92513604(L_1/t_1)^2 + 52.61871380(L_1/t_1) - 203.31146800$
$\mathbf{x_2}$	$w_2 = 1.67522600(L_1/t_1)^2 - 25.03371000(L_1/t_1) + 103.71340000$	$\mathbf{u_2}$ $o_2 = 0.83964140(L_1/t_1)^2 - 21.02727600(L_1/t_1) + 72.83884500$
	$y_2 = -8.86512400(L1/t1)^2 + 135.59096000(L_1/t_1) - 586.68820000$	$p_2 = -4.63776216(L_1/t_1)^2 + 118.40275820(L_1/t_1) - 435.56693700$
	$z_2 = 7.08191200(L_1/t_1)^2 - 104.65630000(L_1/t_1) + 512.74670000$	$q_2 = 4.63853728(L_1/t_1)^2 - 125.20698260(L_1/t_1) + 466.63988100$
$\mathbf{x_3}$	$w_3 = -1.35822400(L_1/t_1)^2 + 20.42690000(L_1/t_1) - 87.43150000$	$\mathbf{u_3}$ $o_3 = -0.71100732(L_1/t_1)^2 + 17.03310940(L_1/t_1) - 54.19886400$
	$y_3 = 7.14083000(L_1/t_1)^2 - 109.57385000(L_1/t_1) + 488.51500000$	$p_3 = 4.03706172(L_1/t_1)^2 - 98.62418440(L_1/t_1) + 343.48347900$
	$z_3 = -5.56422400(L_1/t_1)^2 + 82.89234000(L_1/t_1) - 429.50100000$	$q_3 = -4.13615496(L_1/t_1)^2 + 106.12657620(L_1/t_1) - 376.29620700$
$\mathbf{x_4}$	$w_4 = 0.46360800(L_1/t_1)^2 - 7.10582000(L_1/t_1) + 32.33030000$	$\mathbf{u_4}$ $o_4 = 0.23206404(L_1/t_1)^2 - 5.23082580(L_1/t_1) + 14.06902800$
	$y_4 = -2.26002000(L_1/t_1)^2 + 34.09340000(L_1/t_1) - 161.89600000$	$p_4 = -1.46270892(L_1/t_1)^2 + 33.65652340(L_1/t_1) - 108.23339400$
	$z_4 = 1.39475200(L_1/t_1)^2 - 19.00862000(L_1/t_1) + 122.75440000$	$q_4 = 1.80358040(L_1/t_1)^2 - 42.56730800(L_1/t_1) + 143.29263000$
$\mathbf{x_5}$	$w_5 = -0.01452000(L_1/t_1)^2 - 0.14084000(L_1/t_1) + 0.11700000$	$\mathbf{u_5}$ $o_5 = -0.06152400(L_1/t_1)^2 + 1.52215000(L_1/t_1) - 5.64135000$
	$y_5 = -0.03922000(L_1/t_1)^2 + 2.87704000(L_1/t_1) - 7.93390000$	$p_5 = 0.44958240(L_1/t_1)^2 - 10.73330800(L_1/t_1) + 41.45668000$
	$z_5 = 0.23207000(L_1/t_1)^2 - 4.42665000(L_1/t_1) + 9.05200000$	$q_5 = -0.62686400(L_1/t_1)^2 + 13.30749000(L_1/t_1) - 45.84185000$

$\mathbf{v_1}$	$e_1 = 0.52168620(L_1/t_1)^2 - 10.40274600(L_1/t_1) + 40.50827500$
	$f_1 = -2.87460888(L_1/t_1)^2 + 59.02951260(L_1/t_1) - 244.21874100$
	$g_1 = 2.57535128(L_1/t_1)^2 - 55.03644860(L_1/t_1) + 237.74906100$
$\mathbf{v_2}$	$e_2 = -1.19245692(L_1/t_1)^2 + 23.63884640(L_1/t_1) - 89.93160900$
	$f_2 = 6.69897676(L_1/t_1)^2 - 137.38894020(L_1/t_1) + 562.81188200$
	$g_2 = -6.06044096(L_1/t_1)^2 + 129.57250620(L_1/t_1) - 557.64280700$
$\mathbf{v_3}$	$e_3 = 0.93773992(L_1/t_1)^2 - 18.43521340(L_1/t_1) + 68.37626900$
	$f_3 = -5.39431972(L_1/t_1)^2 + 110.21873940(L_1/t_1) - 446.98560400$
	$g_3 = 4.95966420(L_1/t_1)^2 - 105.61540400(L_1/t_1) + 453.26091500$
$\mathbf{v_4}$	$e_4 = -0.29988824(L_1/t_1)^2 + 5.85614680(L_1/t_1) - 21.48052800$
	$f_4 = 1.76829276(L_1/t_1)^2 - 35.89944020(L_1/t_1) + 145.07328200$
	$g_4 = -1.69910636(L_1/t_1)^2 + 35.78122020(L_1/t_1) - 155.27394200$
$\mathbf{v_5}$	$e_5 = 0.04044460(L_1/t_1)^2 - 0.84950000(L_1/t_1) + 3.47638500$
	$f_5 = -0.25621680(L_1/t_1)^2 + 5.47814100(L_1/t_1) - 24.00338500$
	$g_5 = 0.28024740(L_1/t_1)^2 - 5.79158500(L_1/t_1) + 26.58564000$

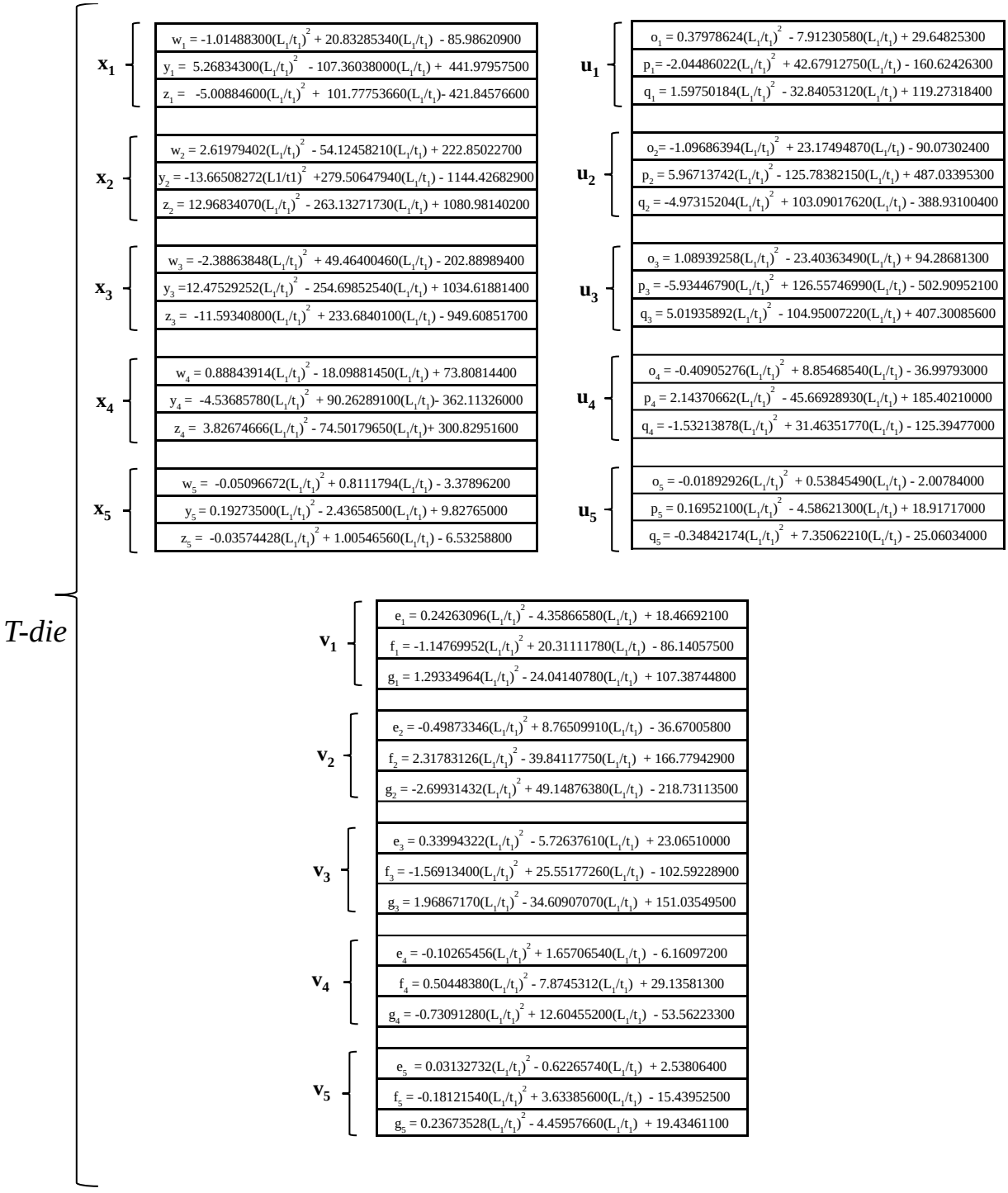
T-die
x1
w1 = -1.01488300(L1/t1)^2 + 20.83285340(L1/t1) - 85.98620900
y1 = 5.26834300(L1/t1)^2 - 107.36038000(L1/t1) + 441.97957500
z1 = -5.00884600(L1/t1)^2 + 101.77753660(L1/t1)- 421.84576600
x2
w2 = 2.61979402(L1/t1)^2 - 54.12458210(L1/t1) + 222.85022700
y2 = -13.66508272(L1/t1)^2 +279.50647940(L1/t1) - 1144.42682900
z2 = 12.96834070(L1/t1)^2 - 263.13271730(L1/t1) + 1080.98140200
x3
w3 = -2.38863848(L1/t1)^2 + 49.46400460(L1/t1) - 202.88989400
y3 =12.47529252(L1/t1)^2 - 254.69852540(L1/t1) + 1034.61881400
z3 = -11.59340800(L1/t1)^2 + 233.6840100(L1/t1) - 949.60851700
x4
w4 = 0.88843914(L1/t1)^2 - 18.09881450(L1/t1) + 73.80814400
y4 = -4.53685780(L1/t1)^2 + 90.26289100(L1/t1)- 362.11326000
z4 = 3.82674666(L1/t1)^2 - 74.50179650(L1/t1)+ 300.82951600
x5
w5 = -0.05096672(L1/t1)^2 + 0.8111794(L1/t1) - 3.37896200
y5 = 0.19273500(L1/t1)^2 - 2.43658500(L1/t1) + 9.82765000
z5 = -0.03574428(L1/t1)^2 + 1.00546560(L1/t1) - 6.53258800
u1
o1 = 0.37978624(L1/t1)^2 - 7.91230580(L1/t1) + 29.64825300
p1= -2.04486022(L1/t1)^2 + 42.67912750(L1/t1) - 160.62426300
q1 = 1.59750184(L1/t1)^2 - 32.84053120(L1/t1) + 119.27318400
u2
o2= -1.09686394(L1/t1)^2 + 23.17494870(L1/t1) - 90.07302400
p2 = 5.96713742(L1/t1)^2 - 125.78382150(L1/t1) + 487.03395300
q2 = -4.97315204(L1/t1)^2 + 103.09017620(L1/t1) - 388.93100400
u3
o3 = 1.08939258(L1/t1)^2 - 23.40363490(L1/t1) + 94.28681300
p3 = -5.93446790(L1/t1)^2 + 126.55746990(L1/t1) - 502.90952100
q3 = 5.01935892(L1/t1)^2 - 104.95007220(L1/t1) + 407.30085600
u4
o4 = -0.40905276(L1/t1)^2 + 8.85468540(L1/t1) - 36.99793000
p4 = 2.14370662(L1/t1)^2 - 45.66928930(L1/t1) + 185.40210000
q4 = -1.53213878(L1/t1)^2 + 31.46351770(L1/t1) - 125.39477000
u5
o5 = -0.01892926(L1/t1)^2 + 0.53845490(L1/t1) - 2.00784000
p5 = 0.16952100(L1/t1)^2 - 4.58621300(L1/t1) + 18.91717000
q5 = -0.34842174(L1/t1)^2 + 7.35062210(L1/t1) - 25.06034000
v1
e1 = 0.24263096(L1/t1)^2 - 4.35866580(L1/t1) + 18.46692100
f1 = -1.14769952(L1/t1)^2 + 20.31111780(L1/t1) - 86.14057500
g1 = 1.29334964(L1/t1)^2 - 24.04140780(L1/t1) + 107.38744800
v2
e2 = -0.49873346(L1/t1)^2 + 8.76509910(L1/t1) - 36.67005800
f2 = 2.31783126(L1/t1)^2 - 39.84117750(L1/t1) + 166.77942900
g2 = -2.69931432(L1/t1)^2 + 49.14876380(L1/t1) - 218.73113500
v3
e3 = 0.33994322(L1/t1)^2 - 5.72637610(L1/t1) + 23.06510000
f3 = -1.56913400(L1/t1)^2 + 25.55177260(L1/t1) - 102.59228900
g3 = 1.96867170(L1/t1)^2 - 34.60907070(L1/t1) + 151.03549500
v4
e4 = -0.10265456(L1/t1)^2 + 1.65706540(L1/t1) - 6.16097200
f4 = 0.50448380(L1/t1)^2 - 7.8745312(L1/t1) + 29.13581300
g4 = -0.73091280(L1/t1)^2 + 12.60455200(L1/t1) - 53.56223300
v5
e5 = 0.03132732(L1/t1)^2 - 0.62265740(L1/t1) + 2.53806400
f5 = -0.18121540(L1/t1)^2 + 3.63385600(L1/t1) - 15.43952500
g5 = 0.23673528(L1/t1)^2 - 4.45957660(L1/t1) + 19.43461100

Chapter 5

Profile extrusion: experimental assessment of a numerical model for heat transfer in the cooling/calibration stage

Abstract

Designing an optimum calibration system that ensures fast and uniform cooling for a complex profile extrusion is always a difficult task in the extrusion industry.
In this work an experimental validation is performed for a numerical code previously developed in OpenFOAM framework, using, for this purpose, an existing industrial calibration system in operation. This code models the heat transfer that occurs between the polymer and the calibrator during the profile extrusion cooling process. The results allow proving the accuracy of the code. In order to demonstrate the applicability of this numerical code to improve the design of the calibration system, a numerical based trial-and-error study was also carried out. As a result, the study led to the proposal of an alternative calibration system, which has a simpler constructive solution and a better performance than the one considered in the industrial case study.

This chapter was adapted from: Rajkumar, A., Habla, F., Fernandes, C., Mould, S., Sacramento, A., Carneiro, O.S. and Nóbrega, J.M. (2017). "Profile extrusion: experimental assessment of a numerical model for heat transfer in the cooling/calibration stage", in preparation for submission in International Polymer Processing.

5.1 Introduction

Extrusion is a continuous manufacturing process used to produce thermoplastic products with constant cross-section such as rods, films, profiles, pipes and sheet. A typical profile extrusion line is shown in Figure 5.1: it comprises an extruder, a die, a cooling /calibration system, a haul-off unit and a saw (Carneiro and Nóbrega, 2012). In this process, the melt from the extruder is pushed through the die that shapes it into the desired geometry; then, the extruded profile is cooled down to a sufficiently low average temperature using one or several calibration units. The haul-off system pulls the extruded profile, assuring a constant extrusion linear velocity, and, finally, the profile is cut at regular intervals by the saw.

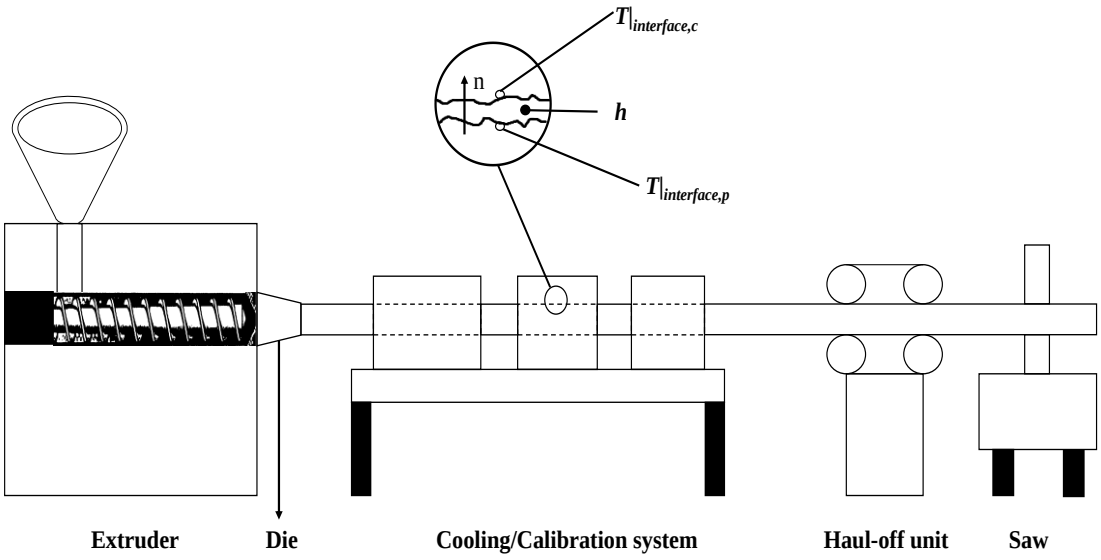

Figure 5.1: Schematic view of a thermoplastic profile extrusion line.

The calibration/cooling system/stage of the extrusion process is responsible for the final

profile dimensions and should ensure sufficient profile strength to withstand the

external forces (such as, gravity, friction, compression and buoyancy) experienced along the production line (Kleindienst, 1973; Michaeli, 1992). The calibration system should also reduce the level of residual thermal stresses induced during cooling, minimizing the temperature gradient developed along the profile cross section (Fradette et al., 1995). Therefore, the calibration/cooling stage should be able to reduce the profile average temperature and its non-homogeneity.

The design process of the cooling/calibration system can be quite difficult, because of the complexity of the profile geometry and also due to the large number of parameters involved. The experimental based way to optimize the design process of these systems can be ineffective and time consuming. Therefore, the use of numerical tools can accelerate the design task, reducing the resources involved.

Due to the growing development of powerful computational hardware and numerical techniques, there has been a significant increase in the use of numerical modeling to study the heat transfer occurring in the cooling/calibration system. Some of the available studies regarding developments in the design of calibration systems assisted by numerical simulation are discussed below. Initially, one dimensional models were used by Kurz (1988) and Menges et al. (1982), to study the cooling of plastic profiles. This approach was limited to ideal conditions, i.e. uniform cooling and uniform thickness extrudates. Later, a two dimensional (2D) approach was developed by Menges et al. (1987) to deal with complex extrudate shapes, where the cooling channels should always run parallel to the profile. Subsequently, this model was extended to handle three dimensional (3D) geometries (Sheehy et al., 1994), where the authors proposed the 'Corrected Slice Method', based on the 2D approach. The performance of the method was tested with real problems, and the predicted values showed a good agreement with the real ones. A 2D

approach was also developed by Pittman et al. (1994), and by Szarvasy (2000). However, due to their 2D nature, those models neglected the heat flux along the extrusion axis Fradette et al., 1995.

Fradette et al. (1996) developed a correlation to describe the interface heat transfer (*h*, in Figure 5.1) between a stainless steel calibrator and a PVC profile, and used it to simulate a real calibration unit, based on the model suggested by Menges et al. (1987). A comparison was made between the numerically predicted temperature and those obtained from experimental measurements. The results showed a fairly good agreement.

In an another work by Reifschneider et al., 2004, the cooling performance and the shaping behavior of a calibrator was studied numerically using a transient FEM based model. It was concluded that the heat transfer coefficient values of the calibrator depend both on the calibrator geometry and on the extrusion flow rate. Later, in this field, an algorithm comprising a non-isothermal 3D code was developed by Nóbrega et al. (Nóbrega et al., 2004; Nóbrega and Carneiro, 2006; Nóbrega et al., 2008). At a first stage of the work (Nóbrega et al., 2004) a non-isothermal 3D code was developed and validated with the analytical solution of a simple problem, with the results obtained from the literature, and with the results predicted by a commercial software (Nóbrega et al., 2004). The main processing parameters and boundary conditions were identified and their relative importance was estimated. Later (Nóbrega and Carneiro, 2006), an optimization routine was coupled, aiming to determine the optimal system design. However, the code was limited to structured meshes, being not able to handle complex geometries, common in industry.

In industrial context, the use of numerical modeling to aid the design of cooling/calibration systems is very limited, mainly due to the lack of knowledge and

experience in numerical modeling, and to the high cost of the numerical packages licenses. Therefore, most of the extrusion industries design their cooling systems based on experimental trial-and-error approaches, which are highly dependent on the

designer's experience.

The use of free open-source numerical modeling codes can motivate the extrusion companies to follow this route to improve their design processes. Having this is mind, a numerical code able to model the heat transfer between the polymer and calibrator phases, which can handle complex cooling systems was recently developed, by Habla et al.(2016), in the open-source computation library OpenFOAM®. In addition, geometry and mesh generators, and an optimization routine were also developed. The validation of this code was done with both the analytical and numerical results of a bench mark case study, but the code was not experimentally assessed.

The objective of this work is to extend the application of the code developed in the previous work (Habla et al., 2016) to industrial context. The assessment of the solver is made using the experimental results obtained from the cooling/calibration system of a swimming pool cover profile production line. After, and in order to demonstrate the usefulness of the developed code, a numerical study is employed to study and to improve the behavior/performance of the referred system.

The remainder sections of this chapter are organized as follows. Section 5.2 provides a brief description of the governing equations and numerical methods employed. The experimental assessment of the code is presented in Section 5.3. Section 5.4 presents a numerical based study aiming to obtain further insights into the calibration system behavior and to identify the best alternatives to improve its performance. Finally, the conclusions of the chapter are drawn in Section 5.5.

5.2 Numerical Modelling Code

The complete derivation of the governing equations to model the heat transfer between the calibrator and the profile is presented in a previous study (Habla et al., 2016). Therefore, only the most relevant details are provided in this section.
The energy conservation equation can be expressed as:

$$\nabla \cdot \left(\mathrm{U}_i \rho_i c_{P,i} T_i \right) - k_i \nabla^2 T_i = 0 \tag{5.1}$$

where T is the temperature, ρ is the density, c_p is the heat capacity, U is the velocity vector, k is the thermal conductivity, and subscript i identifies the material ($i = p, c$ (polymer and calibrator)), in which $\mathrm{U}_c = 0$ since the calibrator is not moving. In real processing conditions, there is a contact resistance at the interface between the polymer and the calibrator (a magnified image of the polymer calibrator interface is shown in Figure 5.1), causing temperature discontinuity between the two domains (Fradette et al., 1995). For contact resistance the following equations are considered (Habla et al., 2016).

$$\left(\dot{\mathbf{q}}_p - \dot{\mathbf{q}}_c \right) \cdot \mathbf{n} = \left(k_p \nabla T_{|interface,p} - k_c \nabla T_{|interface,c} \right) \cdot \mathbf{n} = 0 \tag{5.2}$$

$$T_{|interface,p} - T_{|interface,c} = \frac{\dot{\mathbf{q}}_c \cdot \mathbf{n}}{h} \tag{5.3}$$

where, $\dot{\mathbf{q}}$ indicates the interface heat flux, $\mathbf{n}$ is the interface normal vector pointing from the profile to the calibrator, and h is the interface heat transfer coefficient, which is the inverse of the contact resistance (Habla et al., 2016).

In order to have one governing equation valid for all the domain, a new energy conservation equation was devised Eq 5.4 (Habla et al., 2016), using the conditional

volume averaging technique (Dopazo, 1977; Marschall et al., 2012; Habla et al., 2013).

$$\nabla \cdot \left(\mathrm{U}_m \rho_m c_{P,m} T_m \right) - k_m \nabla^2 T_m = -\nabla \cdot \left[\frac{k_m \nabla \alpha_p - \alpha_p \alpha_c \left(\bar{k}^p - \bar{k}^c \right) \left(\frac{1}{\bar{k}^p} - \frac{1}{\bar{k}^c} \right) h \mathrm{n}}{h \left(\frac{\alpha_p}{\bar{k}^p} + \frac{\alpha_c}{\bar{k}^c} \right) + \nabla \alpha_p \cdot \mathrm{n}} \nabla T_m \cdot \mathrm{n} \right] \quad (5.4)$$

where, T_m is the mixture temperature, α_p and α_c are the volume fraction of polymer and calibrator, respectively, and the overbar notation denotes the conditional volume average of that quantity within the averaging volume (Habla et al., 2016). A detailed information about this issue is available in a previous study (Habla et al., 2016).

Equation 5.4 is used to model the heat transfer between the two phases (polymer and calibrator). The first term of the left hand side, is the advection term and is followed by the diffusion terms, and the interface with contact resistance boundary condition is provided at the right hand side of the equation. The latter term is not null just at the interface ($\nabla \propto_p \; or \; \propto_{\boldsymbol{p}} . \propto_{\boldsymbol{c}}$).

The OpenFOAM® computation library is used to solve the main governing equation (Eq 5.4), which allows to compute the temperature distribution in both domains.

The numerical calculation procedure begins with the initial setting of temperature, volume fraction and the profile velocity. Before solving Eq 5.4, the mixture field quantities are calculated explicitly, and then introduced into it. The equation is solved only once in each time step, until a steady state solution is observed.

A second order cellLimited leastSquares scheme is used for the approximation of the gradient terms, and the Gauss scheme is considered for the Laplacian and divergence

terms. The mixture temperature (T_m) has to be interpolated onto the cell-faces, for the calculation of the convection term, and it is done by a second-order Gamma scheme.

To obtain fast convergence rates, a geometric-algebraic multi-grid (GAMG) solver in conjunction with a diagonal incomplete-Cholesky smoother is used. The numerical solution was considered to be converged at the time where no change in the value of the outlet average temperature field is observed, and the overall residuals obtained is 10^{-6}.

5.3 Experimental Assessment

In this section, the numerical code developed by Habla et al.(2016) is validated with the experimental results obtained from a real case calibration system used for the production of a polycarbonate swimming pool cover. The cooling/calibration system used in the production line of this profile is given in Figure 5.2.

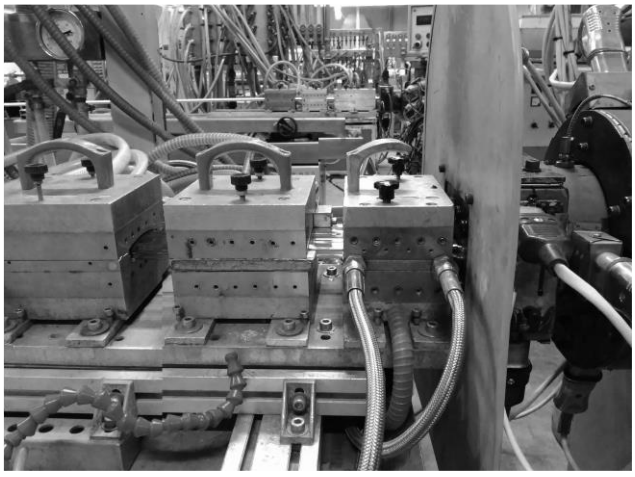

Figure 5.2: Cooling/calibration system used in the production line of the swimming pool cover profile

As can be seen, the cooling/calibration system consists of three calibrators, made of stainless steel, separated by short annealing zones. The swimming pool cover is a

complex profile (see Figure 5.3) with uneven thickness, and the outer surface of the profile is in contact with the calibrator material.

For experimental validation purposes, during the production run of the swimming pool cover profile the surface temperature of the profile was measured at different locations along the length of the cooling/calibration system, using a FLIR thermal imager (FLIR). Due to the extrusion line set up (See Figure 5.2), it was only possible to measure the temperature at the top surface of the profile because it was not possible to focus the device (FLIR thermal imager) on the other cross section regions of the profile. Therefore, two different cross section regions (CSRs) at the top surface of the profile (see Figure 5.3) were selected to perform the temperature readings.

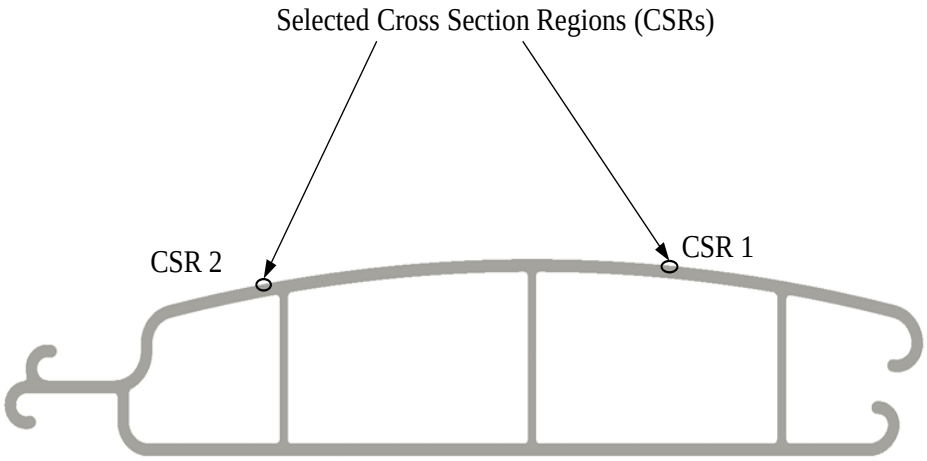

Figure 5.3: Swimming pool cover profile and selected cross section regions (CSRs) where the temperature was measured

It is impossible to measure the temperature of the profile inside the calibrators, so the data were collected at the calibration system inlet (inlet of the first calibrator) and outlet (outlet of the third calibrator), and at the annealing zones.

5.3.1 Geometry and boundary conditions

The complete details about the system geometry and the processing conditions were used in order to replicate the process numerically. Figure 5.4 shows the lateral view of the real case cooling/calibration system and corresponding dimensional details. Each calibrator unit has different values of length and height, and the width (150 mm) is same for all. The calibrators' cooling channels have a zigzag layout (see Figure 5.5), and a constant diameter of 6.75 mm. The complete calibration system was design by the industrial company, based on previous experience.

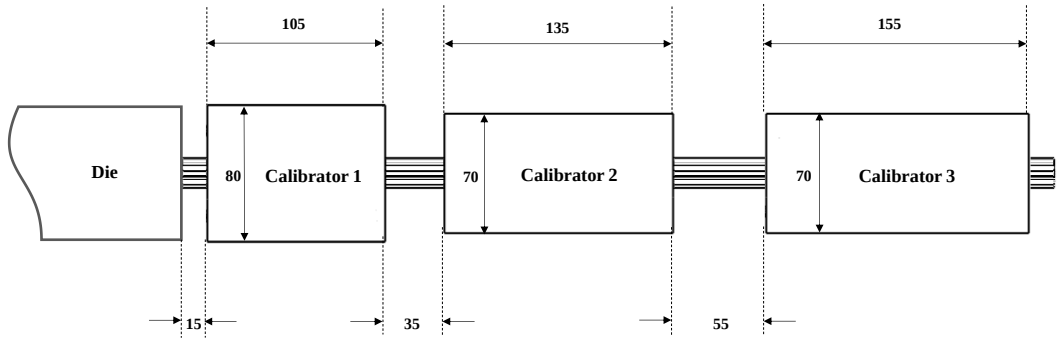

Figure 5.4: Lateral view of the cooling/calibration system used for the production of the swimming pool cover profile. (Dimensions in mm)

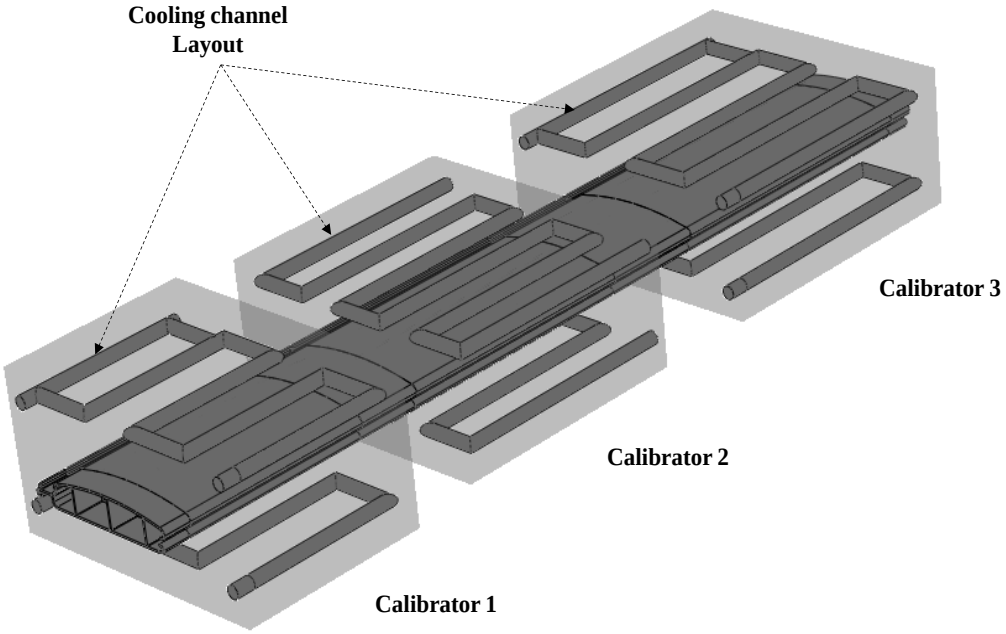

Figure 5.5: Cooling channel layouts adopted in the calibrators used for the production of the swimming pool cover profile

In order to provide slow cooling during the cooling process, a higher temperature was used for the first two calibrators. To do so, these calibrators were set at 70°C and the last one was set at 18°C. This setting was done based on the experience got in well succeeded previous productions with polycarbonate. A thermal regulator was used to heat the cooling fluid circulating in calibrators 1 and 2.

In terms of numerical modeling, proper boundary conditions should be provided at the profile and calibrators. The external surface of the profile and calibrators are subjected to natural convection boundary condition. Regarding the other sections in the geometry, the Dirichlet boundary condition is assumed at the modeling domain inlet (extrusion die exit) and at the cooling channels' surfaces. Furthermore, an

adiabatic boundary condition is considered at the modeling domain outlet and interior walls of the profile (Nóbrega et al., 2004). A clear picture of the boundary conditions employed for this case study is given in Figure 5.6.

The thermal and physical properties of the calibrator and the profile are provided in Table 5.1.

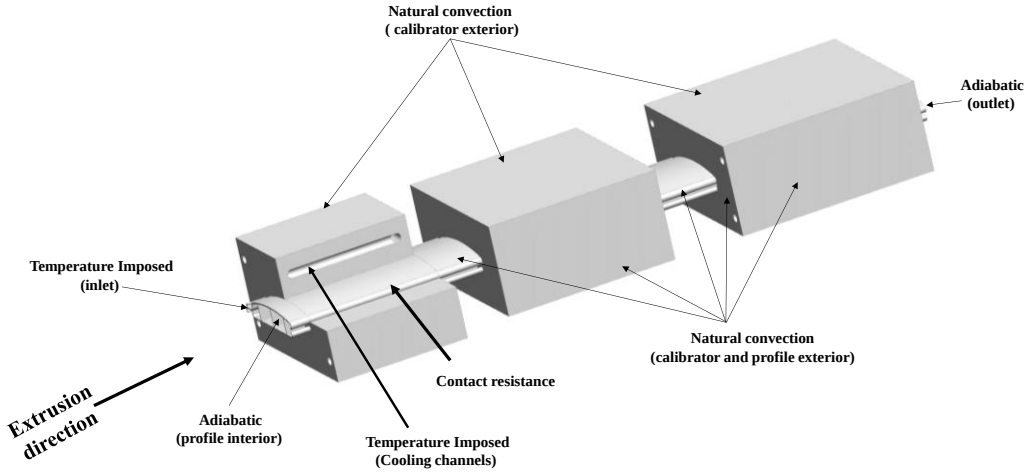

Figure 5.6: Temperature boundary conditions used for the numerical study of the real case calibrator system

Table 5.1: General properties and processing conditions used in the numerical simulation

Profile material : Polycarbonate	k_p **(W/mK)** c_p **(J/KgK)** ρ_p **(kg/m3)**	**0.255** **1808** **1090**
Calibrator material : Stainless steel	k_c **(W/mK)** c_c **(J/KgK)** ρ_c **(kg/m3)**	**28.5** **510** **7740**
Air convection heat transfer coefficient (free convection) (*W/m2K*)	**5**	
Profile-calibrator convection heat transfer coefficient (*W/m²K*)	**500**	
Linear extrusion speed (*m/min*)	**1.28**	
Inlet profile temperature (°C)	**228**	
Room temperature (°C)	**18**	

5.3.2 Mesh sensitivity analysis

A mesh sensitivity analysis was performed to evaluate the degree of refinement needed to get results independent of the mesh, which will be used in the subsequent studies. Three different meshes having 558,662 (M1), 4,431,414 (M2), and 35,189,840 (M3) computational cells, were considered in this study, being the meshes generated using the SnappyHexMesh (Gisen, 2014) utility, one of the tools available in OpenFOAM framework.

As an initial comparison, the temperature evolution along the calibration system length at three different profile cross section points (P1, P2 and P3), were determined for each

mesh, and was shown in Figure 5.7, where P1 and P2 are the cross section points at the outer surface of the profile, and P3 is located at the middle of the center rib in the

profile (see Figure 5.7)).

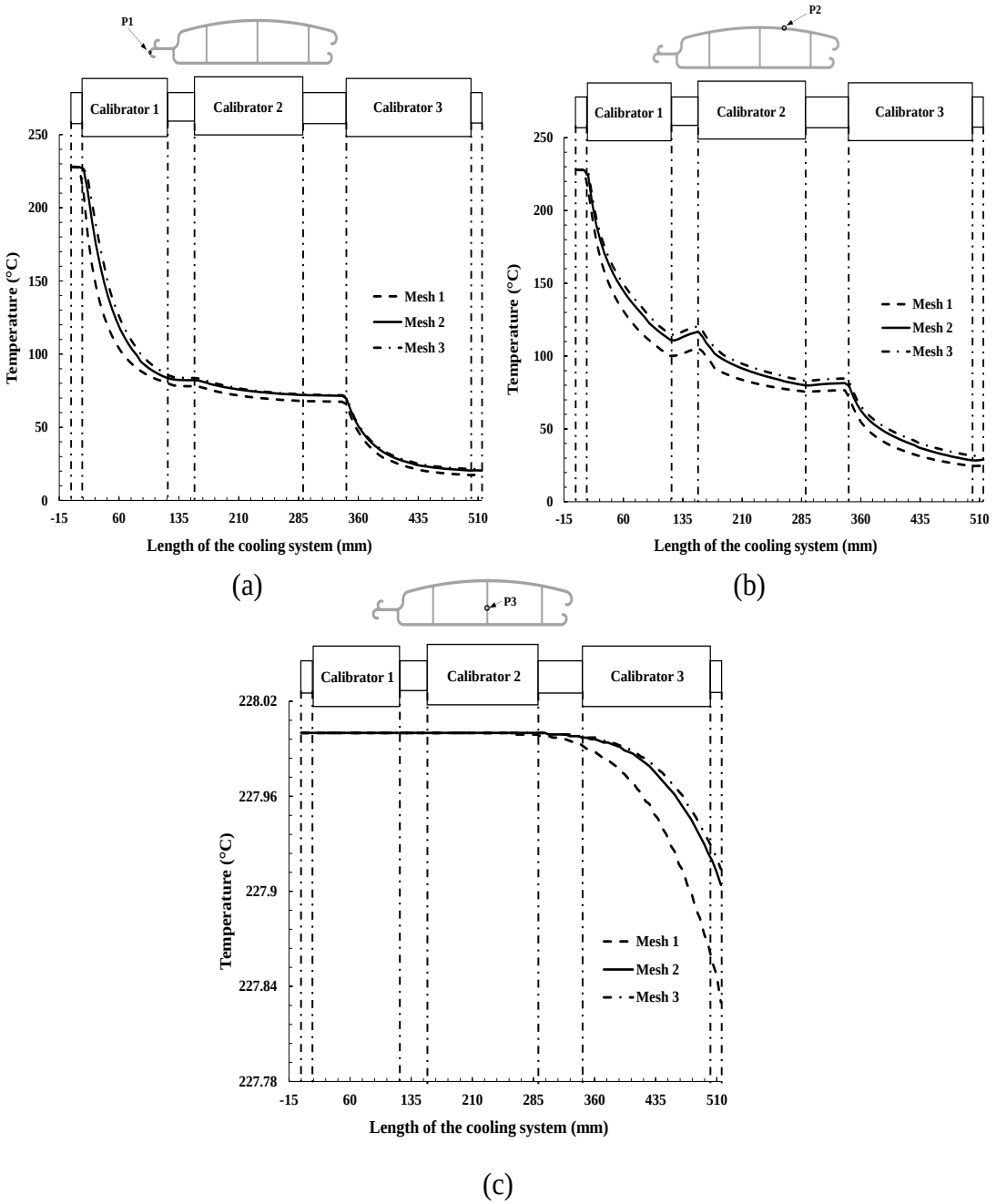

Figure 5.7: Temperature results along the cooling system length of the mesh refinement study, at different profile cross section points: (a) P1, (b) P2 and (c) P3

As one can observe from Figure 5.7(a) and (b), for the cross section points P1 and P2

the temperature decreases inside the calibrators and a small rise in temperature is observed in the annealing zones (clearly visible in P2 (see Figure 5.7(b)), due the heat flow from the hotter inner zone of the profile to the colder outer one. For both cross section points (P1 and P2) a sharp reduction of the temperature occurs in the first calibrator unit, where the difference between the calibrator and polymer surfaces are higher. For the cross section point P3, only a very small reduction in temperature was observed in the second annealing zone/calibrator 3 This is because P3 is located at the center rib of the profile (see Figure 5.7(c)), which is not in contact with the calibrators. In all the cases, the temperature distribution predicted with M2 is similar to that obtained with the most refined mesh (M3).

The average ($\overline{T}$) and the standard deviation (σ_T) of the temperature distribution at the outlet profile cross section were also calculated for the studies performed, using Eq 5.5 and 5.6, respectively.

$$\overline{T} = \frac{\sum_{i=1}^{n} T_i A_i}{A_T} \tag{5.5}$$

$$\sigma_T = \frac{\sum_{i=1}^{n} (T_i - \bar{T})^2 A_i}{A_T} \tag{5.6}$$

where, n is the number of computational cell faces at the outlet cross section, and T_i and A_i are the cell face temperature and area, respectively. A_T is the outlet profile cross section area. For the analysis, the average and standard deviation temperature distribution values were normalized with the values from the most fined mesh (M3). The results are given in

Figure 5.8, where the average temperature at the outlet of M2 shows a maximum relative difference of circa 1.3% with respect to the finer mesh (M3).

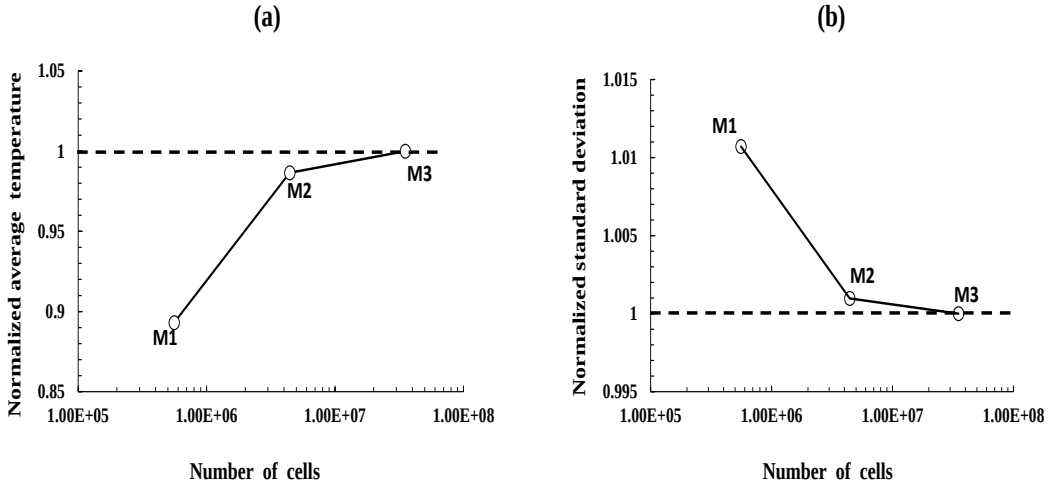

Figure 5.8: Results of the mesh sensitivity analysis, for the replicated real case calibration system geometry, normalized with those obtained with the finer mesh: (a) average temperature at the outlet; (b) standard deviation of temperature distribution at the outlet

Based on the results of the mesh sensitivity analysis, it can be concluded that M2 (having circa 4.5 million computational cells) provides a considerable accuracy within an acceptable simulation time. Therefore, this level of refinement was employed for the subsequent studies performed in this work. The typical mesh corresponding to M2 is illustrated in Figure 5.9.

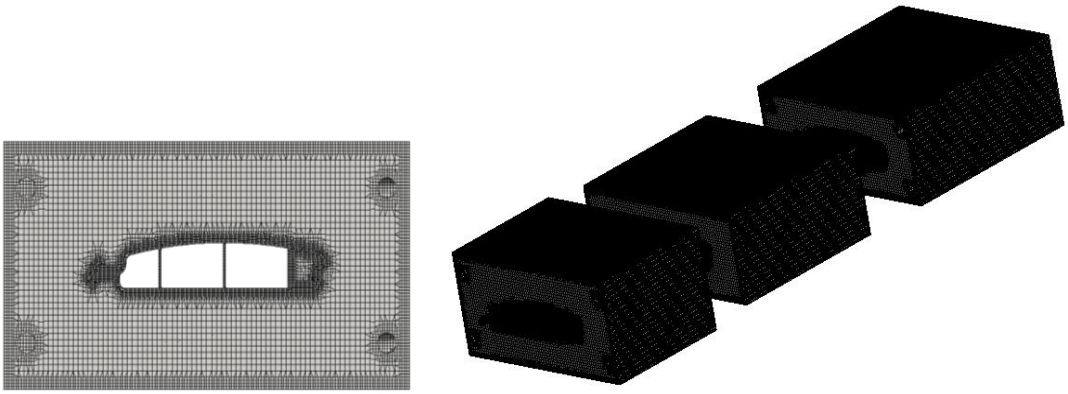

(a) (b)

Figure 5.9: Selected mesh (M2) used to replicate the real case calibration system geometry: (a) Front view; (b) 3D view

5.3.3 Results and discussion

The information about the locations where the temperature of the profile was measured was indicated in section 5.3. While performing the experimental measurements, a set of five temperature readings were collected from the defined locations (CRSs, indicated in Figure 5.3) along the length of the calibration system. These data were used to compute the profile average temperature and standard deviation, at each location.

Regarding the numerical results, the temperature was computed after averaging the temperatures corresponding to a number of domain points located at the cross section regions (CSRs) under study.

Figure 5.10 shows the comparison between the experimental measurements and the numerical results, evidencing the good agreement between both.

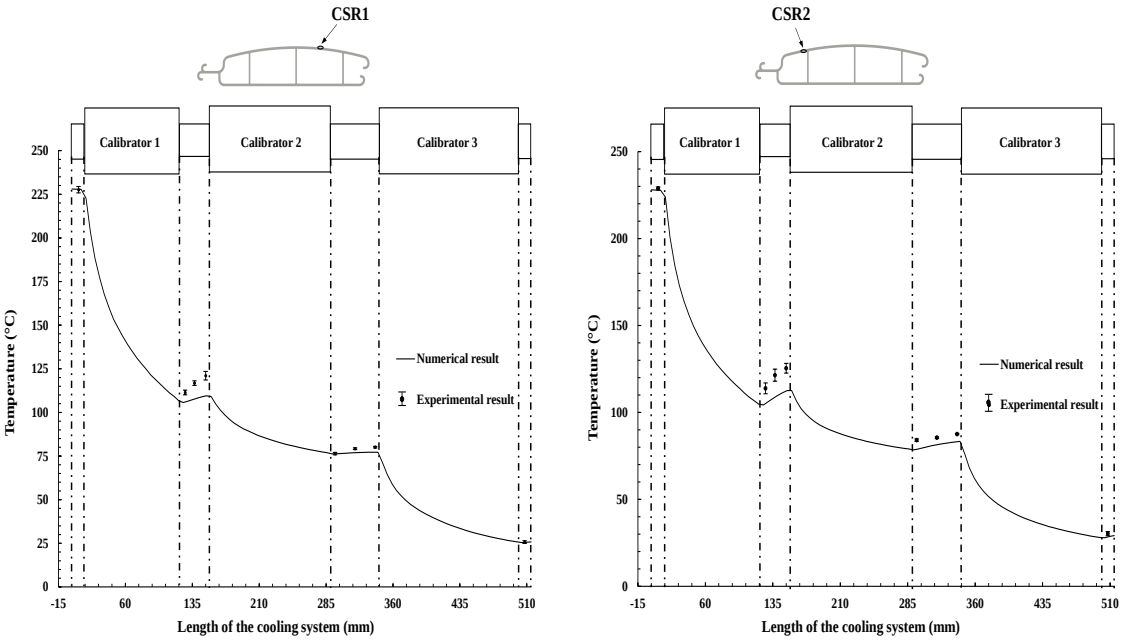

Figure 5.10: Experimental and numerical temperature results determined at the top surface of the profile: (a) CSR1 and (b) CSR2

Notice that the maximum difference between the experimental and numerical temperature values was observed near the inlet of the second calibrator unit for, both CSRs. Comparatively, the CSR2 location provides the higher relative error (circa 8.6%). On the other hand, the results at other locations show minor differences, mainly near the outlet of the calibrator system where the difference observed between the numerical prediction and the experimental result was very low, where in the CSR2 show a maximum relative error of circa 1.56 %.

As a conclusion, the results obtained prove the accuracy of the numerical code developed by Habla et al.(2016), making it a suitable tool to aid the design of the cooling/calibration stage of profile extrusion lines.

5.4 Calibration system design

This section comprises a set of studies performed to demonstrate the advantage of using a numerical code (Habla et al., 2016) to support the design of a calibration system. For this purpose, a numerical based trial-and-error approach was used to identify a better alternative to the original calibration system (reference case) presented in section 5.3. The goal is to reduce the average and standard deviation of the temperature distribution at the outlet profile cross section, when compared to the reference case.

An open source software, Salome, was used to generate the geometries and the corresponding meshes for the various trials involved in this study (Habla et al., 2016). In search for an alternative cooling system, the numerical trial-and-error study holds some restrictions. The total length of the reference case calibration system is maintained constant in all the numerical trials, i.e. the total length assigned for the calibrators is kept constant. The same applies to the annealing zones and to the diameter of the cooling channels.

The boundary conditions used for all the numerical trials were the same indicated in Section 5.3.1 (see Figure 5.6), with the exception of the temperature imposed in the cooling channels of the calibrators.

5.4.1 Cooling channel layout

The main objective of this section is to propose an alternative calibration system to be used in the production of the swimming pool cover profile, with manufacturing advantages. The manufacturing process can be simplified by using straight cooling channels instead of the complex zigzag ones, so the search for an alternative cooling/calibration system is focused on straight cooling channels.

The study starts with two initial numerical runs; i) a first trial, named as (cc6), where each calibrator unit has six cooling channels, and, ii) a second trial, named as (cc12), where each calibrator unit has twelve cooling channels. The latter trial case (cc12) is similar to the reference case concerning to the number of cooling channels.
The same dimensional setup and cooling fluid temperatures used for the reference case (see section 5.3) are used to perform these initial runs (cc6 and cc12). The calibration system geometries of both trials are shown in Figure 5.11.

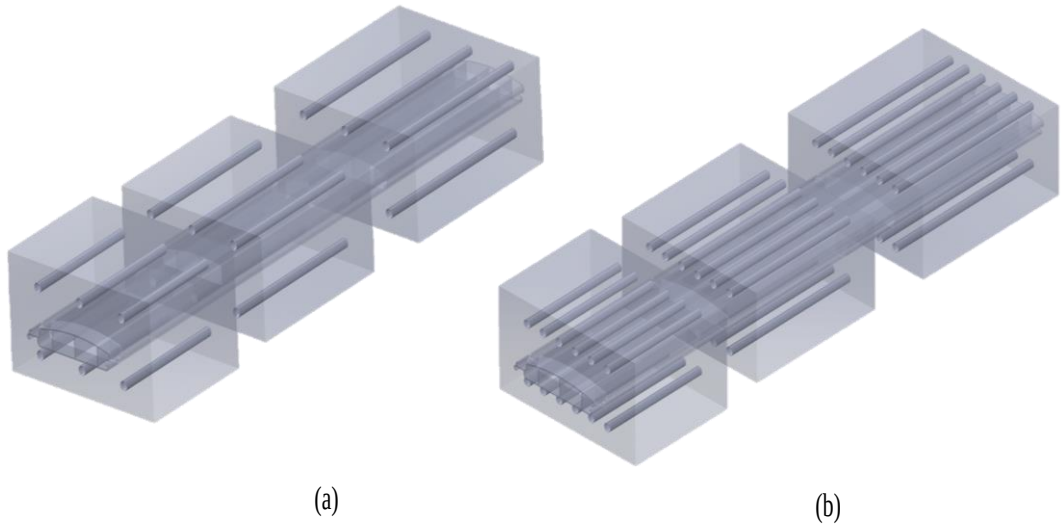

Figure 5.11: Layout of the cooling channels considered in the initial trials: (a) cc6; (b) cc12

The average and standard deviation of temperature distribution at the outlet profile cross section, predicted from these trials (cc6, cc12) and from the reference case are presented in Table 5.2.

Table 5.2: Field results at the outlet profile cross section for the reference case and initial trials (cc12 and cc6)

Fields predicted at the profile outlet	reference case	cc12	cc6
Average temperature (° C)	46.2	47.2	49.1
Standard deviation of temperature distributions (° C)	51.4	51.2	50.8

A higher average temperature is experienced with trials cc6 (see Table 5.2) and cc12, when compared to the reference case. A reverse situation is observed with the standard deviation of the temperature distribution (see Table 5.2), as expected. The results from trial cc12 show a smaller difference to the reference case, when compared to those of cc6. However, the outlet average temperature given by trial cc6 is around 3ºC higher than the reference case.

Moreover, having in mind the manufacturing advantage of cc6 over cc12, the former (cc6) is considered for possible design improvements.

5.4.2 Length and cooling fluid temperature distribution

This study is performed to propose a suitable length and cooling fluid temperature for each calibrator of the trial calibration system cc6, in order to provide a better cooling performance than the reference case. As a consequence, a number of subsequent numerical trials are performed, by numerically adjusting these two variables (length and temperature of each calibrator).

The variables LC1, LC2 and LC3 are used to represent the lengths (see Figure 5.12) and

the variables TC1, TC2 and TC3 represents the cooling fluid temperatures, of

calibrators 1, 2 and 3, respectively. The total length of the calibrators is given by TCL, where TCL = LC1+LC2+LC3= 395 mm. The annealing zones between calibrators 1 and 2 and between calibrators unit 2 and 3 (see Figure 5.12) are represented by AD1 and AD2, respectively.

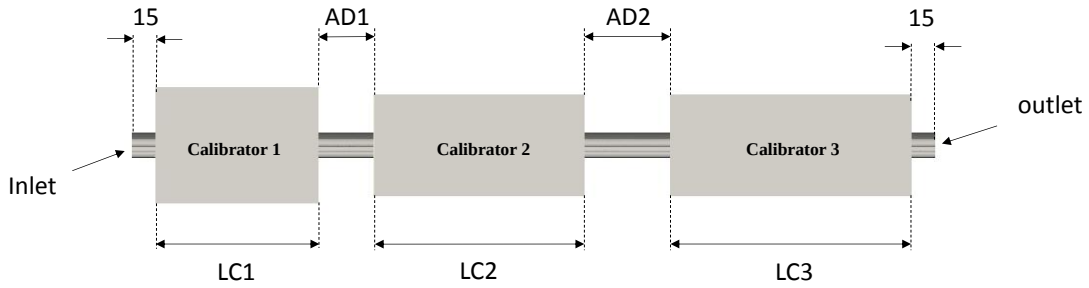

Figure 5.12: Lateral view of the cooling system and variables used for numerical trials. (Dimensions in mm)

The first numerical trial (T1) was done with a calibration system having only one calibrator with a length (LC1) equal to the total calibrator unit length (TCL). The details are shown in Figure 5.13. The temperature of the cooling fluid (TC1) is assumed to be 70 °C, as suggested by the company, based on their previous experience.

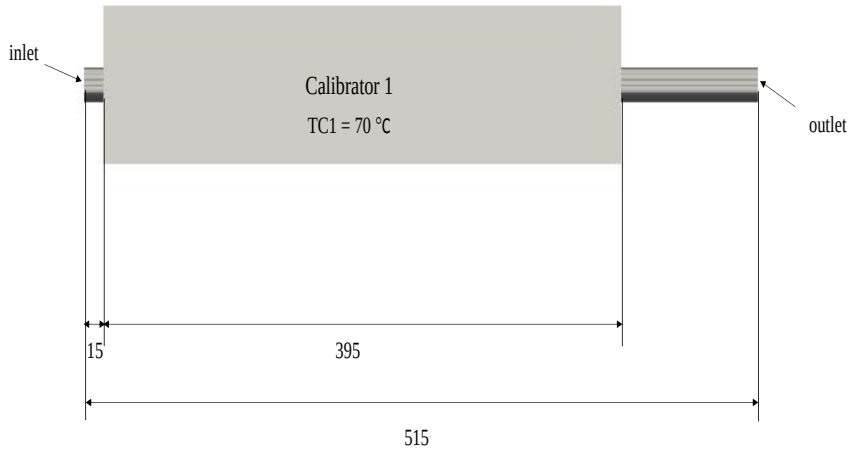

Figure 5.13: Side view of the cooling system designed for T1 (Dimensions in mm)

Trial T1 was performed in order to determine the adequate length of the first calibrator, having into consideration its effectiveness in terms of cooling rate. For this purpose, the evolution of $\overline{T}$ and σ_T along the length of the calibration system was calculated, being shown in Figure 5.14.

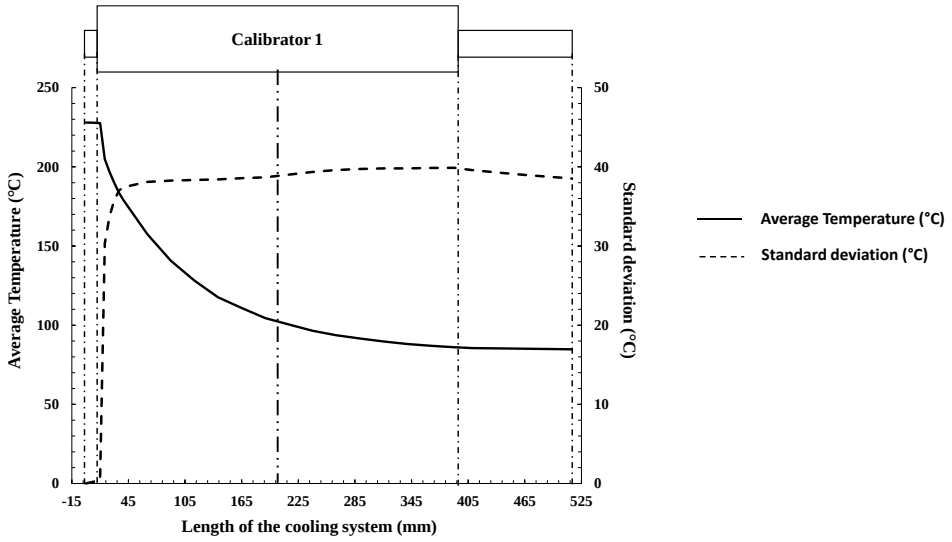

Figure 5.14: Average and standard deviation of the temperature distribution along the T1 calibration system length

One can observe from Figure 5.14 that the average temperature ($\overline{T}$) show a sharp drop up to the middle of the calibrator, and then almost stabilizes. Contrarily, the standard deviation raises within a short initial length of the calibrator unit and then progresses with a very small increase along the calibrator unit length. These results allow to conclude that there is no advantage of having a length for LC1 higher than 50% of the TCL. Based on this, in all the following trials the first calibrator unit length (LC1) was fixed to 50% of the TCL and its temperature (TC1) to 70 °C.

Subsequently, a set of trials were performed by adjusting the length and temperature of calibrators 2 and 3, in order to further improve the calibration system design. Each new trial was based on the results obtained with the previous one. The details about these trials are given in Table 5.3. For the set of trials T1 to T5 an equal length was assumed for both annealing zones (AD1 = AD2 = 45 mm).

Table 5.3: Trials performed to search for the length and temperature of calibrators 2 and 3

Trials	**Length of calibrator units (mm)**			**Cooling fluid temperature (°C)**			**Average temperature (°C)**	**Standard deviation (°C)**
	LC1	**LC2**	**LC3**	**TC1**	**TC2**	**TC3**		
reference case	**105**	**135**	**155**	**70**	**70**	**18**	**46.2**	**51.4**
T2	**197.5**	**118.5**	**79**	**70**	**50**	**30**	**58.4**	**46.7**
T3	**197.5**	**98.75**	**98.75**	**70**	**40**	**20**	**49.5**	**49.5**
T4	**197.5**	**98.75**	**98.75**	**70**	**30**	**18**	**46.2**	**50.3**
T5	**197.5**	**98.75**	**98.75**	**70**	**20**	**20**	**45.2**	**50.3**
T6	**197.5**	**98.75**	**98.75**	**70**	**20**	**20**	**45.2**	**50.2**

The numerically predicted average and standard deviation values of temperature distribution are also presented in Table 5.3, where the results of reference case is also included for comparison purposes.

The results from T2 show a higher average temperature and a lower standard deviation at the outlet profile cross section when compared to the reference case. In order to decrease the average temperature, the next trial (T3) was carried out by decreasing LC2 (and, consequently, increasing LC3, see Table 5.3), because the last calibrator has the lowest temperature, being therefore more effective. Moreover, the cooling fluid temperatures, TC2 and TC3, were also decreased. As a result, the average temperature predict forT3 show a lower value, with respect to T2, with a

corresponding increase in standard deviation. However, when compared to the reference case, the average temperature value is still higher, but better than one obtained in the previous trial, T2 (see Table 5.3).

Considering this, in the next trial (T4) only the cooling fluid temperatures, TC2 and TC3,

were decreased, maintaining calibrator's lengths of T3 (see Table 5.3), to further decrease the average temperature. The results improved since the average temperature predicted for T4 is similar to that of the reference case (see Table 5.3), and the standard deviation is lower.

The next trial (T5) was performed by setting the same cooling fluid temperature for TC2 and TC3, i.e. a lower temperature for TC2 and a slightly higher for TC3, when compared to those used in T4 (see Table 5.3). The objective is to decrease the average temperature while not affecting too much the standard deviation. At this stage the predicted results from T5 satisfies the objective of this numerical study, by providing lower average and standard deviation of temperature distribution at the outlet profile cross section when compared with the reference case (see Table 5.3).

Both T4 and T5 trials provide acceptable cooling performance. However, in an attempt to obtain further improvements, the evolution of the average and standard deviation of temperature distribution along the calibration system length of both trials, were analyzed, and is shown in Figure 5.15.

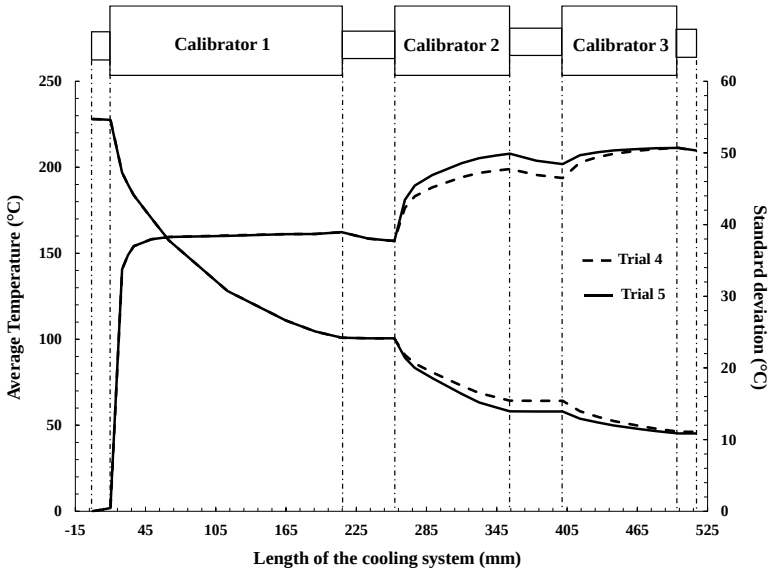

Figure 5.15: Average and standard deviation of the temperature distribution evolution along the calibration system length, for T4 and T5 trials

From Figure 5.15 one can observe that the average temperature inside calibrator 2 drops more in T5 than in T4, because a lower temperature is assumed in this calibrator in T5 (see Table 5.3). As expected, this promoted an increase in the corresponding standard deviation. However, in these T4 and T5 trials the average temperature and the standard deviation converged to closer values in the last calibrator, but still T5 remains as a better choice.

On observing the result of the standard deviation along the calibration system length of T5, it can be seen that the drop of the standard deviation is higher in the second annealing zone (AD2) than in the first. So a final trial (T6) was performed with a small change with respect to T5, where the annealing length AD2 was increased (to 75 mm), forcing a reduction of AD1 to 15 mm. The results predicted from this last trial (T6) did not affect the average temperature at the outlet profile cross section with respect to T5 (see Table 5.3), but the standard deviation decreased slightly (around 0.2% relative to the previous trial, T5).

5.5 Conclusion

The aim of this work was to unveil the capability of a numerical solver developed in OpenFOAM framework to model the heat transfer that occurs during the cooling stage of profile extrusion. For this purpose, an experimental validation was performed considering the cooling of a complex geometry profile in industrial premises, employing the existing cooling/calibration system. The numerical results obtained were in good agreement with those measured during a production extrusion run.

The usefulness of the numerical code was than illustrated by performing a numerical based trial-and-error study intended to provide an alternative cooling/calibration system with better performance than the existing one. Within the constraints considered, new calibration system was proposed, which has a slightly better cooling performance and requires a simpler manufacturing process.

5.6 References

Carneiro, O. S. and Nóbrega J. M. (2012). *Design of Extrusion forming Tools*, Smithers Rapra Technology Ltd.

Dopazo, C. (1977). On conditioned averages for intermittent turbulent flows, *Journal of Fluid Mechanics* **81**(03): 433-438.

FLIR (2016).
URL: http://www.flir.eu/home/.

Fradette, L., Tanguy, P., Hurez, P. and Blouin, D. (1996). On the determination of heat transfer coefficient between PVC and steel in vacuum extrusion calibrators, *International Journal of Numerical Methods for Heat & Fluid Flow* **6**(1): 3-12.

Fradette, L., Tanguy, P., Thibault, F., Sheehy, P., Blouin, D. and Hurez, P. (1995). Optimal design in profile extrusion calibration, *Journal of polymer engineering* **14**(4): 295-322.

Gisen, D. (2014). Generation of a 3D mesh using snappyHexMesh featuring anisotropic refinement and near-wall layers for a hydro power dam tailwater. *Proceedings of the 11th International Conference on Hydroscience and Engineering (ICHE)*.

Habla, F., Dietsche, L. and Hinrichsen, K.O. (2013). Modeling and simulation of conditionally volume averaged viscoelastic two-phase flows, *American institute of chemical engineers Journal* **59**(10): 3914-3927.

Habla, F., Fernandes, C., Maier, M., Densky, L., Ferrás, L.L., Rajkumar, A., Carneiro,

O. S., Hinrichsen, O. and Nóbrega, J.M. (2016). Development and validation of a model for the temperature distribution in the extrusion calibration stage, *Applied Thermal Engineering* **100**: 538-552.

Kleindienst, V. (1973). Effective Parameters for Vacuum Calibration of Extruded Plastic Pipes, *Kunststoffe-German Plastics Stuttgart* **63**: 7-11.

Kurz, H. (1988). Fixing the dimensions of extruded high-mw polyolefin pipes during cooling, *Kunststoffe-German Plastics Stuttgart* **78**(11): 1052-1058.

Marschall, H., Hinterberger, K., Schueler, C., Habla, F. and Hinrichsen, O. (2012). Numerical simulation of species transfer across fluid interfaces in free-surface flows using OpenFOAM, *Chemical engineering science* **78**: 111-127.

Menges, G., Haberstroh, E. and Janke, W. (1982). Systematic lay-out of cooling lines for film, sheet and pipe extrusion plant, *Kunststoffe-german plastics* **72**(6): 332-336.
Menges, G., Kalwa, M. and Schmidt, J. (1987). Finite element simulation of heat transfer in plastics processing, *Kunststoffe-german plastics* **77**(8): 797-802.

Michaeli, W. (1992). *Extrusion Dies for Plastics and Rubber: Design and Engineering Computations,* Hanser publication, Munich.

Nóbrega, J.M. and Carneiro, O.S. (2006). Optimising cooling performance of calibrators for extruded profiles, *Plastics, rubber and composites* **35**(9): 387-392.

Nóbrega, J.M., Carneiro, O.S., Covas, J., Pinho, F.T. and Oliveira, P.J. (2004). Design of calibrators for extruded profiles. Part I: Modeling the thermal interchanges, *Polymer Engineering & Science* **44**(12): 2216-2228.

Nóbrega, J.M., Carneiro, O.S., Gaspar-Cunha, A. and Gonçalves, N. (2008). Design of calibrators for profile extrusion–optimizing multi-step systems, *International Polymer Processing* **23**(3): 331-338.

Pittman, J., Whitham, G., Beech, S. and Gwynn, D. (1994). Cooling and Wall Thickness Uniformity in Plastic Pipe Manufacture: An Experimental Study and Computer Simulations, *International Polymer Processing* **9**(2): 130-140.

Reifschneider, L.G., Kostic, M. and Vaddiraju, S.R. (2004). Computational Design of U-Profile Die and Calibrator, *Antec-Conference Proceedings*.

Sheehy, P., Tanguy, P. and Blouin, D. (1994). A finite element model for complex profile calibration, *Polymer Engineering & Science* **34**(8): 650-656.

Szarvasy, I. (2000). Simulation of Complex PVC Window Profile Cooling During Calibration with Particular Focus on Internal Heat Exchange, *3rd ESAFORM Conference on Material Forming*.

Chapter 6

Conclusions and Future work

6.1 Conclusions

In this dissertation, new and improved methodologies for the design of extrusion forming tools were implemented using open source computational tools.

A new methodology was proposed to design complex extrusion dies for thermoplastics profiles. The open source softwares required to perform various tasks in the design methodology were identified. For this purpose a numerical code capable of dealing with non-isothermal flows of generalized Newtonian fluids was developed in the OpenFOAM framework and verified with the Method of Manufactured Solutions for proper implementation. Later, the die-design methodology was experimentally validated with two industrial case studies (protection bar and swimming pool cover profiles). The results for both case studies were very good. The proposed die design procedure proved to be a much better alternative to the usual experimental based trial-and-error approach followed by many profile extrusion industries.

To support the extrusion die designers with no access to numerical tools, a new die design methodology that circumvent the use of any numerical tool was developed to provide useful guidelines in the design process of complex profile extrusion dies, which can be decomposed in '*L'* and '*T*' shaped elementary geometries. The die design methodology comprises a surrogate model and two alternative design approaches (Average Method and Minimum Method). The surrogate model was devised based on the results obtained from a comprehensive numerical study performed with elementary profiles, namely, '*L*' and '*T*' shaped geometries. The

design methodology was assessed with three different complex geometries. The results obtained proved the efficiency of the proposed methodology in predicting the flow channel geometry resulting in an improved flow distribution at the extrusion die outlet, when compared to the usual initial trials used in industry.

In a second stage, the previously developed surrogate model was improved by considering the influence of the material rheological parameters and the processing conditions. Among these parameters, only the rheological parameter Power-Law index 'n' showed a significant influence on the flow distribution. Therefore, this parameter was included in the surrogate models by performing a new extensive numerical study. The improved die design methodology was tested with different geometries with a relevant range of Power-Law index values. The results obtained enabled concluding that the methodology was applicable for a relevant range of thermoplastic materials, thus proving to be a useful tool for extrusion die designers.

Concerning the calibration/cooling system, a valid experimental assessment was made for a previously developed numerical code used to model the heat transfer occurring at the calibration stage of complex profiles. A very good agreement between the numerical prediction and the experimental measurements was obtained, proving the accuracy of the code in industrial situations. The applicability of the code to improve the calibration system design was demonstrated using a numerical trial-and-error approach. In this study, a better alternative was proposed for a real case calibrator system providing a simpler design with manufacturing benefits.

6.2 Future work

The outcome of this dissertation gained the interest of the profile extrusion industry to use numerical simulations in the design process of the extrusion forming tools. So far, the developed / proposed design methodologies were based on numerical trial and error approaches in which the design of the extrusion die and of the calibration system were carried out separately. Also, the consequent changes on the geometry or the modification of the boundary conditions performed during the design process were still committed to the designer. In the future, the developed numerical codes can be coupled to an optimization algorithm to search the optimum solution for these extrusion forming tools. In this circumstances, the design process will be automated, thus minimizing the designer's intervention.

Regarding the calibration system, the experimental validation of the numerical code proved its adequacy to deal with industrial problems, and an improved calibration system was suggested in this work. However, an experimental implementation of this proposal would be an added confirmation. Furthermore, the implementation of algorithms to evaluate the thermo-mechanical subtleties during the cooling stage would be of paramount importance on predicting details regarding formation of thermal residual stresses.

Moreover, it would be very useful for the profile extrusion industries, if an integrated solver is developed to numerically model the complete process from the extrusion die inlet to the calibrator outlet.